An In Vitro Single Molecule Fluorescence Assay to Study the Spindle Assembly Checkpoint

Kwaku Nyame Opoku

A dissertation

submitted in partial fulfillment of the

requirements for the degree of

Doctor of Philosophy

University of Washington

2016

Reading Committee:

Charles Asbury, Chair

Linda Wordeman

Sue Biggins

Program Authorized to Offer Degree:

Molecular and Cellular Biology

University of Washington

Abstract

Building an *in vitro* Single Molecule Fluorescence Assay to Study the Spindle Assembly Checkpoint

Kwaku Nyame Opoku

Chair of the Supervisory Committee:
Dr. Charles Asbury, Professor
Department of Physiology & Biophysics

Dividing cells rely on a surveillance mechanism at kinetochores called the spindle assembly checkpoint, which emits a diffusible 'wait' anaphase signal when kinetochores are unattached or improperly attached to microtubules. This results in cell arrest, delaying anaphase until stable bioriented kinetochore-microtubule attachments are formed.

The evolutionarily conserved spindle assembly checkpoint kinase, Mps1, has been shown to phosphorylate the core kinetochore component, Spc105, leading to recruitment of the Bub1-Bub3 checkpoint complex. Further phosphorylation of Bub1 by Mps1 also results in the recruitment of the checkpoint protein Mad1 leading to generation of the 'wait' anaphase signal.

Attachment of microtubules to kinetochores results in the silencing of the spindle assembly checkpoint signal. However, how attachment directly results in checkpoint silencing continues to be debated. Studying the checkpoint and how it is silenced has proven a challenge due to the difficulty of directly and unambiguously distinguishing the microtubule attachment status and levels of checkpoint proteins on individual kinetochores *in vivo*. In this dissertation, I developed a fluorescence-based approach to observe the association of checkpoint proteins with single kinetochore particles *in vitro*, where the kinetochore-microtubule attachment status can be controlled and its effect on checkpoint protein levels can be directly observed.

Mps1 is most upstream of the checkpoint signaling cascade and is localized to the core Ndc80 component of the kinetochore. The Ndc80 sub-complex is a major microtubule-binding core component of the kinetochore. Recent studies on checkpoint silencing have focused on Mps1 and how it responds to kinetochore-microtubule attachment since it is most upstream of the signaling cascade and is implicated in the checkpoint. I isolated native budding yeast kinetochore particles carrying fluorescent tags on a core Mtw1 kinetochore component and Mps1. I then examined the kinetochores in the presence of microtubules using a custom-built multi-color Total Internal Reflection Fluorescence (TIRF) microscopy system and single particle assays. I show that the spindle assembly checkpoint can be studied *in vitro*, at the single particle level. The assays I develop also set the stage for checkpoint silencing to be understood.

TABLE OF CONTENTS

LIST OF FIGURES

LIST OF TABLES

ACKNOWLEDGEMENTS

I would like to thank my family for all the support, prayers and encouragement. To my siblings, Kwasi and Akosua, I am a better man because of the two of you. You allowed me to be big brother even though I haven't been around much, and I have learned so much from you than you could ever imagine. I am very proud of who you've grown to become. Daa and Maa, I don't know how to say thank you. From Koforidua all the way to this point you have given up everything so we could live lives you could not. We never lacked clothes to wear, we never lacked a roof over our heads, we never lacked food to eat, we were never kicked out of school because of school fees. You took us to church, taught us the Bible, prayed with and for us. How can I say thanks?

To my extended family, friends and loved ones. I would not have made it this far without you. Agnes Yeboah, you opened the way for me to come to the United States and you continue to set the bar high. Sometimes too high. I am forever grateful. To the Bowers family in Bothell Seattle, my American family. You took a Ghanaian kid who lived across from your son's dorm room in freshman year in as one of your own. Mark, you have been a father to me. Beth you have been a mother to me. You came into my life at a time when I really needed you and I will forever be your son. Mike, Scott, Kiersten and Andy. Thank you for treating me like a brother.

To Mama C. Even before I married your daughter you took me in as a son and loved me like one. Your courage, strength and tenacity amaze me. I will never forget everything you have done for me. You gave me one of those greatest blessings, in your daughter. I could not have wished for a better family to be a part of. To all my in-laws, I thank you for the love, support, encouragement and prayers. Nneka, Olisa, Nnamdi, Chucky, Arinze, Merve and Kennie: thank you very much.

My boys Setri, Edwin, Kofi, Francis and Sydney. We have come very far from Bogstad Manor. Thank you for everything you have done for me. Thanks for the encouragement when things got tough. You are my brothers for life.

To my church family from Ebenezer Presby, LCI Eden Prairie and LCI Tacoma, thank you very much for your love and your prayers. Rev. David and Rev. Sonny thanks for being fathers to me. Rev. Sonny I do not know why you took special interest in me but I would not be the man I am without you.

To all the teachers that helped me along the way: Mrs. Donkor, Ms. Addo, Madam Kugblenu, Mr. Norman, Mr. Koranteng, Mr. Baffoe, Mr. Dzah, Profs. Bill Tomhave, Doug Anderson, Don 'Chopper' Krogstad, Darin Ulness and Julie Rutherford. Thank you. Dr. Victor Barocas for encouraging us to do lab research when I took your Biomechanics class. A very special thank you to Dr. David Odde, one of the many fathers that have made this possible. You gave me a shot and took me in. If you did not hire me to work in your lab, I had no idea where my next meal would come from. When I did not get accepted into grad school the first time, you encouraged me at the elevator on the top floor of Nils Hasselmo. You paid for me to go to conferences and present work and you introduced me to every person you knew. I literally would not have a PhD without you. I will be forever grateful to you and to all the Odde lab members who took me in and taught me science and made pursuing science an attractive endeavor: Clarence, Erkan, Dominique, Brian, Ben B., Becky, Emily, Jordan, Allison, Ben F.

To the MCB program coordinators and directors and to my MCB class, thank you very much. I honestly think we had the best class. Thanks for the encouragement. Thanks for listening. Thanks for sharing your challenges and successes. Thanks for being a part of my life outside of science. Thank you to my committee members Linda Wordeman, Sue Biggins and Fred Rieke

and Akiko Shimamura for all the help and support throughout this journey. You were always available and made room for my unconventional ways. A special thanks to Sue Biggins who has been, practically, a co-mentor to me and opened her lab for me to use.

To my advisor, Chip Asbury. You have been more than a mentor to me. You have been a father to me. Thanks for teaching me how to be a scientist. Thanks for sitting bench-side with me, teaching me one-on-one how to do experiments. Thanks for all the ideas and your constant scientific optimism. No matter how poorly I thought an experiment went, you managed to find the single strand of positivity there was to find in it. Your passion and dedication to science and to your work is the kind I hope to emulate. Thanks for having an open door for all things, even outside of science. You have encouraged me through the worst and the best. I am very grateful that you took a chance on me. Thanks to Asbury Lab members past and present, especially Hugo who introduced me to all things TIRF and kinetochores, and Yi who played an integral role in pushing this study to where it is now. Thanks to Krishna, Powers, Franck, Driver, Yusko, Megan, Aida and the undergrads. Thanks to all members of the Seattle Mitosis Club, especially members of the Biggins Lab: Guppy and Matt, you were teachers and an encouragement. Thank you, Lori, for fighting the Mps1 battle with me. Thanks to Nicole, Steven, Laura and Aimee for your help with kinetochores.

Finally, to my wife, Ifeanyi, bone of my bone and flesh of my flesh. Words cannot express what you mean to me. We have been through a lot over the years. You have been there at my worst. You have been first to celebrate the good news and first to pray and encourage me out of the bad. Thank you for constantly reminding me that I belong. There are better days ahead: ‘small small’.

I am who I am, and I am where I am because of undeserved grace and favor. To God be the Glory!

DEDICATION

To my parents, 'Papa JT' and 'Auntie Salo'. I have never needed any other role models.

Chapter 1. INTRODUCTION TO MITOSIS

1.1 CELL DIVISION

"When a cell arises, there must be a previous cell…"

This statement made by Rudolf Virchow in 1858 was the first to point to the cell cycle in living organisms comprising repeated cycles of duplication and division. Eukaryotic cell division is a short but exquisite process essential for the faithful inheritance of genetic material. The process of mitosis is divided into different phases (Fig. 1.1). During prophase, which occupies about half the length of mitosis, the cell's nuclear membrane breaks down, and the nucleolus disintegrates. The centrosome or spindle pole, which acts as the microtubule organizing center of the cell duplicates, and the spindle poles migrate to opposite ends of the dividing cell. The chromosomes then condense into sister chromatids, which are linked together at the centromere. The mitotic spindle begins to form as microtubules, emanating from the spindle poles, form attachments to the sister chromatids via kinetochores. As the spindle forms, microtubules begin to form attachments to kinetochores, and drive the sister chromatids to the mid-region (metaphase plate) of the dividing cell. The kinetochore, a multiprotein complex, mediates the interaction between the chromosomes and the microtubules. At metaphase, the sister chromatids align at the metaphase plate. It is essential during metaphase to have all the kinetochores stably attached to microtubules from opposite spindle poles, which pull the sister chromatids apart during anaphase. Chromosome segregation is an extremely accurate process. It is estimated that budding yeast cells lose or gain a particular chromosome once in 100,000 divisions (1). This accuracy is a result of several checkpoints employed by the cell during the cell cycle. The spindle assembly checkpoint acts as a surveillance mechanism that emits a diffusible 'wait' signal and arrests cells with unattached or

improperly attached kinetochores during metaphase. During this metaphase arrest, error correction mechanisms destabilize improper kinetochore-microtubule attachments allowing proper attachments to be formed and stabilized. Once proper stable attachments are formed, the 'wait' signal is silenced and the cell proceeds to anaphase. Shrinking microtubules pull the sister chromatids apart, separating them towards the spindle poles during anaphase. In telophase, many of the processes that happen during prophase are reversed and cytokinesis results in the formation of a constriction at the metaphase plate and splitting of the cell into daughter cells.

1.2 THE KINETOCHORE

The kinetochore is central and critical to cell division, and is assembled on the centromere during cell division. The centromere is the distinct region of chromosomal DNA that powers chromosome movement and regulation during cell division (2). In budding yeast, the most well-studied model organism, approximately 125 base pairs of centromeric DNA specifies the kinetochore, unlike in other eukaryotic organisms where the centromere can span several megabases (3). Approximately, more than 100 kinetochore proteins, each present in multiple copies, have been identified to assemble on the centromere to form the kinetochore complex (4). The kinetochore structure, which is evolutionarily conserved, can be separated into the inner kinetochore, an intermediate region and the outer kinetochore. The inner kinetochore interacts with centromeric DNA. The outer kinetochore forms load-bearing attachments to microtubules and the intermediate region contains proteins which link the inner to the outer kinetochore (Fig. 1.2). The budding yeast kinetochore consists of the core CBF3 complex, which was the first identified kinetochore sub-complex. The CBF3 complex together with the constitutive centromere associated network (CCAN) and Cbf1 protein form the inner kinetochore. The CCAN consists of several sub-complexes including the Ctf19-Okp1-Mcm21-Ame1 (COMA) sub-complex, Mif2 and Cse4. The chromosomal passenger

complex (CPC), comprising Ipl1, Sli15, Nbl1 and Bir1, also forms part of the inner kinetochore but is not considered a core component of the kinetochore. The outer kinetochore components consisting of the Ndc80, Dam1 and Spc105 sub-complexes are connected to the inner kinetochore via the intermediate Mis12 complex (5–7). All of these identified kinetochore components have been shown to exist in multiple copies per kinetochore (8, 9).

The kinetochore also possesses motor proteins, components of the spindle assembly checkpoint, and other microtubule-associated proteins (MAPS). These proteins are transient and, mostly, perform regulatory functions. The regulatory motor proteins include Kip1, Kip3, Cin8 and Kar3. The spindle assembly checkpoint proteins are recruited to the kinetochore and delay mitotic progress to allow the formation of stable microtubule attachments. Components of the checkpoint include Mad1, Mad2, Bub1, Bub3 and Mps1 (7, 10).

1.3 THE MICROTUBULE

The microtubule is a component of the cytoskeleton in cells and functions primarily to provide mechanical support for cell shape and to also aid in the transportation of cellular material to and from different cellular compartments. Microtubules are assembled from α and β tubulin dimers. The tubulin dimers usually polymerize to form 13 linear protofilaments, which assemble into a 25-nm cylindrical structure with a hollow core. Microtubules play a major role in mitosis by helping to form the spindle apparatus, which maintains the shape of the cell. Their stable attachments to kinetochores and ability to pull apart sister chromatids is also a requirement for faithful chromosome segregation.

During interphase, microtubules disassemble, which allows tubulin subunits to reassemble into the mitotic spindle. The centrosome, which is the microtubule organizing center of the cell duplicates and localize to form spindle poles at the opposing ends of the mitotic spindle. Polar

microtubules generally grow from the centrosome with the minus end of the microtubule anchored at the centrosome and the plus end undergoing dynamic instability (11). Dynamic instability refers to the ability of microtubules to switch between assembly and disassembly via guanosine triphosphate (GTP) hydrolysis during their lifetime. Dynamic instability is very essential in mitosis as it allows rapid reorganization of the spindle when necessary. Furthermore, dynamic instability helps to generate the force required to push and pull on chromosomes during mitosis (12).

Early in prometaphase, microtubules undergo a period of 'search and capture' via dynamic instability until they form proper attachment to kinetochores (13). The kinetochore forms different types of attachments to microtubules: In a monotelic attachment only one sister kinetochore attaches a microtubule. In a syntelic attachment, both sister kinetochores attach to microtubules from a single spindle pole. A merotelic attachment results from one or both kinetochores forming attachments to microtubules from both spindle poles. In an amphitelic attachment, each kinetochore is attached to microtubules from only one spindle pole, usually resulting in biorientation (14). Unstable monotelic and syntelic kinetochore-microtubule attachments are detected by the spindle assembly checkpoint mechanism (Fig. 1.3). This mechanism arrests the cell, and allows time for error correction mechanisms to destabilize these attachments for proper stable amphitelic attachments to be formed. Ipl1 kinase has been shown to destabilize improper attachments via phosphorylation of its kinetochore component substrates (15, 16). Merotelic attachments are not found in budding yeast cells since each kinetochore attaches to only a single microtubule (17). Proper error correction and spindle assembly checkpoint function is necessary to preserve the fidelity of cell division.

1.4 THE SPINDLE ASSEMBLY CHECKPOINT

The first spindle assembly checkpoint components, Budding Uninhibited by Benzimidazole (Bub1, Bub3) and Mitotic Arrest Deficient (Mad1, Mad2, Mad3), were initially discovered via genetic screens in budding yeast (18, 19). The Monopolar Spindle 1 (Mps1) component was initially discovered as a gene important for spindle pole body duplication (20, 21) and was found later to also play a major role in checkpoint signaling (22). Although these highly conserved proteins are known to be recruited to form a signaling pathway that results in the arrest of cells in mitosis when there are improper or unattached kinetochores, the question of exactly what they respond to continues to be debated. One theory proposes that the kinetochore senses tension between itself and the microtubule. Early experiments supporting this theory involved using a micromanipulator to pull on an unattached chromosome. Applying tension in this manner was shown to result in progress to anaphase (23). In a second theory, the checkpoint is believed to respond to kinetochore-microtubule attachment alone in the absence of any tension. Similarly, in a separate experiment in support of this second theory, the last unattached kinetochore in a monotelic PtK1 cell was destroyed using laser ablation. The cell proceeded to anaphase with, presumably, no tension in the mono-oriented chrosome (24). The attachment versus tension debate continues due to several reasons. Laser ablation of the kinetochore does not necessarily completely eliminate kinetochore-microtubule tension, and in the case of the micromanipulation experiment, tension has been shown to increase microtubule occupancy of kinetochores in eukaryotic cells, possibly, through stabilization of the microtubule attachments (25). All in all, these experiments suffer from an inability to clearly distinguish tension from attachment, since the two phenomena are interdependent. The continuing debate will benefit greatly from single particle assays that can directly distinguish between the two.

In the current prevailing checkpoint signaling pathway model, lack of microtubule attachment and/or tension results in the recruitment of Mps1 kinase to the kinetochore (26–29). Mps1 phosphorylates its substrate, Spc105, which results in the recruitment and localization of the Bub1-Bub3 complex to the kinetochore (30–32). Mps1 also phosphorylates Bub1 resulting in the recruitment of Mad1 to the kinetochore (33).

Mad2 has been shown to exist in two conformations: the closed conformation, C-Mad2, can bind stably to Mad1. Free Mad2 exists in an open confirmation, O-Mad2, and cannot bind to itself but is transformed to C-Mad2 when it binds to another C-Mad2 (34–36). Thus, the Mad1/C-Mad2 recruited to the kinetochore through phosphorylation of Bub1 acts as a template to cycle Mad2 on and off the kinetochore. Mad2 is converted from the open to the closed conformation when it attaches to kinetochore bound C-Mad2 (37). The C-Mad2 also binds to Cdc20 (35, 38).

Cdc20 is a direct activator of the anaphase-promoting complex or cyclosome (APC/C), which is an E3 ubiquitin ligase that regulates the metaphase to anaphase transition of a dividing cell. Cdc20 forms part of the mitotic checkpoint complex (MCC), which also consists of C-Mad2, Bub3 and Mad3. When the MCC binds to the APC/C it prevents it from targeting securin and cyclin B for degradation. Securin protects cohesin from being cleaved by separase, while cyclin B binds to Cyclin-dependent kinase 1 (Cdk1) to promote cell cycle progression. Thus, degradation of securin and cyclin B results in the cleavage of cohesin by separase, which acts as molecular scissors cleaving the cohesin complex that holds sister chromatids together and promotes their transition from metaphase to anaphase. In the prevailing ‘template’ model the spindle assembly checkpoint is activated due to improper kinetochore-microtubule attachment

when free O-Mad2 is converted to C-Mad2, which binds to Cdc20, and inhibits the ability of Cdc20 to bind to and activate APC/C resulting in mitotic arrest (Figs. 1.4 and 1.5) (37–39).

Given these discoveries, it has become important in recent years to fully understand the role of Mps1 in the spindle assembly checkpoint signaling pathway since it seems to be most upstream and its ability to phosphorylate its substrates is crucial to the checkpoint signaling cascade.

1.5 MONOPOLAR SPINDLE 1 (MPS1)

Mps1 was first discovered in budding yeast as a protein necessary for the assembly and duplication of the spindle pole body, and was later shown to be a kinase that demonstrated autophosphorylation (20, 21). In recent years, Mps1 has emerged as a critical factor in the establishment and maintenance of the checkpoint signal, and has also been shown necessary for the silencing of the 'wait' signal (22, 40–42). Studies position Mps1 most upstream of the spindle assembly checkpoint signaling cascade, and it localizes to the calponin homology (CH) domain of the Hec1 component of the Ndc80 sub-complex (29, 43, 44). CH domains are actin-binding regions mostly found in cytoskeletal proteins and have also been shown, more recently, to be involved in microtubule binding (45, 46).

Mps1 kinase phosphorylates threonine residues in the methionine-glutamate-leucine-threonine (MELT) motifs of Spc105. This phosphorylation regulates the recruitment of Bub1 and Bub3 to the kinetochore (30, 32, 47). Furthermore, Mps1 also phosphorylates the middle region of Bub1 resulting in the recruitment of Mad1 to the kinetochore (33, 48, 49). It is this recruitment of Mad1 coupled with C-Mad2 that acts in the manner of a prion-like template, converting O-Mad2 to C-Mad2 for Cdc20 binding and subsequent mitotic checkpoint complex formation. Understanding the role of Mps1 is critical to understanding checkpoint silencing.

Two models have been proposed to explain the role of Mps1 in checkpoint silencing as microtubules form attachments to kinetochores. The direct competition model argues that microtubule attachment directly competes with Mps1 for binding to the kinetochore, and thereby prevents Mps1 from phosphorylating its substrates (50, 51). The mechanical switch model, on the other hand, argues that end-on microtubule binding to kinetochores doesn't necessarily compete with Mps1 for kinetochore binding but renders it inactive, in an 'off' state, and prevents it from being able to phosphorylate its substrates. Experiments supporting the models have several limitations including the use of recombinant protein fragments. Also, bulk assays used in the experiments do not address heterogeneity in individual kinetochores nor differentiate between different types of kinetochore-microtubule attachments. To overcome these challenges, I utilized native yeast kinetochores instead of protein fragments. Using single molecule biophysical techniques also enabled me to assess single kinetochore particles, and how lateral, end-attached and tip tracking of the single kinetochores affect Mps1 association. Specifically, I leveraged a recently developed method of isolating intact native single kinetochores (52) and Total Internal Reflection Fluorescence (TIRF) microscopy to provide more direct evidence as to how Mps1 responds to different modes of microtubule attachment.

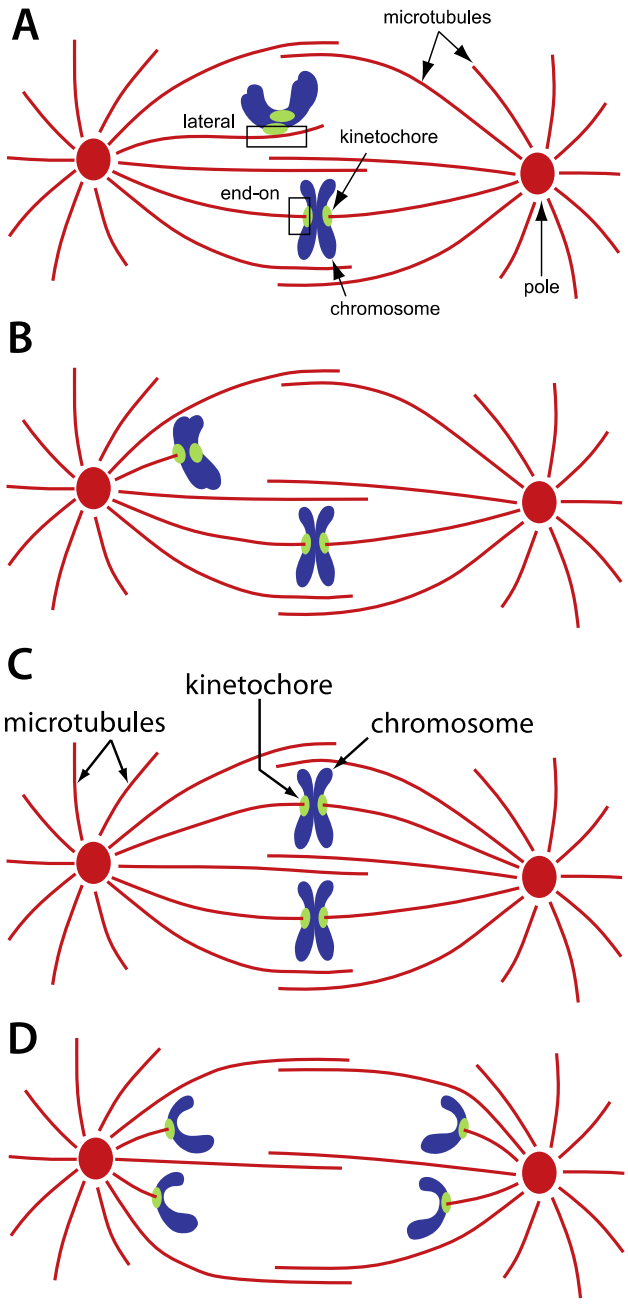

Figure 1.1: Mitosis occurs in several distinct stages. (A) Microtubules begin to grow and form attachments to kinetochores. The microtubules (red) emanating from the spindle pole body (red dot) form initial lateral attachments to the kinetochore (green). The lateral attachments are converted to end-on attachments (B &C) as the cell progresses to metaphase. In metaphase, the chromosomes are aligned in the middle (metaphase plate) of the dividing cell. (D) Stable attachments result in sister chromatid separation as the microtubules disassemble to opposite poles.

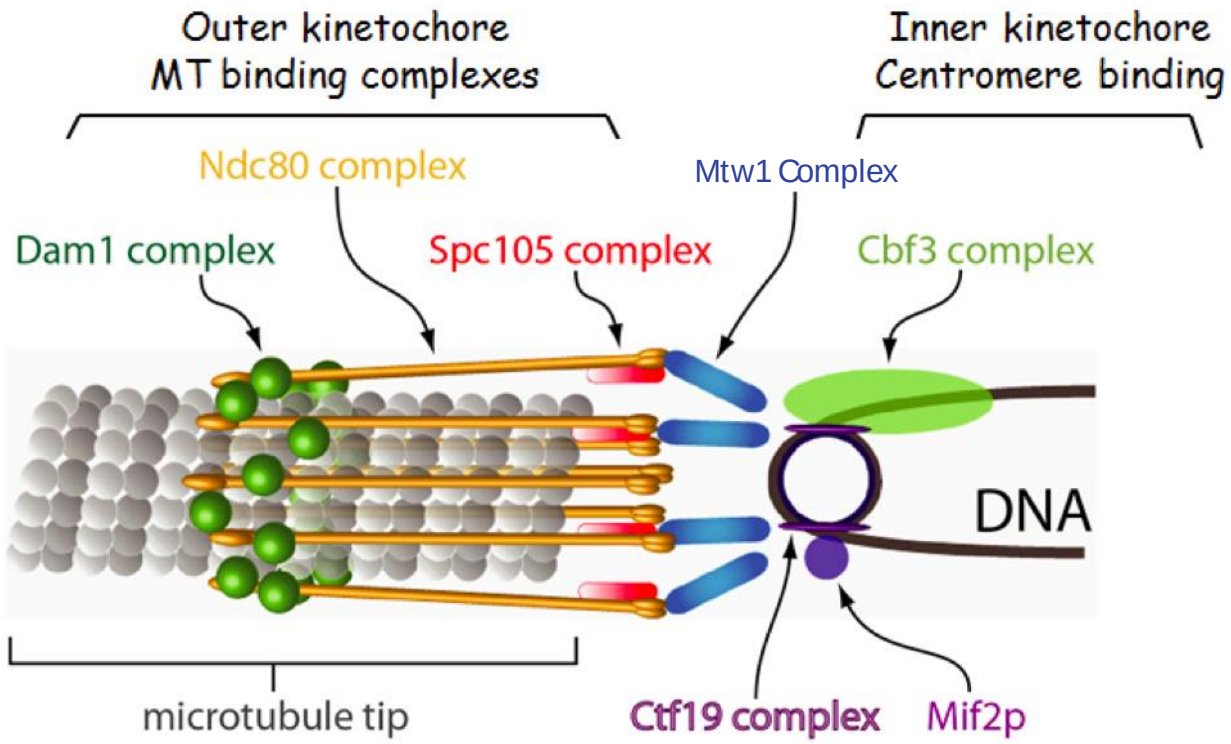

Figure 1.2: Schematic showing kinetochore components. The kinetochore complex can be subdivided into the inner kinetochore, which binds to centromeric DNA and the outer kinetochore, which binds to the microtubule. An intermediate region comprising proteins such as the Mtw1 complex holds the inner and outer components of the kinetochore together.

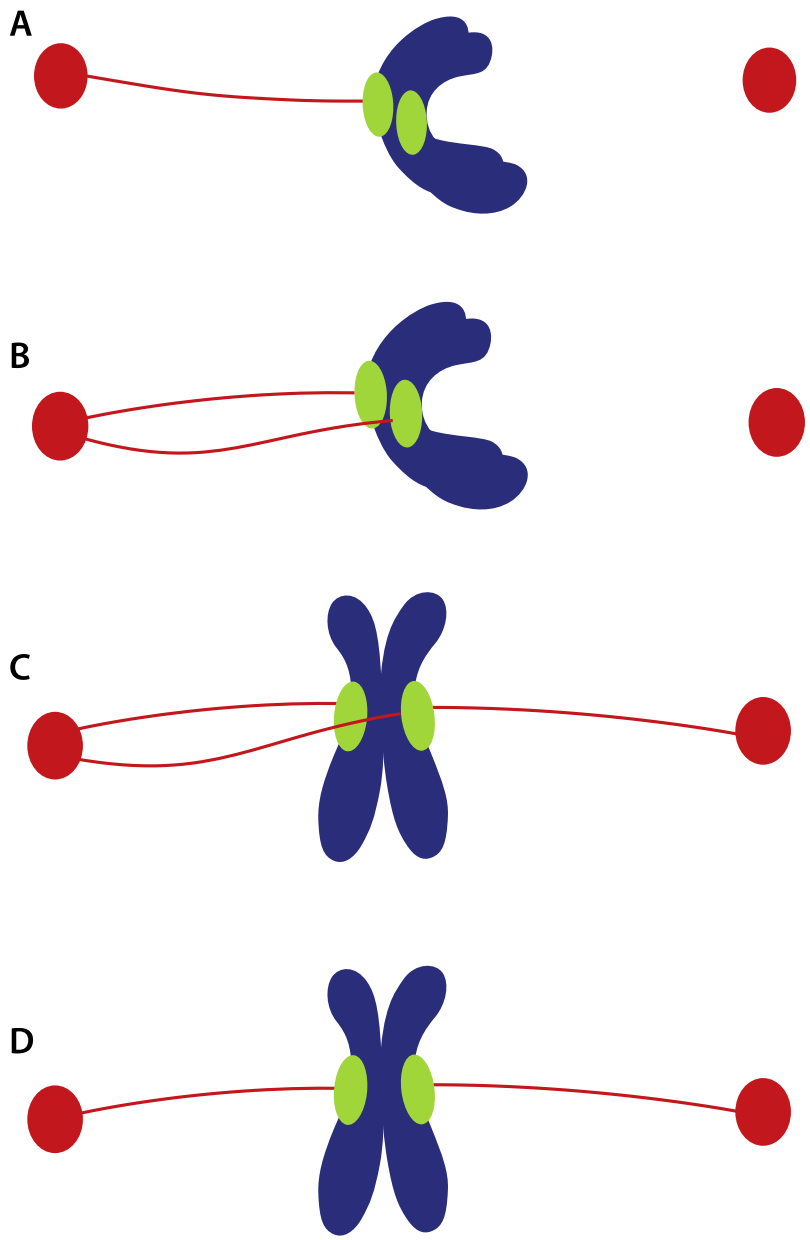

Figure 1.3: Microtubules and kinetochores can form different attachments during mitosis that may lead to errors. (A) In a monotelic attachment, only one of the sister chromatids is stably attached to a microtubule. (B) In a syntelic attachment, both chromatids are attached to microtubules from the same pole. This usually results in both chromosomes being pulled towards the same pole during anaphase, if uncorrected. (C) Merotelic attachments result from one of the sister chromatids being attached to microtubules from both poles. This, however, does not occur in budding yeast cells, where each kinetochore attaches to only a single microtubule. (D) Amphitelic attachments result from microtubules attaching sister chromatids to opposite poles.

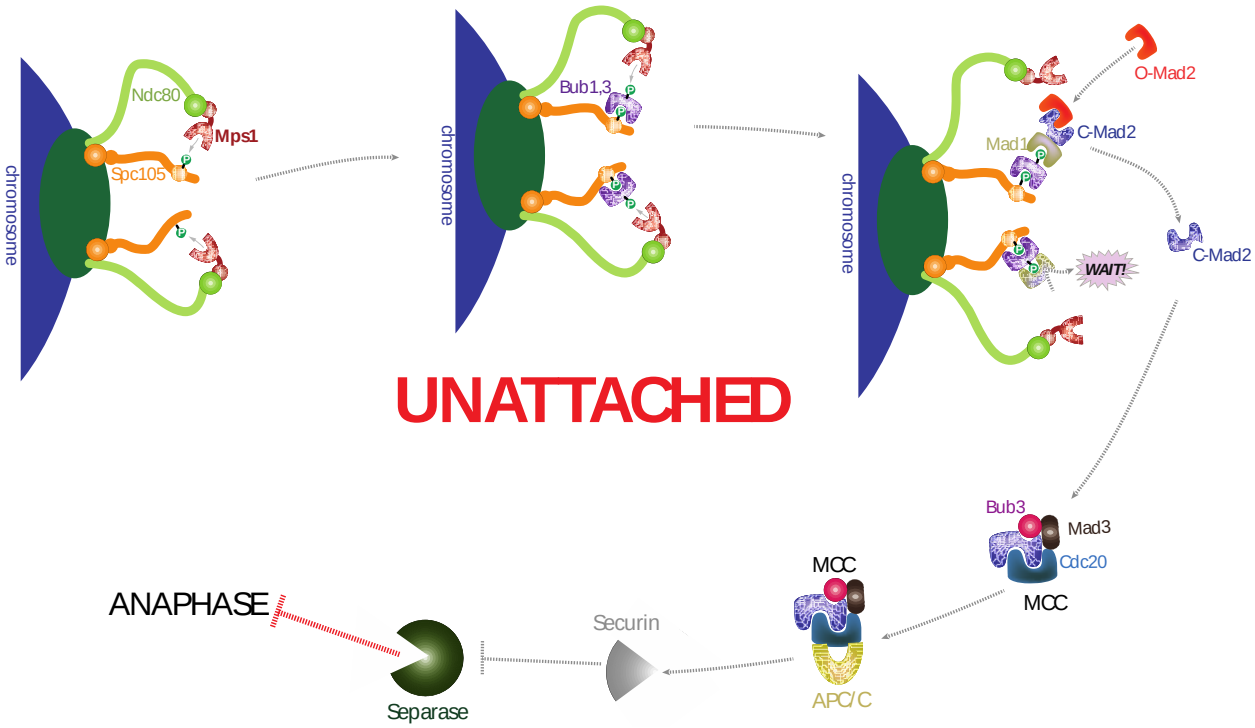

Figure 1.4: The spindle assembly checkpoint signaling cascade in a cell with an unattached kinetochore. In an unattached kinetochore, Mps1 phosphorylates Spc105, which results in Bub1-Bub3 recruitment. Mps1 also phosphorylates Bub1, which results in Mad1-Mad2 recruitment. The Mad2 recruited is in the closed conformation (C-Mad2). This C-Mad2 acts as a template converting O-Mad2 to C-Mad2. The C-Mad2 then binds to Cdc20 to form the mitotic checkpoint complex with Bub3 and Mad3. The MCC prevents the activation of the APC/C. The APC/C is, thus, enable to degrade securin and cyclin B, which act to protect the cohesin holding together sister chromatids from being cleaved by separase.

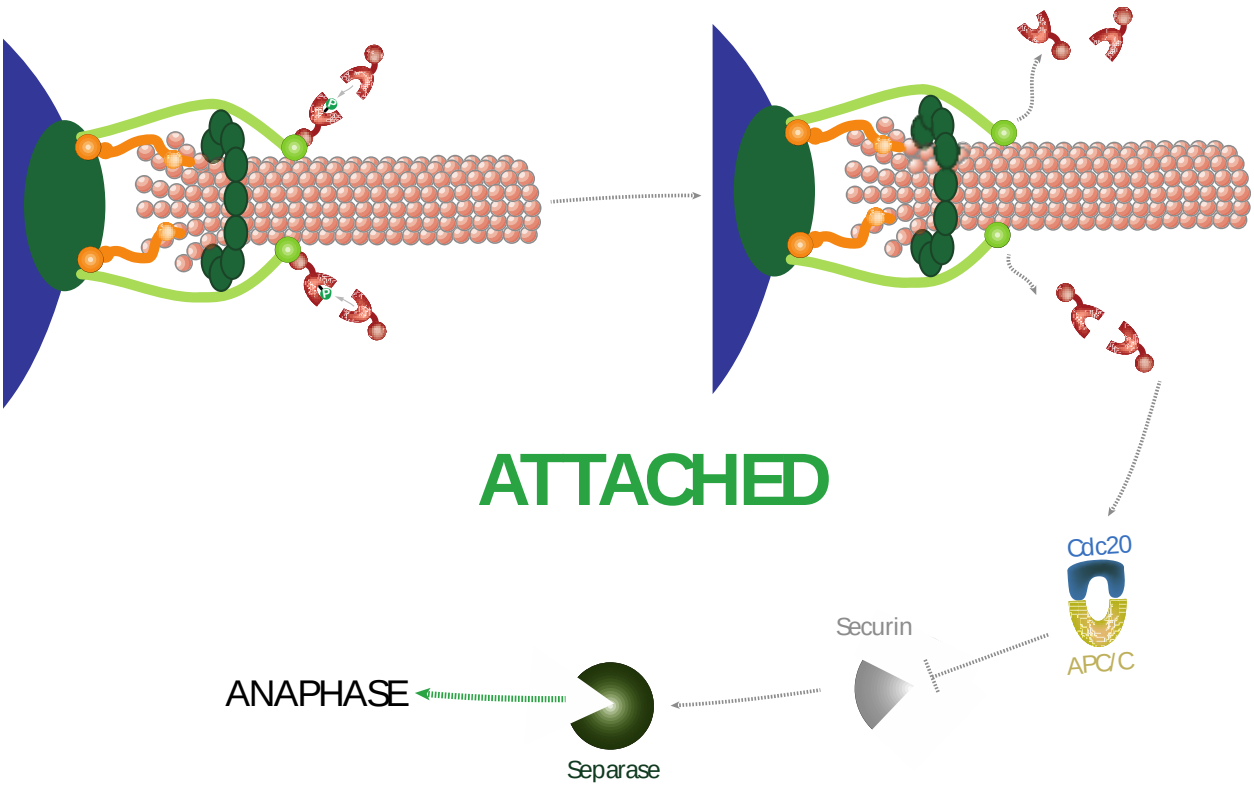

Figure 1.5: The spindle assembly checkpoint signaling cascade in a cell with properly attached kinetochores. When microtubules stable bioriented attachments with kinetochores, Mps1 is unable to phosphorylate Spc105. This inability to phosphorylate Spc105 results in the silencing of the checkpoint as Cdc20 can bind APC/C. APC/C is activated and targets securin and cyclin B for degradation. With securin degraded, separase can cleave cohesin to achieve progress to anaphase.

Chapter 2. INTRODUCTION TO SINGLE MOLECULE BIOPHYSICS

Conventional ensemble experimental techniques have been, and continue to be, used to provide insight into complex biological and chemical reactions. These techniques, however, generally provide wholesale averaged-out information about molecular properties of interest. Advances in single molecule techniques have increased further understanding of biological and chemical phenomena, allowing properties to be examined one molecule at a time.

Unlike in ensemble experiments, single molecule techniques allow the measurement of single molecular properties. With single molecule techniques, distributions can be directly measured and heterogeneity in samples can be directly observed. Sometimes systems being studied may possess multiple states, which may go undetected in ensemble experiments. Single molecule experiments also allow the binding and unbinding rates of molecules to be directly measured. Furthermore, events that happen simultaneously and are very challenging to distinguish in ensemble experiments may also be easily studied using single molecule techniques. Molecular forces as well as the response of molecules and systems to mechanical manipulation can be measured in single molecule studies. Finally, single molecule experiments provide much higher sensitivity than ensemble experiments. This is especially useful in experiments where sample concentrations are lower than normal. Molecules that are present at low concentrations *in vivo* can be studied more easily at similar concentrations in single molecule studies *in vitro* (53).

Multiple single molecule techniques have been invented over four decades, which provide complementary, and sometimes, corroboratory information about important complex biological and chemical phenomena.

2.1 Methods and Applications of Single Molecule Techniques

One of the pioneering studies in single molecule biophysics was done by Hirschfield, where he was able to detect, using an optical microscope, a single fluorescent antibody molecule (54). Around the same period, discrete changes in current were recorded from single ionic channels from the membrane of denervated frog muscle via patch clamping (55). Since then, several single molecule techniques have been developed and continue to be advanced including, but not limited to, magnetic tweezers, optical tweezers and atomic force microscopy (AFM). These techniques allow molecules to be manipulated and molecular forces to be measured. Other techniques such as TIRF, confocal microscopy and Förster Resonance Energy Transfer (FRET) allow properties such as particle intensity, lifetimes and movement to be measured and tracked. Each of these methods brings with it unique characteristics that allows it to be used for studying very different systems and answering myriad scientific questions.

Magnetic tweezers utilize magnetic fields to manipulate and characterize single molecules. Magnetic tweezers not only provide the means to apply forces in a linear fashion to single molecules, but also provide the advantage of applying torque to individual single molecules (56–58). This has been especially useful in the study of DNA structure and function as well as proteins related to DNA (59). Magnetic tweezers can also be useful in studying mitosis since they can be used to generate force. In a recent experiment, magnetic tweezers were used to determine the force required to maintain the spindle in the middle of intact nematode cells (60).

Optical tweezers were first introduced through seminal work by Arthur Ashkin and colleagues, when they observed the optical trapping of dielectric particles in water using a single-beam gradient force trap (61). The technique was further improved to trap and cool neutral atoms, which eventually led to Steven Chu being awarded the 1997 Nobel Prize in Physics. Further

provements in optics and microscopy have led to the implementation of optical tweezers in answering complex biological, chemical and biophysical questions ranging from characterizing molecular motors to determining the force required to stabilize a kinetochore-microtubule attachment (52, 62). When a highly focused laser beam is directed at a nano or micron-sized dielectric particle, the particle experiences light-scattering and gradient forces as it encounters the laser. The scattering forces exert in the direction of light propagation, while the gradient forces pull along the spatial gradient of the intensity of the light. When the gradient forces exceed the scattering forces, the dielectric particle is attracted to the highest intensity region of the focused beam, causing it to be trapped in this position. Subsequently, by changing the position of the laser beam, the dielectric particle can be manipulated. In modern single molecule experiments, the dielectric particles act as handles to which molecules of interest can be attached (63–65). When coupled with a piezo, stage nanometer precision manipulation can be achieved.

The Atomic Force Microscope (AFM) is a type of scanning probe microscope with very high resolution on the order of up to fractions of a nanometer. Since its invention in 1986 by Binnig and colleagues, the AFM has become a mainstay in studying molecular structure and processes at the single particle level (66). The main components of an AFM, generally, include a piezoelectric stage, a cantilever with a narrow tip, and a detector. By pushing the cantilever into a sample of interest, the height of the sample can be measured. The force between the cantilever tip and the sample can also be measured by pulling the cantilever up. The pushing and pulling of the cantilever can be detected through various means including optical deflection using a photo-detector, current measurement and other methods (67). Recent developments in instrumentation as well as image acquisition and sample preparation have propelled the used of AFM in studying mitosis. AFM has

been, especially, useful in determining the surface tension and internal pressure generated by round dividing cells (68, 69).

Single molecule fluorescence methods aim to eliminate noise from the focal plane, and confocal microscopy is one of the methods that enables this to be achieved. Singe molecule confocal microscopy is performed either through a continuous wave or a pulsed laser. Confocal microscopy has been used extensively in single molecule studies to study cell biological phenomena (70). Other single molecule fluorescence methods used include FRET and TIRF, which have been used extensively in single molecule biological experiments. FRET allows molecular distance measurement. The transfer of energy from a molecule with a fluorescent donor attached to a specific site to a second molecule with a fluorescent acceptor can be measured using FRET (71). I used TIRF microscopy in my assays due to its outstanding signal-to-noise ratio, which proved to be very important in single particle counting. The technique is further described below.

2.2 TOTAL INTERNAL REFLECTION FLUORESCENCE (TIRF) MICROSCOPY

TIRF microscopy is very useful for limiting the excitation and detection of fluorophores to a thin section. It allows selective visualization of particles within a region of approximately 200 nm within the specimen. Restricting the depth in which fluorophores can be excited in a specimen results in high signal-to-noise ratio and high contrast. Essentially, sources of illumination outside of this region, including those from the buffer and other particles, is eliminated. Furthermore, photobleaching and photodamage of fluorescently particles that are out of the focal plane are greatly reduced.

When a laser encounters an interface with two different refractive indices, some of the light is partially reflected and partially refracted through the interface. At a critical angle, the refracted

light travels parallel along the plane of the interface. When the light travels from a material with high refractive index to a material with low refractive index (such as from glass to water) at an angle slightly past the critical angle, it undergoes total internal reflection. The basis for TIRF microscopy rests on the fact that at this boundary, an evanescent wave is generated that penetrates the low refractive index material up to about a thickness of 200 nm. This evanescent wave can be used to selectively excite fluorophores that are very close to this boundary while simultaneously avoiding any background noise from outside this slice (Fig. 2.1). The evanescent wave is an electromagnetic field that decays exponentially with perpendicular distance from the interface. This allows it to reach the small depth that is necessary to excite fluorophores close to the interface (72).

TIRF provides researchers the ability to directly observe biochemical events, including interactions between molecules and kinetic rates. Unlike ensemble biochemical experiments that provide average properties of molecules and tend to require larger samples, TIRF has provided a way to study the stoichiometry of cellular molecules and proteins with minute amounts (73–75). Other cell biological questions that have benefited greatly from TIRF include molecular assembly and disassembly, cargo transport, and molecular movements in cells. The technique has allowed direct observation of these events in real time (76–78).

One of the questions that remains debated in the field of mitosis, and more specifically the spindle assembly checkpoint, is whether it responds to attachment or tension between kinetochores and microtubules. This is because in ensemble experiments and in *in vivo* cell biological studies it is virtually impossible to separate tension from attachment. However, native yeast kinetochore isolation in recent years has opened the field to allow this question to be answered using single molecule techniques (52). My goal is to isolate these native kinetochores and build assays that

allow these fundamental questions about the kinetochore and checkpoint proteins to be explored. Combining TIRF and isolated kinetochores allows specific kinetochore proteins to be tagged and studied through direct observation and manipulation.

2.2.1 *Fluorescent Probes for TIRF Microscopy*

One of the most important factors to consider when planning single molecule fluorescence studies is the type of fluorescent probe to use. Fluorescent probes allow the structure and dynamics of a molecular target to be explored. when the target molecule is tagged with the fluorescent probe. Fluorescent proteins such as GFP and mCherry are commonly used in labeling molecular targets for biochemical assays, and although they have properties that make attachment to any target protein easy, poor photophysical properties such as poor photon output and photoblinking, and slightly larger size make them not the most ideal for single molecule studies (79). Fluorescent dyes, which are small, bright and photostable organic molecules are often used in TIRF microscopy. They usually rely on thiol groups of single cysteines or reactive moieties of unnatural amino acids for incorporation into a target molecule, and include those from the 'Cy' and 'Alexa' family (80). In our study of the spindle assembly checkpoint in budding yeast, we tagged kinetochore protein targets with SNAP- and CLIP-tags, which allowed the incorporation of organic Alexa Fluor dyes.

2.2.2 *Use of SNAP- and CLIP-Tags for TIRF Microscopy*

We began our spindle assembly checkpoint studies with GFP and mCherry, but eventually switched to organic dyes due to low photon count and difficulty in clearly distinguishing signal from background noise. To incorporate these organic fluorescent probes,

we used SNAP- and CLIP-tags, which allow covalent attachment of the probes to the kinetochore proteins.

The SNAP-tag is a modified form of the DNA repair enzyme, human O^6-alkylguanine-DNA-alkyltransferase (AGT). The ~20-kDa SNAP-tag undergoes a self-labeling reaction with O^6-benzylguanine derivatives to form a covalent bond (81). The SNAP-tag can, therefore, be fused to any protein target of interest and, subsequently, labeled with a specific organic dye via covalent interaction.

The ~20-kDa CLIP-tag was engineered from the SNAP-tag to react specifically with O^2-benzylcytosine derivatives in a similar covalent reaction (82). These two tags allow simultaneous labeling of proteins with two different probes due to orthogonal and complementary substrate specificities (Fig. 2.2). In our assays, we used a polymerase chain reaction (PCR) technique to integrate the CLIP- and SNAP-tags into the endogenous loci of the Mtw1 protein and a checkpoint protein, respectively. CLIP-Surface Alexa Fluor 647 and SNAP-Surface Alexa Fluor 549 dyes were then added to label the CLIP- and SNAP-tagged proteins in solution, respectively. The fluorophores were very distinguishable from background noise when compared to GFP- and mCherry-labeled proteins (Fig. 2.3).

2.2.3 *Surface Preparation and Particle Immobilization for TIRF Microscopy*

Immobilizing particles onto a coverslip is paramount to single particle observation, and can be very time consuming. Coverslips used in TIRF microscopy must be thoroughly cleaned to eliminate impurities that tend to be auto-fluorescent. This is especially important if fluorophores with low photon count are being used because the impurities make it extremely hard to distinguish noise from actual signal. Once the coverslip is cleaned, the next step is to ensure that its surface is sufficiently passivated. This prevents non-specific adsorption of particles onto the glass surface.

Preventing non-specific adsorption helps to avoid protein malfunction or denaturing induced by the coverslip surface (83). Most organic fluorophores used in single molecule fluorescence assays tend to be hydrophobic and will readily adsorb to glass slide surfaces non-specifically. Surface passivation also helps to thoroughly remove any unbound dye that may be left over from the protein labeling reaction. To prevent this from happening, the coverslip surfaces are usually coated with a protective layer. Bovine serine albumin (BSA) is a common protective layer used for coverslip surfaces. When pre-adsorbed to a coverslip surface, it acts as a blocker, preventing non-specific binding of particles. Polyethylene glycol (PEG) is the most common surface blocking agent used in TIRF studies. One approach to generating a PEG protective layer involves, first, amino-silanizing the coverslip surface. This process results in the deposition of primary amines onto the coverslip surface which react to ester groups on the PEG (84–86).

A third approach which has gained popularity in recent years is phospholipid bilayer deposition. This procedure is easier to handle, and mimics a more natural environment for cellular particles (87). The bilayer is developed by resuspending dehydrated phospholipids in an aqueous solution. This is followed by sonication, which in the formation of small unilamellar vesicles. The phospholipids, when fed into a flow chamber, form a bilayer that coats the coverslip surface.

Most of these protective layers are usually doped with biotin, a small and stable protein, which does not interfere with any of the actual reactions of interest in the system. Biotin forms the strongest known non-covalent interaction with avidin, and this interaction is exploited for specific adsorption of particles in single molecule fluorescence assays (88, 89).

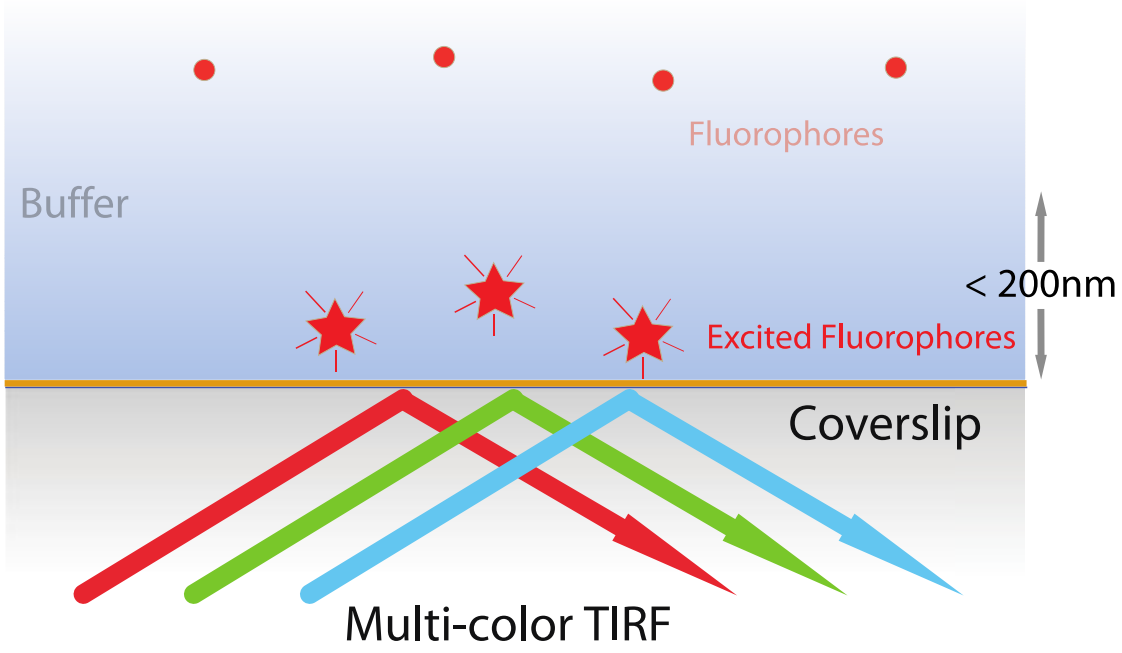

Figure 2.1: TIRF microscopy allows direct observation of fluorophores within a thin slice. When a laser beam reaches a coverslip-buffer boundary, it undergoes total internal reflection past a critical angle. An evanescent wave reaching depths of approximately 200 nm is generated, which TIRF microscopy relies upon to excite fluorophores that reside within this depth. Background fluorescence from the buffer and other particles are eliminated, resulting in high contrast and high signal-to-noise ratio.

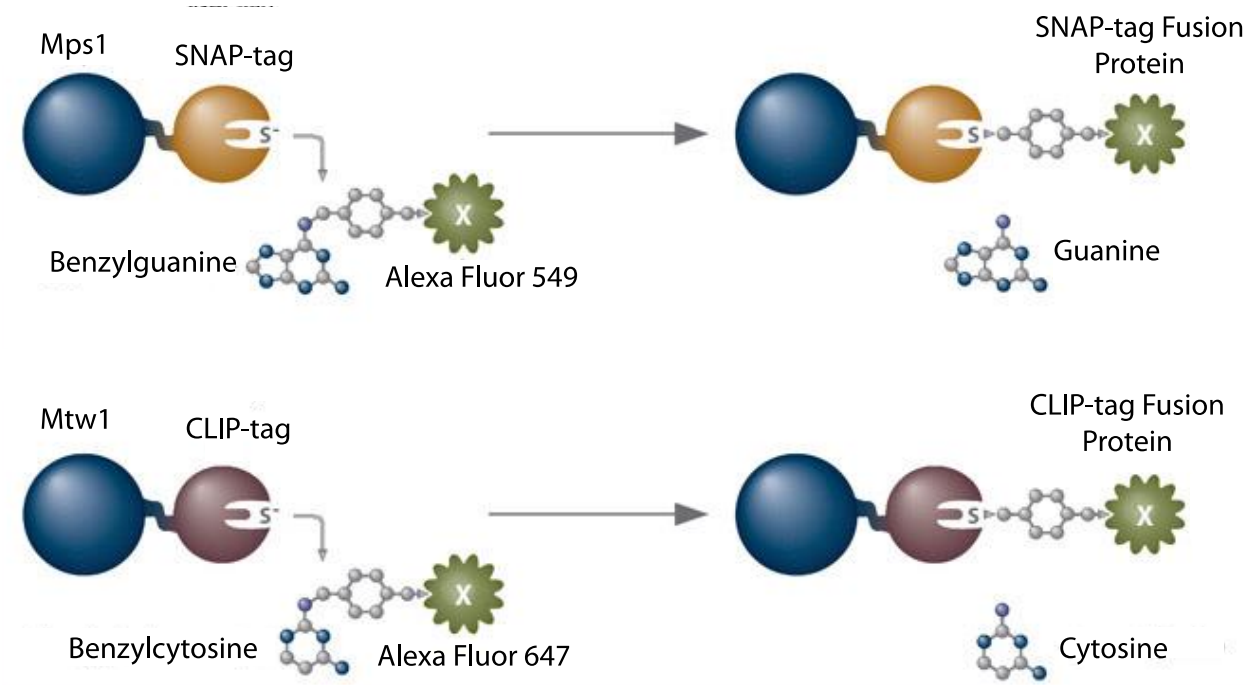

Figure 2.2: SNAP- and CLIP-tags allow covalent labeling of proteins with bright, photostable organic dyes. SNAP- and CLIP-tags are small proteins derived from a DNA repair enzyme that react with benzylguanine and benzylcytosine residues, respectively. They can be tagged to a protein of interest. Addition of Alexa Fluor dyes results in the covalent interaction between the residues. Since they bind to different residues, they offer the advantage of complementarity in labeling the same complex for TIRF observation.

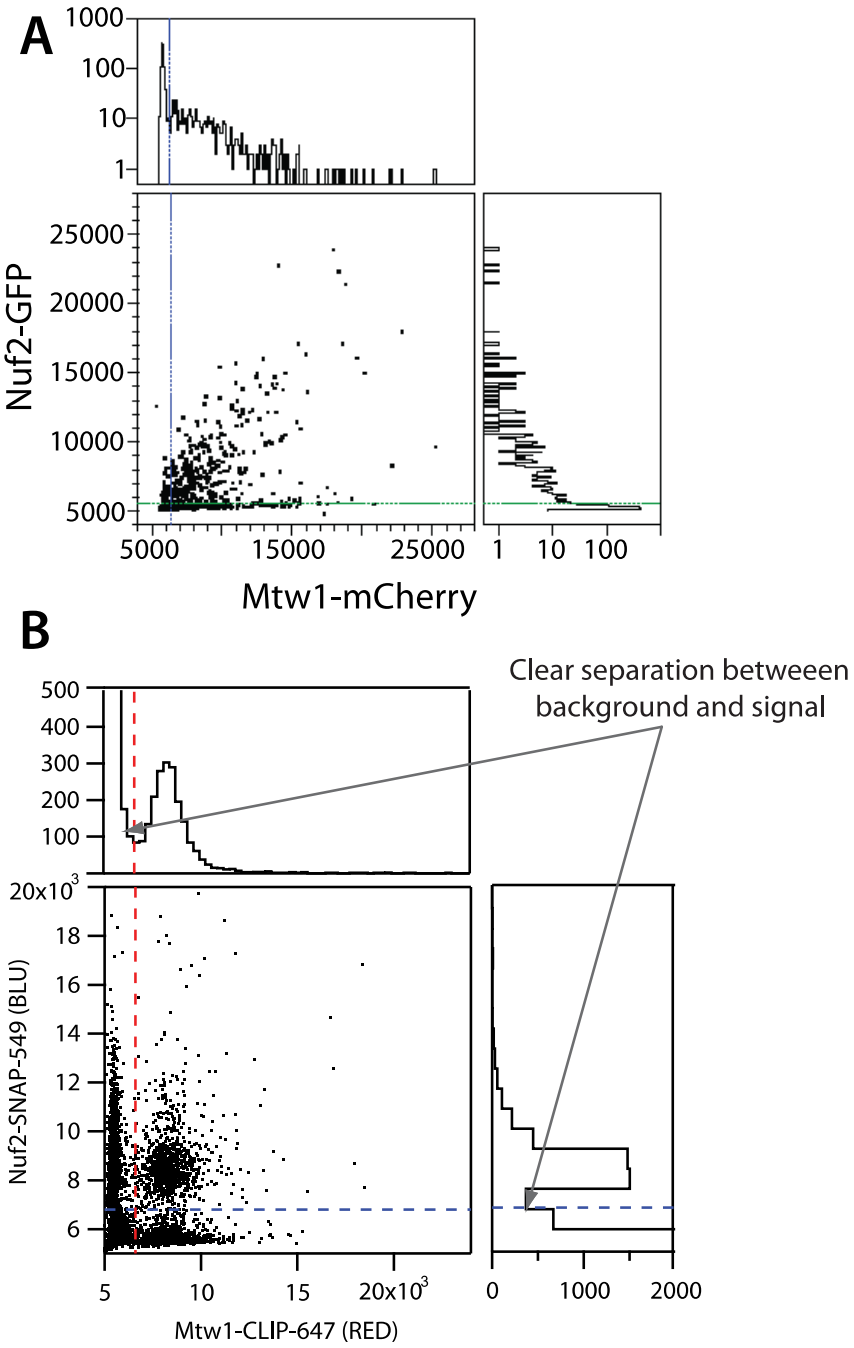

Figure 2.3: SNAP- and CLIP-tagged kinetochores produce bright and photostable particles that are clearly distinguishable from background noise. Images collected and analyzed showed that, compared to GFP and mCherry, the SNAP- and CLIP-tagged kinetochores exhibited bright spots that showed clear separation from background fluorescence.

Chapter 3. DEVELOPMENT OF IN VITRO ASSAYS TO STUDY THE SPINDLE ASSEMBLY CHECKPOINT

Our understanding of cell division has grown by leaps and bounds since the days of Walther Flemming (90). The various stages a cell goes through are well understood. The organization of the spindle apparatus and the role of microtubules and kinetochores in cell division have been identified, and continue to be explored (91). The various checkpoints employed by the cell during its cycle to ensure the fidelity of chromosome segregation have been well established. Knowledge about the spindle assembly checkpoint proteins that were first discovered in the 1950s have expanded to a point where its signaling pathway has been mapped out to the molecular level (39, 92). Advancements in instrumentation and molecular techniques have been greatly beneficial to understanding the spindle assembly checkpoint. How the checkpoint is silenced at the molecular level is advancing and needs more studies at the molecular level. One of the main advantages that single molecule TIRF brings to this field is its ability to isolate specific events in the checkpoint cascade and allow direct visualization.

My goal was to develop a combination of specific single molecule pull down (SiMPull) assays that will allow the interaction between kinetochores and microtubules to be probed at the level of single kinetochores (93). To do this, we first isolated functional native yeast kinetochores that were doubly tagged with SNAP- and CLIP-tags for observation in TIRF. I also developed assays for the kinetochores and microtubules to be specifically pulled down onto a coverslip. I then developed specific assays that included microtubule attachment under different conditions. Kinetochores can bind laterally to microtubules. They can also bind end-on, and tip-track with dynamic microtubules. I designed *in vitro* experiments to mimic all these physiological scenarios of kinetochore-microtubule binding. Finally, we developed a way to

properly analyze all the images and data that were collected from these assays. These are all highlighted below.

3.1 Isolation of Kinetochore Particles With Fluorescent Tags

Kinetochore particles were isolated via affinity-purifying the Dsn1-6His-3Flag protein, similar to previously described methods (52, 75, 94). We firs grew specific budding yeast cell strains at a 2 L volume overnight. Once an optical density (OD) of 2 was reached, the cells were centrifuged and then resuspended in buffer with protease inhibitors (65 mL H_2O, 130 µL phenylmethylsulfonyl fluoride (PMSF)) at a smaller volume. After a second round of centrifugation, the cells were again resuspended in lysis buffer (25 mM HEPES pH 8.0, 2mM $MgCl_2$, 0.1 mM EDTA, 0.5 mM EGTA, 0.1 % NP-40, 15 % glycerol, 150 mM KCl) with protease and phosphatase inhibitors. The cells were then frozen overnight, and lysed in a Freezer/Mill® (SPEX SamplePrep) while submerged in liquid nitrogen. The lysed cells were then ultracentrifuged at 98,500 g for 90 minutes at 4 ^oC to obtain cell lysates. Dynabeads that had been previously conjugated with α-Flag antibodies were then added to the extract and incubated for 3 hours, with constant rotation at 4 ^oC. After the immunoprecipitation, the Dynabeads were washed three times in buffer with 2 mM dithiothreitol (DTT), and then twice in BH buffer without the DTT. The Dynabeads were then suspended in buffer containing 30 µM SNAP-Surface® 549 and CLIP-Surface® 647 dyes (New England BioLabs) for 25 minutes at room temperature with gentle agitation. After the labeling incubation, the Dynabeads were again washed twice in buffer. Kinetochore proteins were then eluted from the Dynabeads by gentle agitation in an elution buffer (0.5 mg/mL 3Flag peptide in buffer) at room temperature for 30 minutes. Each sample preparation was run on an SDS-PAGE gel and imaged via typhoon scan

for analysis of fluorescent bands. The gels were also silver stained to observe components of the isolated kinetochores.

3.2 Dye Labeling of Kinetochores and Comparison Between Mitotic & Meiotic Kinetochores

SNAP- and CLIP-tags were used to label the isolated kinetochores. For the purposes of our experiments, the SNAP- and CLIP-tags were integrated into the endogenous loci of the checkpoint protein and core kinetochore protein, respectively. The SNAP- and CLIP-tags enable specific covalent binding of fluorophores of interest. For my specific case, SNAP-Surface 549 Alexa and CLIP-Surface 647 Alexa dyes were used for labeling the checkpoint protein and core kinetochore protein, respectively. To proceed with my experiments, I needed to ensure that the kinetochore proteins were efficiently and fully labeled with the dyes of interest. I performed two separate titration experiments using Mtw1-CLIP-647 and Nuf2-SNAP-549 kinetochores to determine the concentration of Alexa dyes that were required to saturate SNAP- and CLIP-tagged kinetochore molecules.

During the kinetochore purification for the titration experiment, I split the Dynabeads into 6 equal volumes after immunoprecipitation. SNAP-Surface 549 and CLIP-Surface 647 Alexa dyes were added to the Dynabeads at the following concentrations: 0 µM, 2 µM, 10 µM, 15 µM, 30 µM and 60 µM. I incubated the Dynabeads for 25 minutes at room temperature with gentle agitation. After the incubation period, I eluted the kinetochores and separated the kinetochore components on an SDS/PAGE gel. I scanned the gel for fluorescent signal on a typhoon scanner, and also silver stained the gel to identify the kinetochore components (95). I quantified the fluorescent typhoon scan by calculating the integrated pixel square density for each band. I found that for the SNAP-Surface 549 Alexa dye, SNAP-tagged molecule saturation

was reached at ~2 μM. On the other hand, saturation for the CLIP-Surface 647 Alexa dye was reached at ~30 μM. Saturation of SNAP- and CLIP-tagged kinetochore components is useful for answering several scientific questions, especially, when protein count is necessary (Fig. 3.1).

One such example of the importance of saturating tagged molecules with the organic dyes was evident in our efforts to determine if kinetochores in the first stage of meiosis had more microtubule binding elements than mitotic kinetochores. This was the first test-case where we successfully used quantitative fluorescence to estimate numbers of labeled molecules per kinetochore particle, and to compare these estimates across different experimental conditions.

Meiosis is an essential type of cell division in sexually reproducing organisms that generates sperm and eggs with haploid chromosomes. Two rounds of cell division, meiosis I and meiosis II, occur during the process of meiosis even though the DNA is replicated only once. The second cell division, meiosis II, is similar to mitosis. However, meiosis I is a distinct type of cell division, which results in homologous chromosome pairing and segregation (96, 97).

During meiosis I, sister chromatids co-migrate to the same spindle pole, as homologous chromosomes segregate. It has been proposed that meiosis I depends on fusion of sister kinetochores (98–101). If this hypothesis were true, then kinetochores purified from budding yeast cells undergoing meiosis I would possess more microtubule binding elements than mitotic kinetochores. If the microtubule binding elements are, thus, SNAP- and CLIP-tagged and saturated with dye, then the fluorescence levels could be compared to determine if the hypothesis were true. To confirm this hypothesis, we purified kinetochore particles doubly-labeled with SNAP-Surface Alexa 549 dye on Nuf2 and CLIP-Surface Alexa 647 dye on Mif2 (an inner kinetochore component) at the right dye concentrations required for tagged molecule saturation. The kinetochores were then visualized using TIRF microscopy. Using particles that exhibited

single-step photobleaching behavior as a baseline, we determined that kinetochore particles isolated from meiosis I cells contained more Nuf2 molecules than those from mitotic cells. We counted 6.5 ± 2.8 molecules for meiosis I Nuf2 molecules, and 3.8 ± 1.3 for mitotic Nuf2 molecules (95).

3.3 Slide Preparation for Single Molecule Fluorescence Assays

As mentioned earlier, slide cleaning and passivation are very essential to TIRF assays. All the experiments I performed were done in flow chambers made of a glass slide and a 24 mm x 40 mm glass coverslip, which were held together by double-sided tape. The double-sided tape strips used as spacers were separated by about 3 mm in width to create the flow chamber. At this width, I estimated that each flow chamber contained approximately 5 µL volume of fluid at any point in time (Fig. 3.2).

Prior to creating the flow chamber, the glass coverslips and slides needed to be thoroughly cleaned. I placed the coverslips on a glass rack and cleaned them in a benchtop plasma cleaner for 5 minutes. Rows of double-sided tape were then laid on the glass slide, perpendicular to its long edge. The coverslip was then placed on the glass slide and pressed to create the flow chambers with the double-sided tape acting as spacers. The tape also created a seal necessary to prevent leakage of buffer from the flow chambers during experiments. The slides were, next, placed on a 60 ^{o}C hot plate for ~30 minutes and pressed again to create an even tighter seal between the coverslip and glass slide. In experiments where multiple chambers were created on the same slide, nail polish was used to seal the flow chambers. The nail polish acted as barriers to prevent buffer overflow into adjacent chambers during pipetting. At this stage, the glass slide flow chambers were ready for passivation and experiments.

3.4 MICROTUBULE PREPARATION AND POLYMERIZATION

For our experiments to be successful, they required both dynamic as well as stabilized microtubules that could be detected at the single particle level using TIRF microscopy. The microtubules I used in my experiments were purified from bovine brain. Bovine tubulin purification was performed as previously described (102). Briefly, calf brains were extracted, cleaned and homogenized at 4 °C. This process allowed microtubules from the samples to depolymerize, and was followed by ultracentrifugation to clarify the lysate. Glycerol and GTP were added to the lysate at 37 ^{o}C to promote re-polymerization, followed by ultracentrifugation. The pellets formed from ultracentrifugation were resuspended under cold treatment and ultracentrifuged again. This cycle of polymerization and depolymerization was repeated one more time, and the harvested tubulin after the last cycle was aliquoted and stored at -80 °C.

To grow taxol-stabilized microtubules, I first mixed 2 µL of Alexa-Fluor-488 labeled tubulin in 98 µL of unlabeled tubulin obtained from bovine brain at a concentration of 1 mg/mL. Next, I mixed 6.4 µL of the premixed tubulin with 24.4 µL of microtubule polymerization buffer (7 µL dimethyl sulfoxide (DMSO), 24 µL 5x BRB80, 5 µL $MgCl_2$, 12 µL 10 mM GTP, 74 µL H_2O). This mixture was then incubated at 37 ^{o}C for an hour. After the incubation period, I added 200 µL of warm BRB80 with 10 µM taxol to the solution, and centrifuged at 37 ^{o}C at 100,000 g for 10 minutes in an ultracentrifuge machine. I discarded the supernatant, and resuspended the pelleted microtubules in BRB80 with 10 µM taxol, making sure to avoid clumps. The method described here was used to generate all the fluorescent microtubules required in my experiments that required taxol-stabilized microtubules. In the other says, I grew dynamic microtubules off seeds that were anchored to a coverslip surface.

3.5 Lipid Preparation for Flow Chamber Surface Passivation

To ensure that the fluorescent particles I imaged during my experiments were specifically tethered to the coverslip surface, I utilized a phospholipid-based passivation surface. These phospholipids form unilamellar vesicles that spontaneously form supported bilayers on the plasma-cleaned coverslip surface. The bilayer prevents non-specific adsorption of soluble proteins and small molecules. However, with the addition of biotinylated head groups in the phospholipid, molecules of interest such as the kinetochores or microtubules can be specifically anchored to the lipid surface via a biotin-streptavidin interaction.

To do this, 12 μL of 25 mg/mL 1-palmitoyl-2-oleoyl-*sn*-glycero-3-phosphocholine (POPC) was added to 4 μL of 0.1 mg/mL 1,2-dieoleoyl-*sn*-glycero-3-phosphoethanolamine-N-(cap biotinyl) sodium salt (biotinyl-cap-PE). This was then dissolved and thoroughly mixed in 84 μL of chloroform in a glass test tube. The lipid mixture was then dried in the test tube by blowing nitrogen over the mixture for about 5 minutes, while simultaneously rotating the test tube. The phospholipid mixture was further dried via a vacuum desiccator overnight. Prior to use, I added 300 μL BRB80 buffer (80 mM PIPES, 1 mM $MgCl_2$, 1 mM EGTA pH 6.9) to the test tube. I then rehydrated the dried lipid in the aqueous solution by vigorously vortexing the test tube. I, next, sonicated the rehydrated phospholipid at 50 % duty cycle and low power setting using a tabletop sonic dismembrator with a probe. The sonication converted the rehydrated phospholipid (milky color) into a clear liquid made of small unilamellar vesicles (Fig. 3.2). The clear phospholipid mixture, at this stage, to be fed into the coverslip flow chamber for kinetochore tethering.

3.6 Specific Attachment of Kinetochores to Phospholipid Surface & Single Particle Confirmation

The initial experiments I performed were to determine if I could detect doubly-labeled single kinetochore particles in an *in vitro* assay. This required specifically anchoring the kinetochore particles to the surface of a biotinylated phospholipid bilayer in the glass slide flow chamber. Once anchored, the slide was set up on the piezo stage of our custom-built TIRF microscope, and image acquisition was performed. I acquired multiple snapshots of different fields of view for each experiment using a raster sequence algorithm.

First, I fed 10 μL of BRB80 into the coverslip flow chamber to wet the glass surface, and followed this step by feeding in 10 μL of the sonicated phospholipid mixture. After approximately 4 minutes of incubation at room temperature, I washed the flow chamber to rid it of any impurities with 50 μL of BRB80. I followed this step with 10 μL of 0.25 mg/mL Streptavidin (Sigma-Aldrich) in BRB80 in the flow chamber, and allowed a 4-minute incubation reaction period. After the incubation, I washed the flow chamber again with 50 μL BRB80, and then introduced 20 μM Penta-His Biotin Conjugate (Qiagen) in BRB80 into the flow chamber. After a 5-minute incubation, I introduced kinetochore particles diluted in BRB80 at a concentration equal to ~140 pM Dsn1 (usually 1 μL kinetochore stock solution in 99 μL) into the flow chamber. After an incubation period of 5 minutes, which allowed the kinetochore particles to adsorb to the coverslip surface through the Penta-His Biotin Conjugate, I washed the flow chamber with 50 μL of BRB80 and set up the slide on the microscope for image acquisition (Fig. 3.3). A raster algorithm was developed to rapidly acquire images for each sample, using custom LabView software. The raster occurred while the image was maintained in the same focal plane.

For every experiment I performed, I also determined how effective the specific adsorption of particles to the biotinylated phospholipid bilayer was. I confirmed passivation by comparing four flow chambers under different conditions. In the first flow chamber, I fed in only kinetochores onto the plasma-cleaned glass surface, without a phospholipid bilayer or linkers (biotin-streptavidin). In the second flow chamber, I created the biotinylated phospholipid bilayer and then fed the kinetochores into the flow chamber without the Streptavidin or Penta-His antibody. I also set up a third flow chamber, where I fed in all the components of the assay minus the Penta-His antibody. I compared all three flow chambers above to a normal experiment (Fig. 3.4). In these assays, I found that the biotinylated phospholipid bilayer, when devoid of impurities, was effective in preventing non-specific adsorption, and that the linkers (biotin, Streptavidin & Penta-His antibody) were required to specifically anchor the kinetochores onto the phospholipid surface.

Each glass slide I used for every experiment, contained 3 flow chambers. The first two chambers served as control. In the first control chamber, I always fed in the phospholipid bilayer and kinetochores only. The second chamber contained the phospholipid bilayer with streptavidin and kinetochores, but no Anti-Penta-His antibody. This helped to ensure that for each experiment I was only looking at a majority of specifically tethered kinetochores. Seldom, the control flow chambers would fail. I defined a failed passivation as one where I could detect more than ten kinetochore particles non-specifically adsorbed. Passivation, was one of the main crutches of these assays, and if passivation worked, an experiment was highly likely to be successful. Problems in passivation were mostly due to impurities in the lipid or buffer. Also, the coverslips were, sometimes, not properly cleaned. This would usually result in defective phospholipid bilayer formation. Holes sometimes formed on the in the bilayer, resulting in the kinetochores

being directly adsorbed to the glass. This was sometimes evident as clumps of kinetochore particles in various fields of view. The advantage, however, of using the system described above was that defective phospholipid mixtures or unclean coverslips could be easily discarded and remade, unlike other passivation procedures that require tedious and time-consuming preparation.

3.7 Attachment of Kinetochores to Microtubules

3.7.1 *Lateral Attachment of Kinetochores to Microtubules*

During cell division, microtubules initially make lateral attachments to kinetochores through a 'search and capture' mechanism, which involves assembly and disassembly of the microtubules. Once these lateral attachments are made, they are subsequently converted to end-on attachments, which are then pulled to the spindle poles as the cell transitions from metaphase to anaphase. I wanted to confirm that the checkpoint-labeled kinetochores we isolated could make lateral attachments to microtubules *in vitro* and that these attachment events could be directly observed using TIRF microscopy.

To do this, I first fed 10 μL of BRB80 buffer into the flow chamber, and followed that with 10 μL of the phospholipid mixture. After 4 minutes of incubation at room temperature, I fed 50 μL of BRB80 into the flow chamber to wash it. I then introduced 10 μL of 0.25 mg/mL Streptavidin (Sigma-Aldrich) in BRB80 into the chamber and let it incubate for 4 minutes. After the incubation period, I washed the chamber again with 50 μL BRB80, and then fed 10 μL of 0.05 mg/mL biotin anti-Tubulin-α Antibody (BioLegend) into the chamber. After a 5-minute incubation period, I performed another chamber wash with 50 μL BRB80 plus 0.1 mg/mL κ-casein. Next, I immobilized 10 μL of the fluorescent taxol-stabilized microtubules diluted in

BRB80 (with 0.1 mg/mL κ-casein) unto the flow chamber surface, and allowed an incubation of 5 minutes. After the 5 minutes, I washed the flow chamber again and fed kinetochore particles diluted in BRB80 plus 0.1 mg/mL κ-casein at a concentration equal to ~140 pM Dsn1 into the chamber. The kinetochores were allowed 5 minutes to bind to the immobilized taxol-stabilized microtubules. After the incubation, I performed a last chamber wash with 50 µL BRB80 (with 0.1mg/mL κ-casein), and performed image acquisition on the microscope.

3.7.2 *End Association of Kinetochores to Microtubules ('Flip' Assay)*

We developed an assay called the 'flip' assay to mimic the end-on attachment that kinetochores make with microtubules after they transition from an initial lateral attachment. I specifically anchored fluorescent kinetochores to the biotinylated phospholipid surface via the biotin-streptavidin-biotin-(Anti-His)-(Dsn1-His) linkage. I then obtained fluorescent microtubules, and vortexed them gently to obtain appropriate microtubule lengths suitable for this experiment. In this experiment, it was essential to use microtubules that were between the lengths of 5 µm and 10 µm. This is because the longer the microtubules, the more likely they were to make lateral attachments instead of end-on attachments. The gently-vortexed microtubules were then introduced into the flow chamber and allowed to bind to the specifically anchored kinetochores. Through thermal diffusion, most of the microtubules that were introduced into the flow chamber formed end-on attachments to the already adsorbed kinetochores. The other ends of the microtubules freely swiveled in solution until they eventually made attachments with other tethered kinetochores. I then imaged the end-associated particles after a 5-minute incubation period.

3.7.3 *Attachment of Kinetochores to Disassembling Microtubules ('Disassembly' Assay)*

During cell division, stable end-on attached kinetochores are pulled towards the spindle poles as the cell progresses from metaphase to anaphase and the spindle assembly checkpoint is satisfied. During this period, the kinetochores track processively with disassembling microtubules *in vivo*. I wanted to test the fluorescently labeled isolated kinetochores to ensure that they could track with dynamic microtubules in my *in vitro* assay.

To test this, I first fed 10 μL of BRB80 into a plasma-cleaned flow chamber to wet the glass surface, and then followed with 10 μL of the sonicated biotinylated phospholipid mixture. Next, I introduced 10 μL of 0.25 mg/mL Streptavidin in BRB80 into the chamber. After an incubation period of 5 minutes, I introduced 10 μL of unlabeled biotinylated Guanosine-5'-[(α,β)-methyleno]triphosphate (GMPCPP) seeds diluted in BRB80 into the flow chamber. As the GMPCPP seeds bound to the chamber surface via its biotin heads I prepared a buffer consisting of 0.1 mg/mL κ-casein, 1 mM GTP, 250 μg/mL glucose oxidase, 25 mM glucose, 30 μg/mL catalase, 1 mM DTT, and 1.5 mg/mL fluorescent tubulin in a total volume of 49 μL. I also added 1 μL of fluorescent kinetochores to the buffer, and fed 30 μL of the prepared buffer into the flow chamber. I let the slide incubate at room temperature for 10 minutes as fluorescent microtubule extensions grew from the specifically anchored GMPCPP seeds. After the 10-minute incubation, I set up the slide on the TIRF microscope and proceeded to induce disassembly of the microtubules via buffer exchange using 15 μL BRB80 plus 0.1 mg/mL κ-casein. Microtubule disassembly was induced while simultaneously acquiring images on the microscope.

3.8 TOTAL INTERNAL REFLECTION FLUORESCENCE (TIRF) IMAGE ACQUISITION AND ANALYSIS

3.8.1 *Custom-built Multi-color TIRF Microscopy*

Total internal reflection fluorescence microscopy allowed imaging of the fluorescent kinetochore particles within a thin focal plane with nanometer precision, essentially reducing background noise from the specimen sample. Our TIRF system was built on an inverted Nikon microscope with three solid-state diode lasers at 488 nm, 561 nm and 647 nm for excitation. The lasers had a maximum power of 100 mW. Photon emission was collected on three highly sensitive electron multiplying charge coupled device (EMCCD) cameras. The lasers were set up with an adjustable incident angle allowing easy TIRF alignment and possible switch between TIRF, epi-fluorescence and oblique illumination. TIRF alignment was done using a CCD camera. The camera was mounted at a view port and images observed from the eyepiece were used for the alignment.

3.8.2 *Image Registration*

Since our experiments require multiple fluorescence color channels (488 nm, 561 nm, 647 nm lasers), it was very important to have accurate image registration across all three channels. Image registration errors tend to occur mostly because of the differences in the optical paths of the different lasers that are used. For example, the doubly tagged kinetochore components when excited are split into two images per their respective wavelengths, and recorded separately on their respective cameras. The two channels will invariably map onto different positions due to their different imaging paths. In my experiments, image registration

was especially important because our analyses required position determination for colocalization calculation.

Image registration was done as previously described (103–105). I made a 1 in 1000 solution of 0.2 μm TetraSpeck microspheres (ThermoFisher) and fed 10 μL of it into a plasma-cleaned flow chamber. The bright and photostable TetraSpeck microspheres were visible across all three color channels. Following this, I identified a single microsphere without any neighboring microsphere in a field of view as a fiducial marker on the TIRF microscope. I then raster-scanned the microsphere using a custom LabView algorithm (Fig. 3.5). At each position of the raster scan, I collected images in each of the three channels. Control points for each of the image spots in each of the channels were then determined by fitting each spot with a two-dimensional Gaussian function. A mapping was calculated using control points from one of the channels, which was designated as fiducial. The mapping that was calculated was then applied to the other channels to align them with the fiducial (106). Each time I performed an image registration, I also tested the registration data generated and calculated the accuracy of the registration by determining a target registration error. Given the custom nature of our instrumentation and temperature fluctuations, it was essential to perform image registration routinely during the year to ensure accuracy in colocalization calculations.

3.8.3 *Image Analysis*

To analyze the data, I calculated the colocalization of the particles. Here, I defined colocalization as the number of identified fiducial Mtw1 spots above background noise that also had corresponding checkpoint protein (Mps1) spots above background noise. For each experiment, I plotted all the spots identified from all fields of view (FOVs) on a scatter dot plot as shown in Figure 3.6. I used histograms to distinguish background noise from actual spots. The

histograms I generated allowed thresholds to be set for both the Mtw1 and checkpoint particle brightnesses (Fig. 3.6). Next, I determined for each FOV in the sample dataset, the number of Mtw1 particles that had a checkpoint particle in the same location. This was done after the image registration was performed. Once an Mtw1 particle above threshold was identified, I recorded the corresponding checkpoint particle brightness. A checkpoint brightness level above threshold was recorded as an uncolocalized spot and vice versa.

I performed a titration experiment to ensure that the data I was collecting were from single kinetochore particles (Fig. 3.7). To do this, I prepared 6 plasma-cleaned flow chambers, and specifically anchored kinetochores onto biotinylated phospholipid bilayers on the flow chamber surfaces using linkers, as described before. I fed a different concentration of kinetochore particles into each flow chamber. This resulted in densities per FOV of between 50 and 400 particles. I then calculated the mean colocalization for each flow chamber after performing image acquisition, and showed that the colocalization did not change.

I collected large amounts of images for each experiment with the help of a modified focus detection system. We utilized a 1064 nm laser for the focus detection. The incident beam from the laser was reflected at the coverslip-buffer interface of our flow chamber, reflected back to the objective lens, and translated due to a shift in the position of the sample. The shift in the sample was detected by a position-sensitive detector (PSD). The focus detection allowed a raster acquisition of multiple FOVs, while the focal plane was kept in focus (107). In all, I collected approximately 160 FOVs and 200 spots per field for each experiment. I estimate that on average, the results from each experiment were determined from 96,000 colocalized or uncolocalized Mtw1 particles. I determined an overall mean colocalization across FOVs for each experiment.

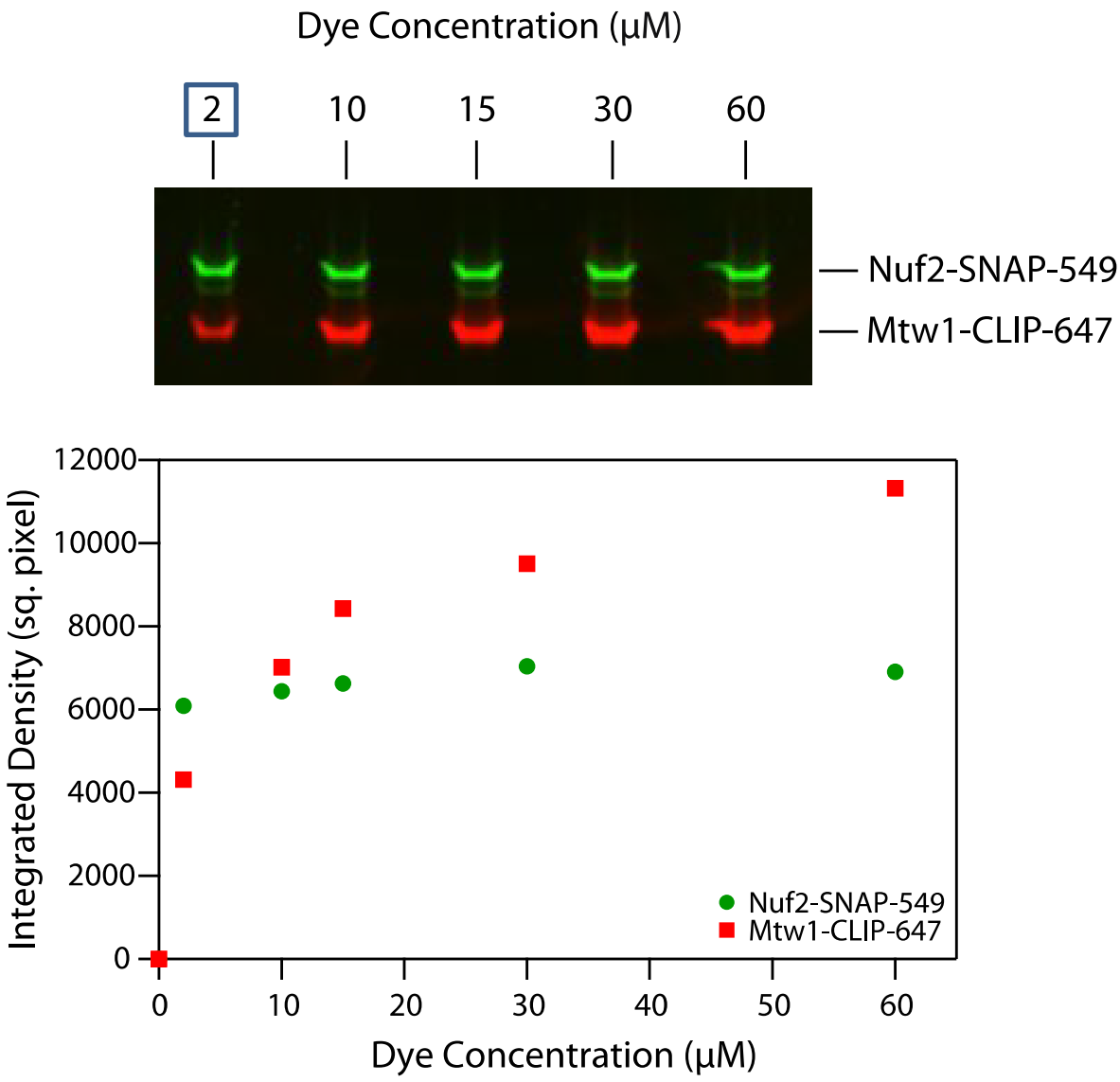

Figure 3.1: SNAP and CLIP maximal labeling with Alexa dyes. Alexa-Fluor-549 and Alexa-Fluor-647 dyes were used to label the SNAP- and CLIP-tagged proteins, respectively. To obtain maximal labeling of the kinetochores, a titration experiment using increasing concentrations of the dyes. Maximal labeling for the SNAP- and CLIP-tags were reached at 2 µM and 30 µM, respectively.

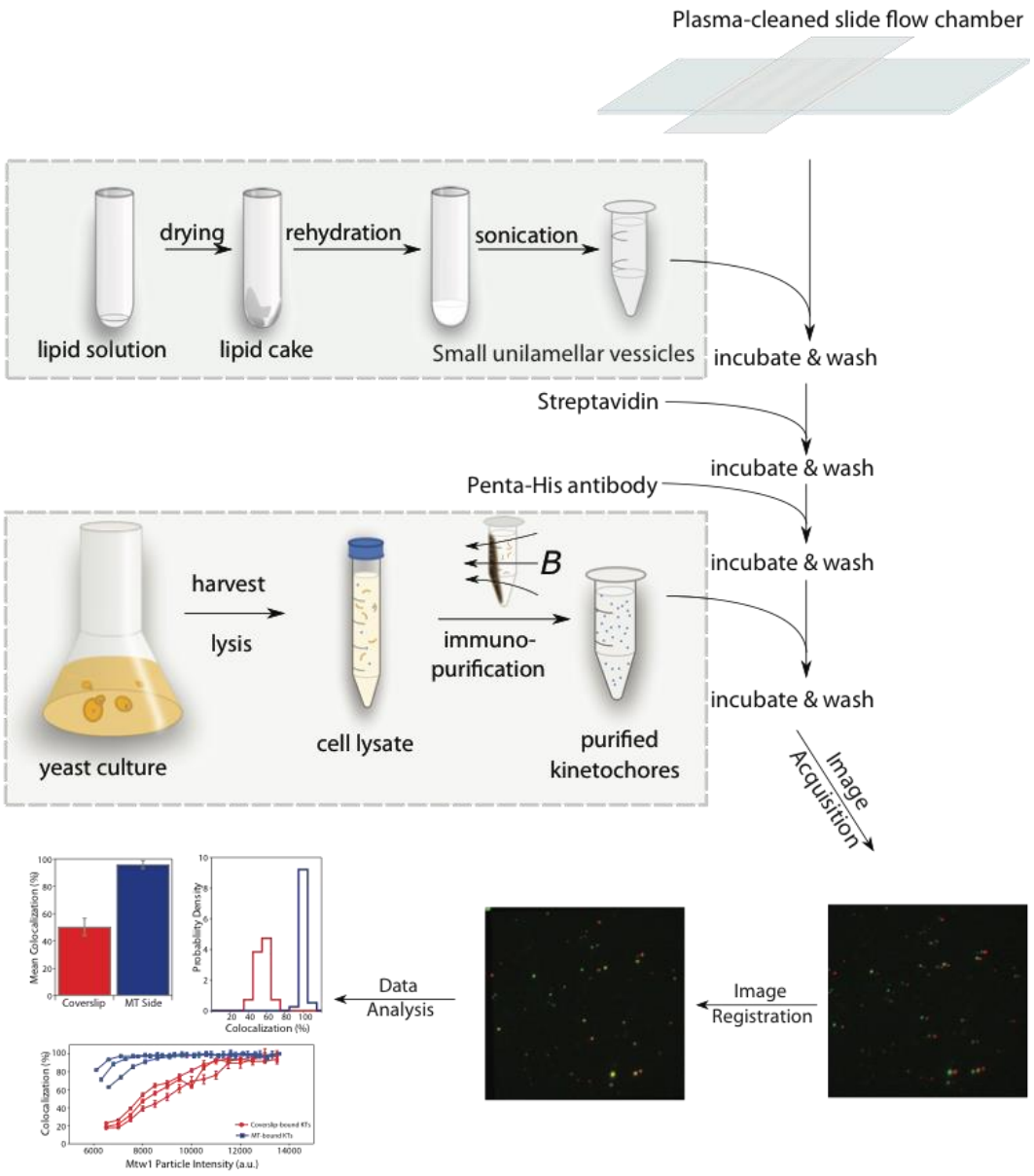

Figure 3.2: The experimental assay developed allows direct observation and analysis of single kinetochore particles. We development an experimental assay that included making a glass slide with flow chambers. The flow chambers were plasma-cleaned and coated with a phospholipid bilayer for passivation. Isolated kinetochores were specifically anchored to the surface of the phospholipid bilayer via a biotin-streptavidin linkage, and directly observed using TIRF microscopy. Image registration allowed colocalization levels of particles to be calculated with high precision.

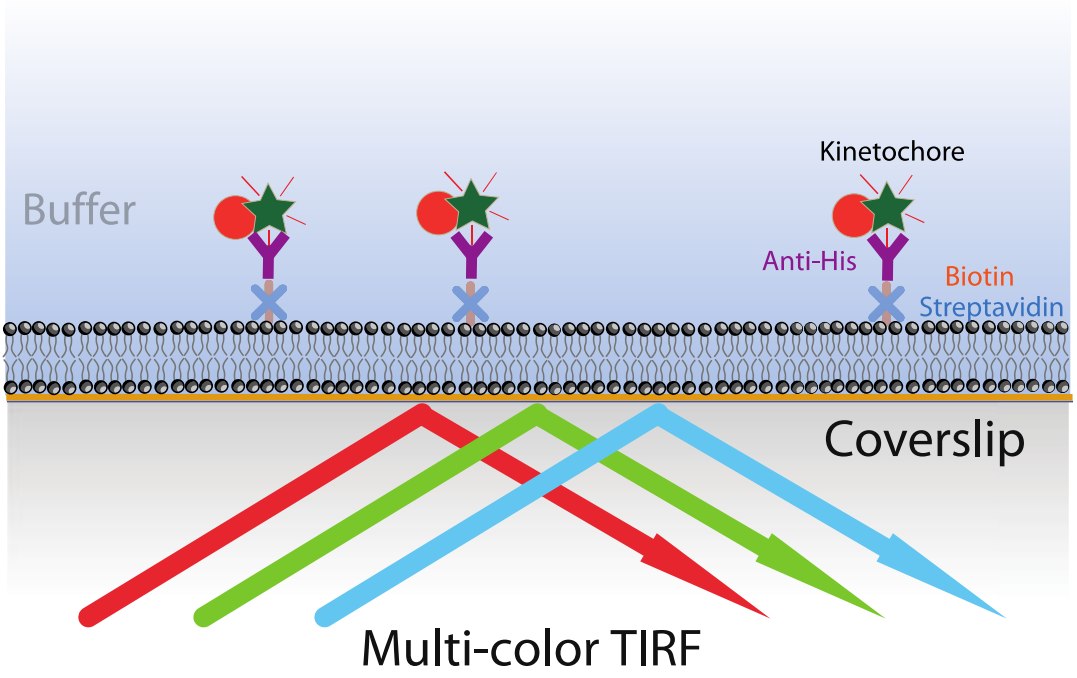

Figure 3.3: Glass slide flow chamber setup for particle visualization using TIRF. To visualize fluorescent kinetochores using TIRF, the flow chamber was plasma-cleaned and passivated using a phospholipid bilayer doped with biotin. The kinetochores were then linked through a biotin-Streptavidin-biotin-(Anti-His)-(Dsn-His) interaction. The glass slide was then placed on the microscope piezo stage and the kinetochores were directly visualized.

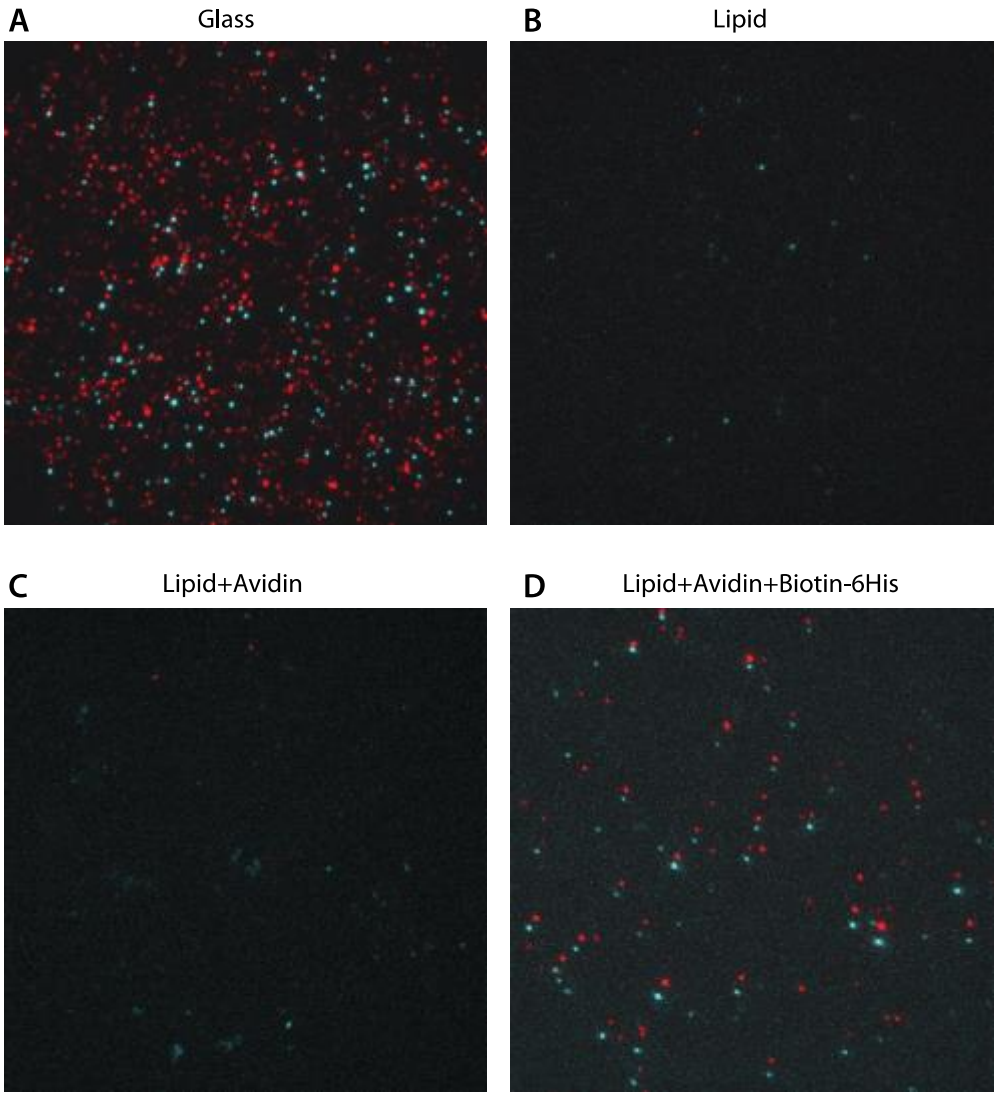

Figure 3.4: The phospholipid bilayer passivates the coverslip surface effectively and increases specific adsorption of kinetochore particles. In (A) the isolated kinetochores were immobilized unto a plasma-cleaned coverslip surface without a phospholipid bilayer or linkers. The kinetochores were non-specifically bound to the surface. To test the passivation, the kinetochores were immobilized onto a phospholipid bilayer in (B), and onto a bilayer with Streptavidin in (C). In both cases, since there was no Anti-His antibody the kinetochores were unable to bind, demonstrating good passivation of the coverslip surface. In (D) when the Anti-His antibody was included before addition of the kinetochores, the kinetochores were specifically adsorbed through the Dsn1-His tag.

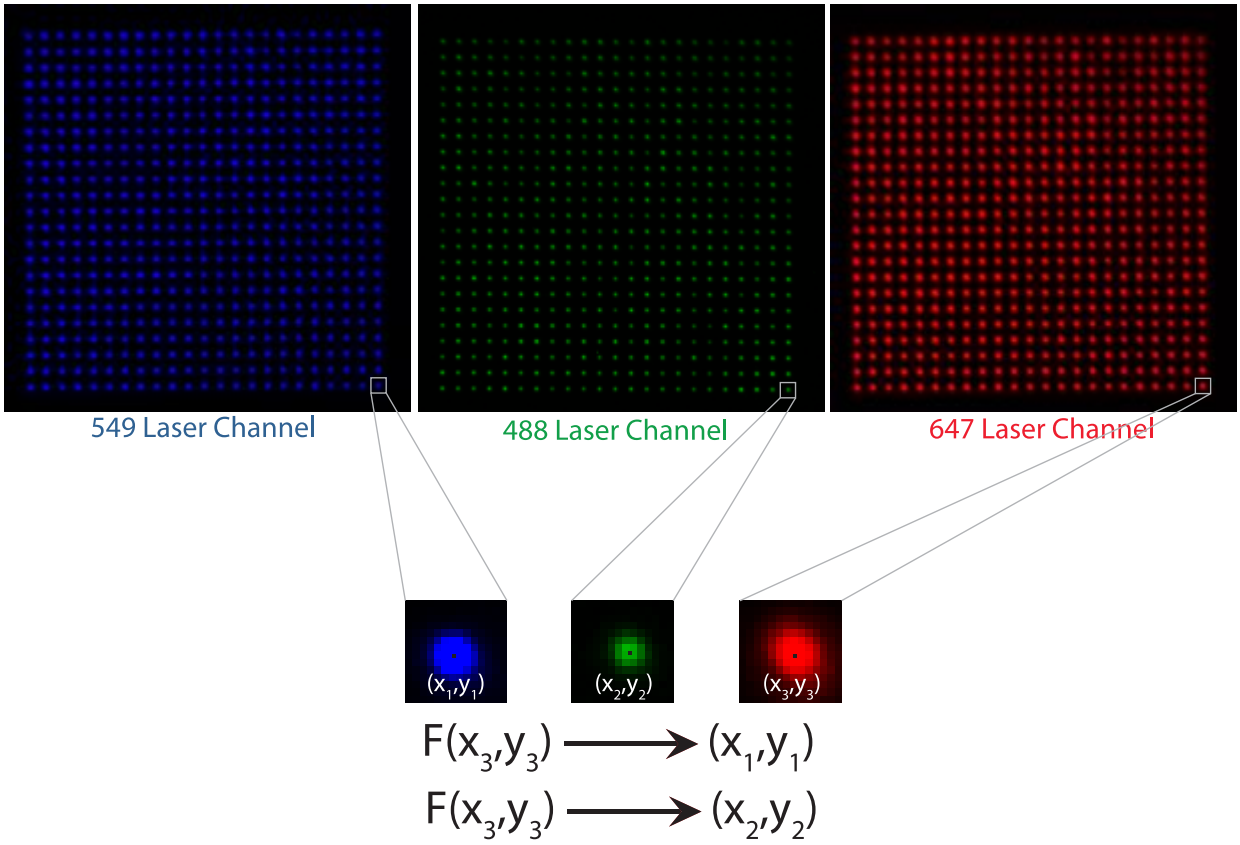

Figure 3.5: Image registration ensures particle colocalization is correctly calculated. A TetraSpeck bead that could be excited in all three laser channels was raster-scanned across an entire field of view, as shown. The center of each spot generated from the raster scan was determined, and used to generate a map that was applied to all the images. This process eliminated registration errors from the imaging system, enabling colocalization calculation.

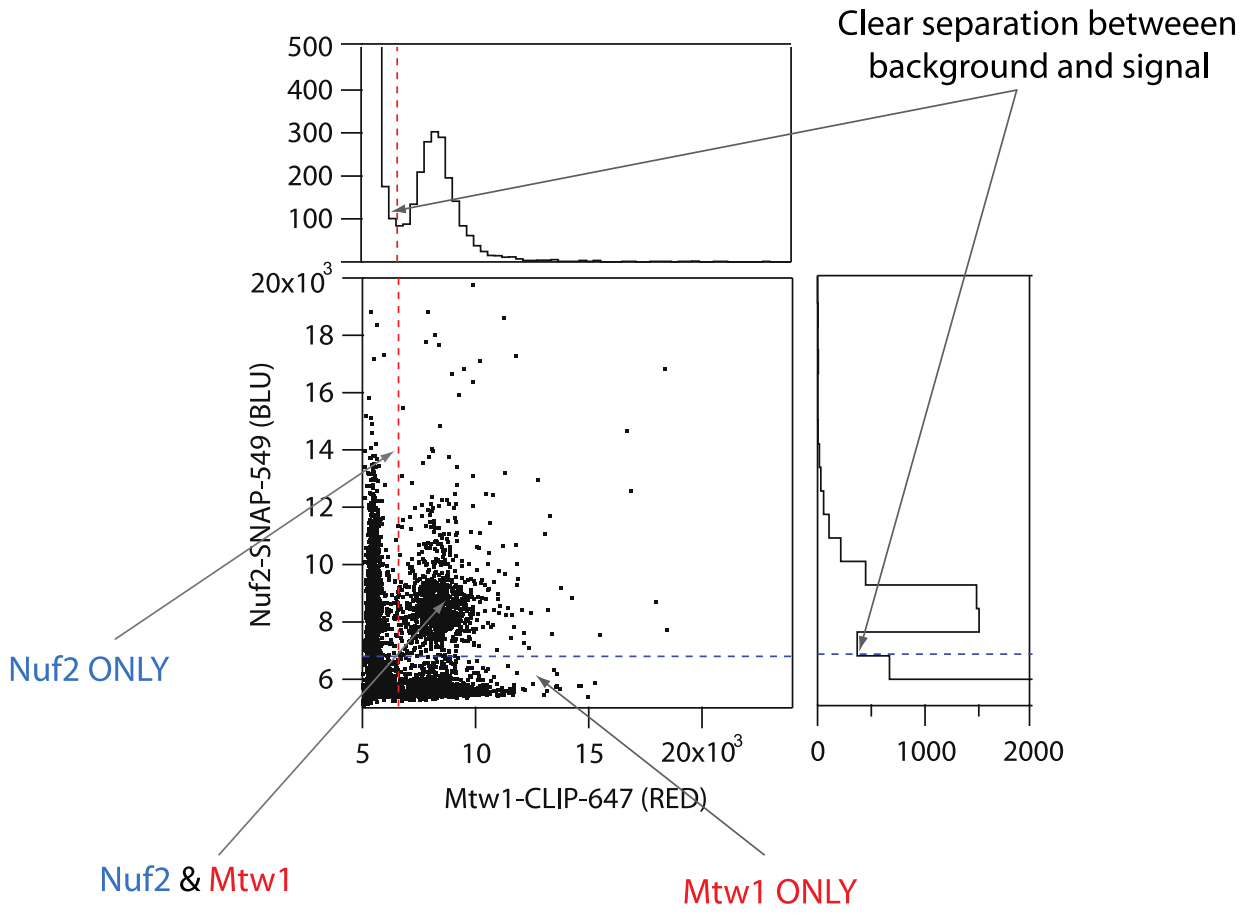

Figure 3.6: A scatter plot is generated to calculate colocalization of the kinetochore particles. To calculate the colocalization, all the fluorescent spots that were detected during TIRF image acquisition were plotted on a scatter plot as shown, with the Mtw1 (fiducial marker) signal intensity on the X-axis and the checkpoint protein of interest on the Y-axis. Histograms were plotted for each channel and used to generate thresholds to identify signal above background noise. The top-right quadrant of the scatter plot contains all the spots (actual particles above noise) that were colocalized. The colocalization was calculated by dividing all the spots in the top-right quadrant of the scatter plot by all the Mtw1 spots above noise (bottom-right quadrant).

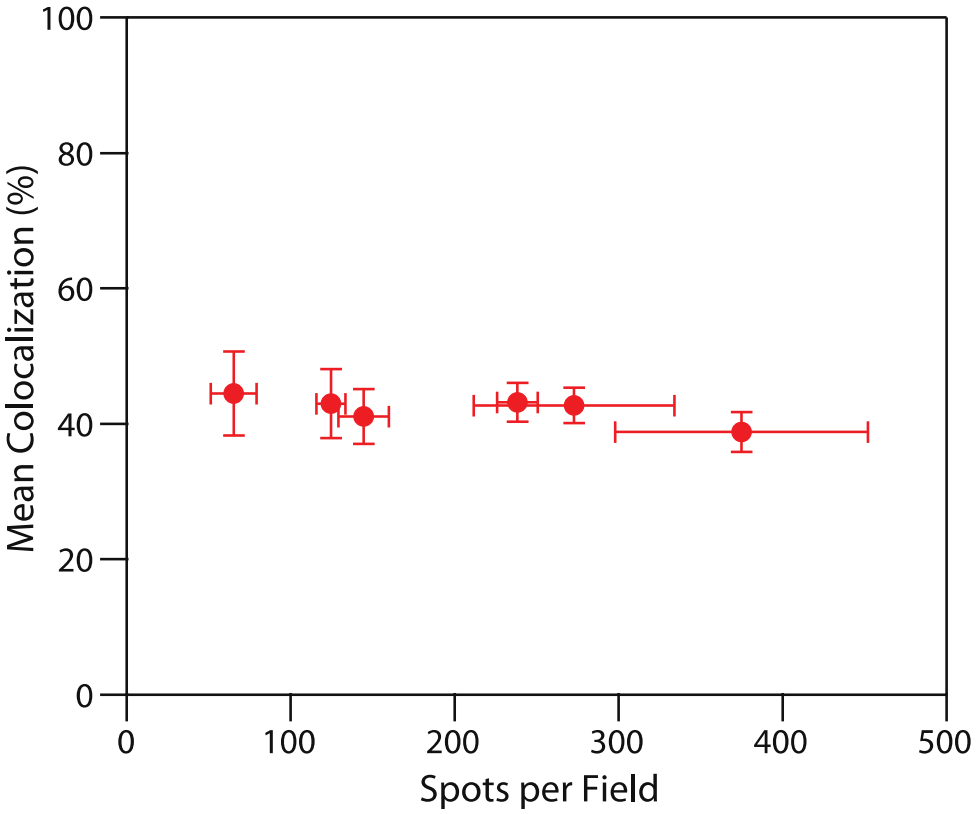

Figure 3.7: Single kinetochore particles are specifically adsorbed to the phospholipid bilayer. To ensure that single particles were being observed in the experiments, a dilution series experiment was performed. Flow chambers with increasing concentrations of specifically adsorbed kinetochore particles were imaged and analyzed. The mean colocalization percentage calculated did not change within a range of 50 to 400 particles per field of view. This confirmed single particle observation in the assays.

Chapter 4. ASSOCIATION OF MPS1 KINASE WITH ISOLATED YEAST KINETOCHORES IS NOT STRICTLY COMPETITIVE WITH MICROTUBULE ATTACHMENT

Adapted from manuscript in preparation

Kwaku N. Opoku, Lori B. Koch, Yi Deng, Sue Biggins, Charles L. Asbury

4.1 ABSTRACT

Accurate mitosis depends on a surveillance system called the spindle assembly checkpoint. The checkpoint acts at kinetochores, which attach chromosomes initially to the sides of spindle microtubules and later to dynamic microtubule ends. When a kinetochore is unattached or improperly attached, the checkpoint kinase Mps1 phosphorylates various kinetochore components, catalyzing the generation of a diffusible 'wait' signal to block anaphase chromosome segregation. When a kinetochore becomes properly attached, this signal is somehow silenced to allow anaphase to proceed. Several models have been proposed to explain how Mps1 is selectively silenced at microtubule-attached kinetochores. In competitive binding models, Mps1 and microtubules compete for binding to the kinetochore, either directly or allosterically, such that proper microtubule attachment is sufficient to release Mps1 from the kinetochore. Alternatively, microtubule attachment could affect the kinase activity of Mps1 or its access to substrates, without necessarily causing its release. Here we describe an in vitro approach that enables unambiguous assessment of the attachment status of individual kinetochore particles while simultaneously monitoring their levels of associated Mps1. We find that fluorescent, active Mps1 is stably retained on native kinetochores purified from budding

yeast. Mps1 levels are not reduced when a kinetochore binds laterally to the side of a microtubule, nor when it tracks processively with a disassembling end. Thus, association of a kinetochore with Mps1 is not strictly competitive with microtubule attachment. In the future, our approach could be combined with fluorescent biosensors to test directly for attachment-dependent changes in Mps1 kinase activity or substrate access.

4.2 INTRODUCTION

Chromosome missegregation during mitosis causes aneuploidy, a hallmark of cancer and chromosomal birth defects (108–110). To prevent missegregation, cells rely on a surveillance system called the spindle assembly checkpoint, which acts at kinetochores, the specialized multiprotein complexes that attach chromosomes to spindle microtubules. When a kinetochore is unattached or improperly attached, a hierarchy of checkpoint proteins is selectively recruited to the kinetochore, where they generate a diffusible 'wait' signal that prevents anaphase chromosome segregation. A kinetochore may cycle between unattached, laterally attached to the sides of microtubules, or end-attached to growing or shortening microtubule tips before a proper attachment is established. The checkpoint proteins are then released to silence the 'wait' signal and allow anaphase to proceed (23, 24, 92). The biochemical steps underlying wait-signal generation are becoming clearer (92). However, it remains unclear how the checkpoint distinguishes unattached versus properly attached kinetochores. A major impediment has been the difficulty of directly and unambiguously determining the microtubule attachment status and the level of checkpoint proteins on individual kinetochores in dividing cells.

The checkpoint kinase, Mps1, is vital for establishing and maintaining the wait signal (20, 22, 40–42, 111). Mps1 initiates the checkpoint signaling cascade by phosphorylating key

threonine residues in a core kinetochore protein, Knl1^{Spc105}, thereby recruiting Bub1-Bub3 to the kinetochore (30, 32, 112). Further phosphorylation of Bub1 by Mps1 promotes recruitment of Mad1, which acts as a platform for catalytic generation of the wait signal (33, 48, 49). Mps1 itself associates directly with the Ndc80 complex, a primary microtubule-binding element of the core kinetochore (29, 43, 44, 50, 51). Overexpressing Mps1 in cells or tethering it constitutively to kinetochores is sufficient to induce a checkpoint-dependent delay, even in the absence of obvious defects in kinetochore-microtubule attachment (41, 42, 113, 114). Thus, Mps1 is a signal initiator that associates directly with a major microtubule-binding element of the core kinetochore, making it a strong candidate for modulating the output of the checkpoint in response to kinetochore attachment status (92, 115–117).

Several classes of models have been proposed to explain how Mps1 could be selectively silenced at properly attached kinetochores. In competitive binding models, Mps1 competes with microtubules for binding to the kinetochore (51, 118). This view is supported by the recent discoveries that N-terminal fragments of Mps1 interact directly with microtubule-binding surfaces on the Ndc80 complex and that the Mps1-Ndc80 interaction is inhibited by taxol-stabilized microtubules (50, 51). It is unknown, however, whether such competition can significantly reduce the levels of Mps1 on whole kinetochores, which contain numerous copies of the Ndc80 complex (estimates suggest 8 to 20 copies per kinetochore (119–122)). Also unknown, is how full-length Mps1 would respond in the published competition model assays. Some of the Ndc80 complexes could bind microtubules while others simultaneously retain Mps1. Alternatively, structural rearrangements occurring within a kinetochore upon proper attachment to a microtubule could modulate Mps1's kinase activity (41, 123), or prevent it from

accessing its substrates (114), without necessarily causing its release. It is important to note that in this model Mps1 was seen present on the kinetochore during metaphase.

To test models for checkpoint silencing, we developed a new approach based on direct observation of Mps1 levels on individual yeast kinetochores in vitro. Here, we show that native yeast kinetochore particles can be isolated carrying high levels of stably associated, fluorescent-tagged Mps1 kinase. The individual particles are readily attached to the sides of taxol-stabilized microtubules and, using a new inverted assay, they can be specifically attached to the microtubule ends. Persistent tracking of the particles with disassembling ends can also be reconstituted. In all three scenarios, the particles retain high levels of Mps1 kinase, suggesting that Mps1 and microtubules do not compete directly for binding to these kinetochore particles. With the addition of fluorescent biosensors we anticipate that the single particle approach could be used in the future to test directly for attachment-dependent changes in the kinase activity or substrate access of Mps1 and other kinetochore-associated kinases.

4.3 RESULTS

4.3.1 *Microtubule binding is not sufficient to release Mps1 from kinetochores in a bulk biochemical assay*

Previous work has shown that active Mps1 kinase co-purifies with native kinetochores isolated from budding yeast (30). Given the recent discovery that microtubules competitively inhibit the binding of human Mps1 fragments to the CH domain of truncated human Ndc80 complex (50, 51), we hypothesized that a similar competition might occur in the context of native yeast kinetochore particles. For an initial test for competitive binding versus microtubules, we immunoprecipitated native kinetochores via affinity purification of the Dsn1 protein under

physiological concentrations of salt, as previously described (52), incubated them with taxol-stabilized microtubules, washed, and then analyzed the resin-bound material. Consistent with previous findings, the purification yielded large assemblies including the majority of kinetochore subcomplexes except CBF3 (data not shown). Mps1 was retained on the kinetochores, as expected (30), and the microtubules bound specifically to the kinetochores, but their binding did not reduce the level of kinetochore-associated Mps1 detected by Western blotting (Fig. 1A). The lack of a detectable reduction suggested a lack of competition between Mps1 and microtubules for binding to the kinetochores. However, neither the fraction of microtubule-bound kinetochores nor the stoichiometry of Mps1 associated with them were monitored in this experiment, so the possibility that competition went undetected due to low occupancy could not be ruled out. We therefore sought a fluorescence-based single particle experiment that could enable a more definitive test.

4.3.2 *Isolation and imaging of single kinetochore particles retaining fluorescent-tagged Mps1*

For direct observation of Mps1 levels by fluorescence, we isolated kinetochore particles from yeast strains in which Mps1 and a core kinetochore protein, Mtw1, were tagged with SNAP and CLIP, respectively (Fig. 4.1). These tags allowed the proteins to be efficiently labeled with bright, photostable fluorescent dyes, CLIP-Surface 647 and SNAP-Surface 549, during the purification. In addition to wild-type, we also purified particles carrying a pair of phosphomimetic serine-to-aspartic acid substitutions in the Dsn1 protein, S240D and S250D (Dsn1-2D), which mimics Aurora B phosphorylation at these sites and helps stabilize the association of inner and outer kinetochore components (124, 125). Quantification of fluorescence after SDS-PAGE confirmed the specificity of labeling (Fig. 4.1) and that both tags

became saturated with dye by the labeling protocol (75). Laser trap assays confirmed that the dual-labeled kinetochore particles were fully mechanically functional, forming attachments to growing microtubule tips with normal rupture strength (Fig. 4.2).

To observe individual fluorescent-tagged kinetochores, the particles were tethered sparsely to a coverslip surface and then viewed by multicolor total internal reflection fluorescence (TIRF) microscopy (Fig. 4.3). Non-specific adsorption was prevented by passivating the coverslip with a supported lipid bilayer. The particles were then tethered specifically to the bilayer through a 6xHis tag on the Dsn1 protein, an arrangement that preserves kinetochore function (87, 107). Using Mtw1-CLIP-647 as a fiducial marker, the concentration of kinetochore particles was adjusted to achieve surface densities between 50 and 300 particles per 1475 μm^2 field of view. An automated procedure was used to collect up to 600 images containing over 100,000 particles for each sample.

The purified kinetochore material contained a mixture of dual-color particles carrying both Mps1 and Mtw1, plus particles lacking Mps1 (Figs. 4.3 & Fig. 4.6). The fraction of wild-type particles that retained Mps1 was modest, 19.6 ± 0.05 % (Fig. 4.6), whereas the fraction of phosphomimetic Dsn1-2D particles retaining Mps1 was higher, 48.7 ± 7.6 % (Fig. 4.3). Higher Mps1 colocalization with the Dsn1-2D particles is consistent with previous work showing that these phosphomimetic mutations stabilize the core kinetochore structure (124, 125). It is unlikely to arise from differences in checkpoint function, because cells carrying the Dsn1-2D mutations enter and exit a checkpoint arrest normally, with kinetics that are indistinguishable from wild-type cells (Fig. 4.2). Dsn1-2D also increases colocalization of Ndc80 with the particles (data not shown), indicating a general stabilization of core kinetochore structure. Subcomplexes with just one detectable Mps1 or one Mtw1, identifiable by their single-step

photobleaching behavior served as internal controls, allowing normalization of particle brightnesses and estimation of molar ratios of Mps1 to Mtw1. High occupancy particles, carrying one or more Mps1 molecules per Mtw1, made up a substantial fraction of the population. These results confirm that endogenous Mps1 kinase remains stably associated with the isolated kinetochores and that it is detectable at the single particle level.

4.3.3 *Mps1 is retained on individual kinetochores bound to the sides of microtubules*

Yeast Mps1, like its human homolog, associates directly with the microtubule-binding CH domain of the Ndc80 complex (43). Although microtubules were not directly observed, the competition seen in the experiments with human protein fragments almost certainly occurred via lateral binding of Ndc80 complex to the sides of the microtubules, since purified Ndc80 complex alone shows no preference for the ends of taxol-stabilized filaments (126). Thus, for comparison, we first examined kinetochore particles bound laterally to taxol-microtubules.

Taxol-stabilized microtubules were anchored to a lipid-passivated coverslip and then kinetochores were introduced and allowed to bind sparsely to the sides of the microtubules (Fig. 4.3) (52, 75). Direct competition would imply that association of individual Ndc80 complexes to Mps1 or to microtubules is mutually exclusive – Ndc80 complexes carrying Mps1 should not bind microtubules until they have released their Mps1. However, many of the isolated kinetochore particles are oligomeric, like kinetochores in vivo, carrying multiple Mtw1 molecules and likely a similar number of Ndc80 complexes (8). If some of these bind microtubules, others could retain Mps1, potentially producing a graded rather than a binary relationship at the whole kinetochore level. Nevertheless, in a competitive binding scenario the particles carrying high levels of Mps1 should be inhibited from binding microtubules and,

conversely, particles lacking or carrying lower levels of Mps1 should be enriched among those that do bind microtubules. Just the opposite was observed. The average molar ratio of Mps1 to Mtw1 for the microtubule-bound Dsn1-2D particles, 1.36 ± 0.01, was much higher than for the control population, 0.45 ± 0.01 (i.e., the coverslip-tethered case). The fraction of microtubule-bound Dsn1-2D particles retaining Mps1 was 94.2 ± 3.8 % (Fig. 4.3), roughly double that of the control population. Even the dimmest microtubule-bound particles, carrying just one Mtw1, were very likely to retain one or more Mps1 molecules. These observations indicate that the isolated yeast kinetochore particles can associate simultaneously with Mps1 and with the microtubule lattice in a non-competitive manner.

4.3.4 *Mps1 is retained on individual kinetochores bound to microtubule ends*

Kinetochores initially make lateral attachments to the sides of microtubules (127, 128), but these lateral attachments are converted to end-attachments before proper, biorientation is achieved (129–134). Silencing the checkpoint might require kinetochores to attach specifically to microtubule ends (135, 136). To test for competition specifically between microtubule ends and Mps1 for binding to the kinetochore particles, we developed a 'flipped' assay in which coverslip-tethered kinetochores capture the ends of free, taxol-stabilized microtubules. Kinetochores were tethered to a lipid-passivated surface as described above and then free microtubules (5 – 10 μm in length) were introduced into the flow chamber. Through thermal diffusion, the microtubules tended to attach to the kinetochores primarily by their ends. End-captured microtubules swiveled freely, occasionally also becoming attached via their sides to additional surface-tethered kinetochores (Fig. 4.4). Surface-tethered kinetochores in the same fields of view that had not captured a microtubule served as internal controls. Most of the kinetochore particles that bound

microtubule ends, 93.4 ± 21.4 %, retained Mps1. A smaller fraction of the control particles that did not bind microtubules retained Mps1, 35.2 ± 13.6 %, similar to the retention seen earlier in our experiments without microtubules.

4.3.5 *Mps1 is retained on individual kinetochore particles tracking with disassembling microtubule tips*

For proper chromosome segregation to occur, kinetochores must attach to the tips of disassembling microtubules. The kinetochore first attaches laterally to the side of the microtubule, which is then converted to an end-on attachment as the microtubule shrinks (134). Given this evidence, we hypothesized that the more physiologically relevant attachment to the tip of a dynamic microtubule might be required for Mps1 release. We therefore wanted to determine if Mps1 would release from kinetochores attached to disassembling microtubule tips in our *in vitro* assay. To do this, we first immobilized biotinylated lipid onto a coverslip surface in a flow chamber. Next we introduced Streptavidin, followed by biotinylated GMPCPP seeds. We then introduced a mixture of fluorescent tubulin and isolated fluorescent kinetochores and allowed the tubulin to polymerize off of the tethered guanylyl 5'-α,β-methylenediphosphonate (GMPCPP) seeds. The isolated kinetochores also made attachments to the polymerized microtubules during this incubation period. The assay was performed while maintaining a concentration of free tubulin in the flow chamber. The free tubulin ensured that the polymerized microtubules had a low probability of disassembling.

Next, we induced disassembly of the microtubules via buffer exchange by introducing a low-concentration-tubulin buffer into the flow chamber. The buffer exchange was done on the microscope stage, while simultaneously recording movies of disassembling microtubules with kinetochores attached to their disassembling tips (Fig. 4.5). After collecting several movies over

several experiments, we compared the Mps1 colocalization of the end-associated disassembling kinetochores to kinetochores that were laterally attached to microtubules in the fields of view observed. We calculated a colocalization of 92.9 ± 11.2 % for kinetochores attached to the sides of microtubules and a colocalization of 95.2 ± 21.8 % for kinetochores attached to the ends of the disassembling microtubules (Fig. 4.5). Together, our data indicates that attachment of kinetochores to not just the ends of stable microtubules but also to the ends of disassembling microtubules is insufficient to release Mps1 from the kinetochore.

4.4 DISCUSSION

The spindle assembly checkpoint plays an essential role in maintaining genomic integrity, and understanding the activity of Mps1 and how it responds to microtubule attachment is critical to understanding checkpoint activity. Mps1 recruitment to the kinetochore and phosphorylation of kinetochore components initiates the checkpoint and 'wait' signal. Its release from the kinetochore is also essential to silencing the checkpoint and shutting off the 'wait' signal during cell division. Microtubule attachment is linked to checkpoint silencing *in vivo*. However, direct release of Mps1 through competition with microtubules remains unclear. Currently, there are two models that describe Mps1 response to microtubule attachment. The direct competition model argues that Mps1 and microtubules compete for binding to the kinetochore (51, 118). In a second mechanical switch model, end-on microtubule binding to kinetochores switches Mps1 to an 'off' state by physically separating it and preventing it from phosphorylating its substrate, without necessarily releasing it form the kinetochore (114).

Our work sheds more light on this topic by using *in vitro* assays based on single kinetochore particles and fluorescence microscopy. This allows direct observation of the

interaction between kinetochores and microtubules under various physiologically relevant scenarios. In our study, we use kinetochores isolated from budding yeast carrying fluorescent tags on Mps1 and test them directly by observing the response of Mps1 when bound laterally to the sides, or attached to and tracking the ends of shrinking microtubules.

Although prior experiments provide evidence for direct competition between peptide fragments of Mps1 and Ndc80 for microtubule binding (51, 118), we find that at the level of more intact kinetochore particles microtubules and Mps1 do not strictly compete for kinetochore binding. We can test the mechanical switch model using a fluorescence kinase sensor that allows detection of conformational changes in the presence of microtubules. We propose a third model that involves phosphorylation of Mps1. Mps1 autophosphorylation has been shown to increase the kinase activity of Mps1 and is also required for mitotic progression (123, 137, 138). In a separate experiment, microtubule binding has also been shown to augment Mps1 kinase activity (139). Phosphorylation of Mps1 triggers its release (unpublished), and kinetochores have been shown to contain much higher levels of kinase-dead Mps1(41, 123). We propose that end-on attachment of microtubules and, possibly, tension increases the kinase activity of Mps1 and consequently its release via autophosphorylation.

This model can be tested both at the single particle level using the assays that we have generated to test direct competition between kinetochores and microtubules. In summary, kinetochores can be isolated from yeast with Mps1 and the kinetochores bind to microtubules both laterally and end-on without releasing Mps1. Mps1 release from kinetochores may require autophosphorylation that is enhanced by end-on attachment and tension.

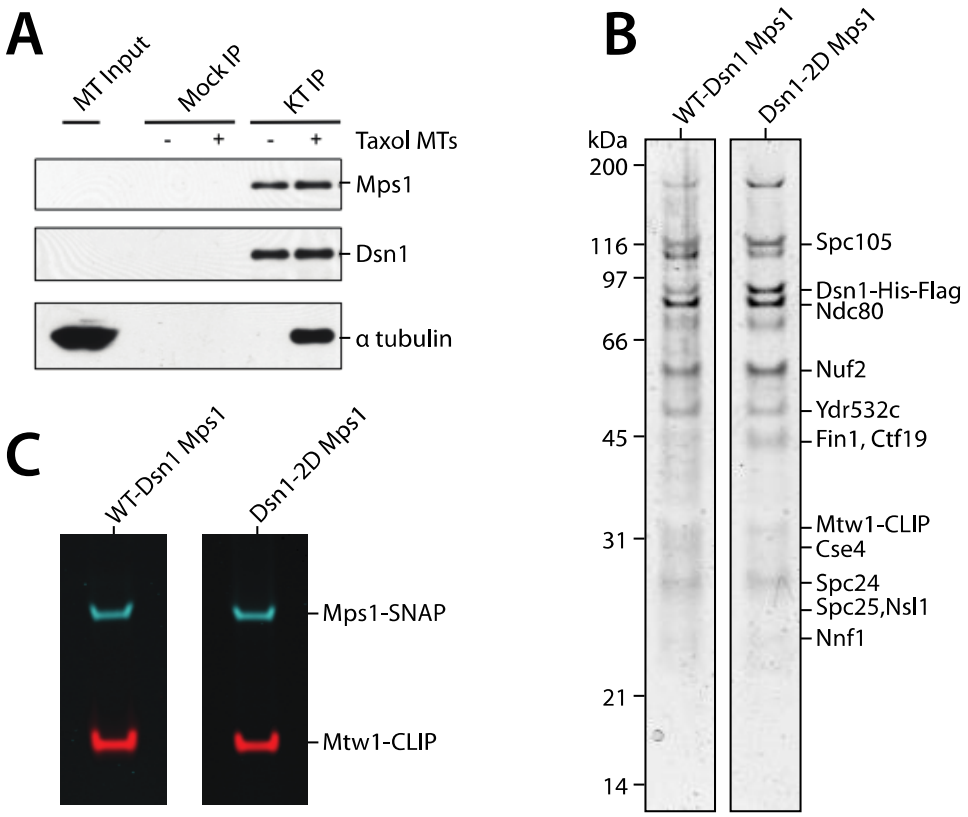

Figure 4.1: Mps1 is not released from kinetochores in a bulk binding assay. (A) Mps1 was detected using a binding assay in the presence of taxol-stabilized microtubules. The lanes in the SDS/PAGE gel from left to right show a microtubule input, a mock immunoprecipitation with and without taxol-stabilized microtubules and kinetochore immunoprecipitation with and without taxol-stabilized microtubules. (B) The relative abundance of core kinetochore proteins that co-purified with Dsn1-His-Flag was similar for both wildtype (WT, SBY12571) and Dsn1-2D (SBY15285) strains. Proteins were separated by SDS/PAGE and detected by silver staining. (C) Typhoon scanning shows that the isolated kinetochore proteins were properly labeled with SNAP on the Mps1 protein and CLIP on the Mtw1 protein.

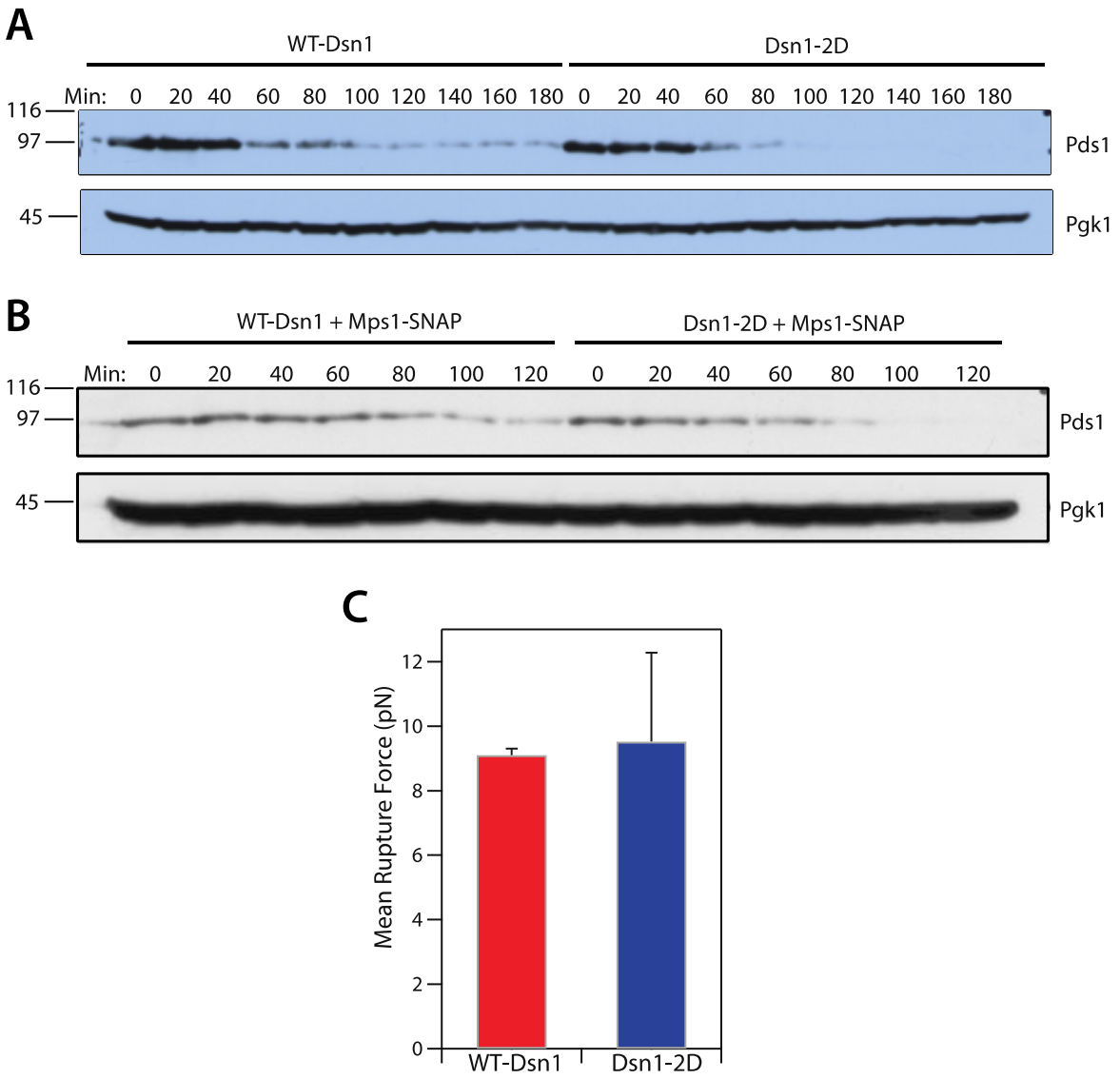

Figure 4.2: Dsn1-2D phosphomimetic mutant strains support normal silencing of the checkpoint 'wait' signal. (A) Wildtype and Dsn1-2D cells were arrested in nocodazole-containing medium and then subsequently released from the checkpoint arrest. Samples were then taken to analyze Pds1 levels by immunoblotting with Anti-myc antibodies at every 20-minute timepoint. (B) Wildtype and Dsn1-2D kinetochores with Mtw1 and Mps1 labeled with CLIP-647 and SNAP-549 dyes were released from checkpoint arrest after a 3-hour incubation in nocodazole-containing medium. Pds1 levels then analyzed by immunoblotting with Anti-myc antibodies. Both sets of cells enter and exit the checkpoint normally. (C) Laser trap assay shows that the Dsn1-2D kinetochores are mechanically functional and rupture at the same force as wildtype kinetochores (*n*=12).

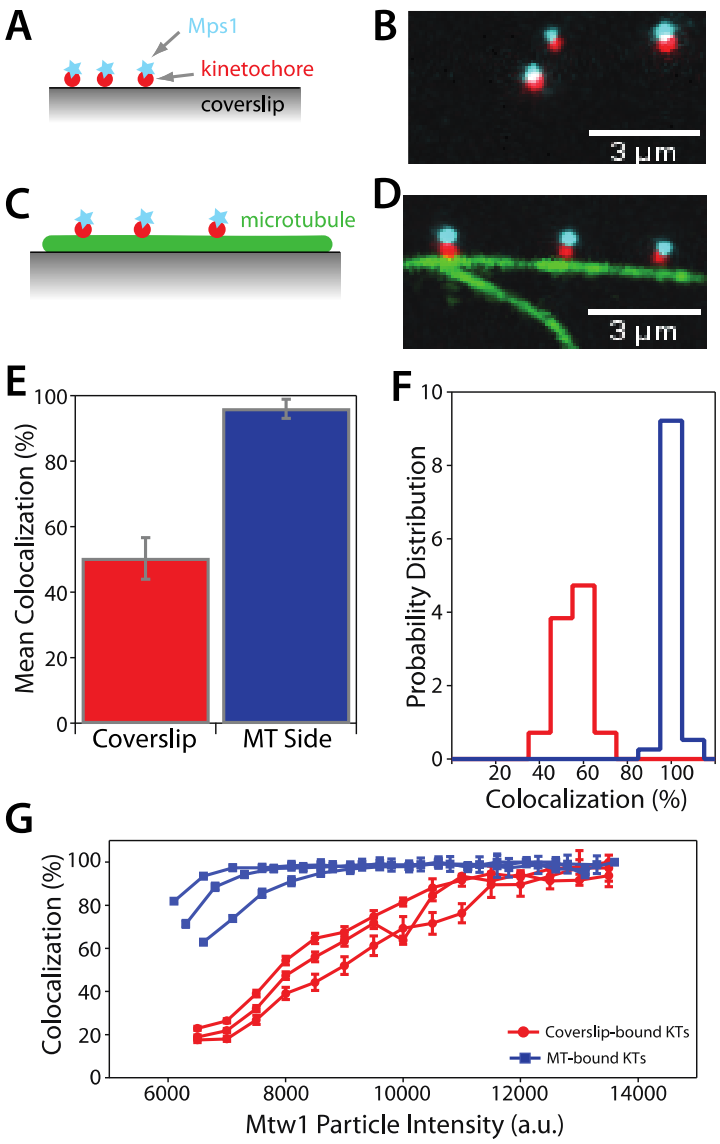

Figure 4.3: Individual kinetochores bound to the side of microtubules retain Mps1. (A) Image showing individual kinetochores specifically linked to a coverslip. The Mps1 protein labeled with SNAP-549 is indicated in cyan and the Mtw1 fiducial protein labeled with CLIP-647 is indicated in red. (B) Schematic of the assay set up for lipid-tethered kinetochores. The kinetochores are immobilized through linkers to a coverslip surface with biotinylated lipid in a flow chamber. (C) Image showing kinetochores linked directly to the side of a microtubule. (D) Schematic of the assay setup in (C). (E) Mean Mps1 colocalization of coverslip-bound kinetochores compared to laterally-bound kinetochores. (F) Probability density comparison between laterally-bound and coverslip-bound kinetochores. (G) Mean Mps1 colocalization compared over increasing Mtw1 particle sizes

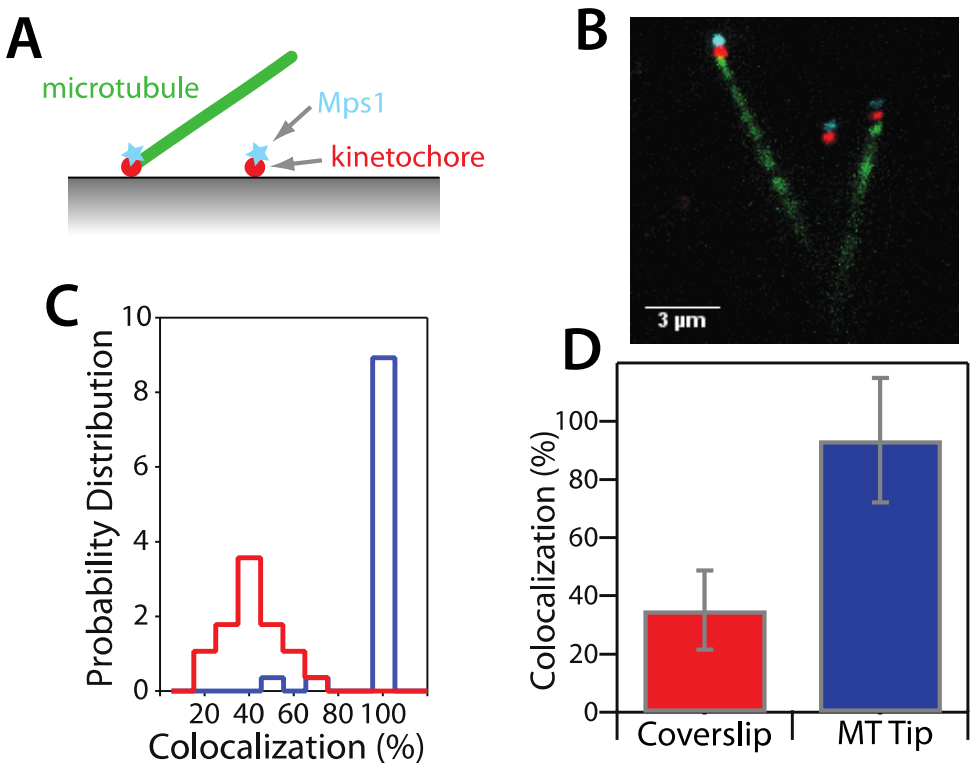

Figure 4.4: Individual kinetochores bound to the ends of microtubules retain Mps1. (A) Schematic of the assay setup for end-associated kinetochores. (B) Image showing end-associated kinetochores. The microtubules have free-flowing ends. (C) Mean Mps1 colocalization of coverslip-bound kinetochores compared to end-bound kinetochores. (D) Probability density comparison between end-associated and coverslip-bound kinetochores

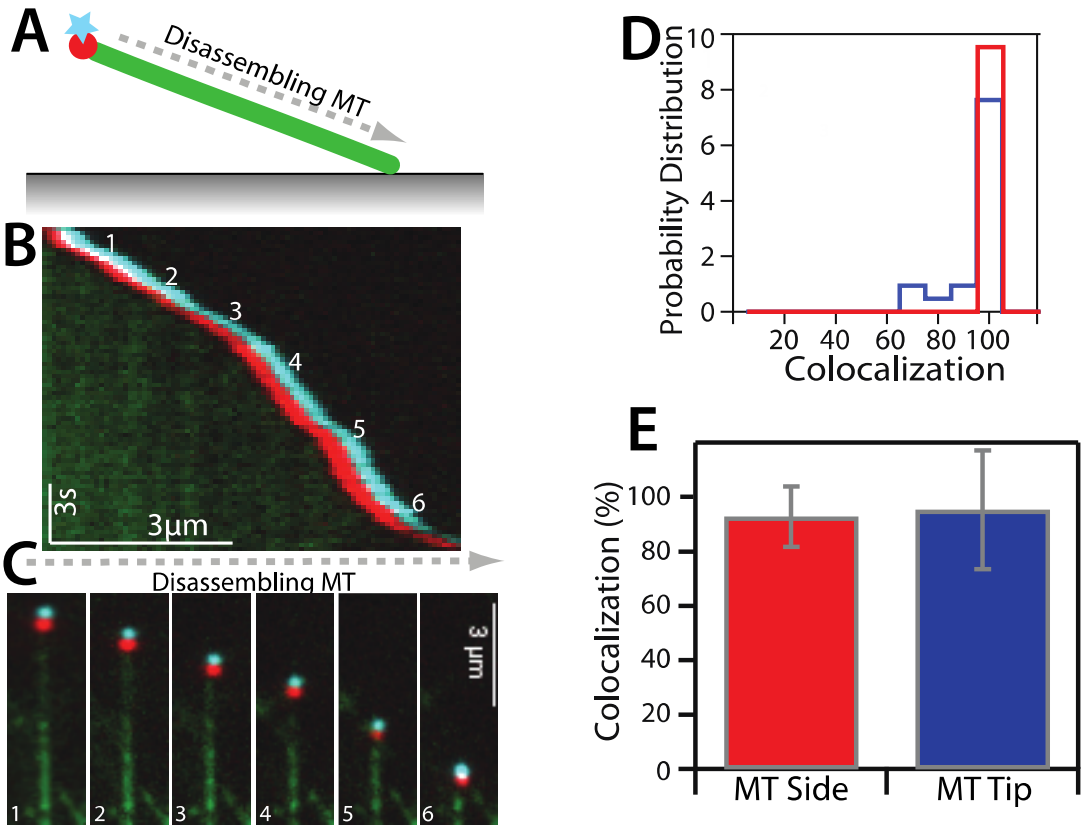

Figure 4.5: Kinetochore particles tracking with disassembling microtubule tips retain Mps1. (A) Schematic of assay setup for tip-tracking kinetochores. (B) Kymograph from a disassembly movie showing disassembling microtubule with end-associated kinetochores. (C) Selected frames from the disassembly movie showing disassembling microtubule with end-associated kinetochore. (D) Mean Mps1 colocalization of side-bound kinetochores compared to tip-tracking kinetochores. (E) Probability density comparison between side-bound kinetochores and tip-tracking kinetochores

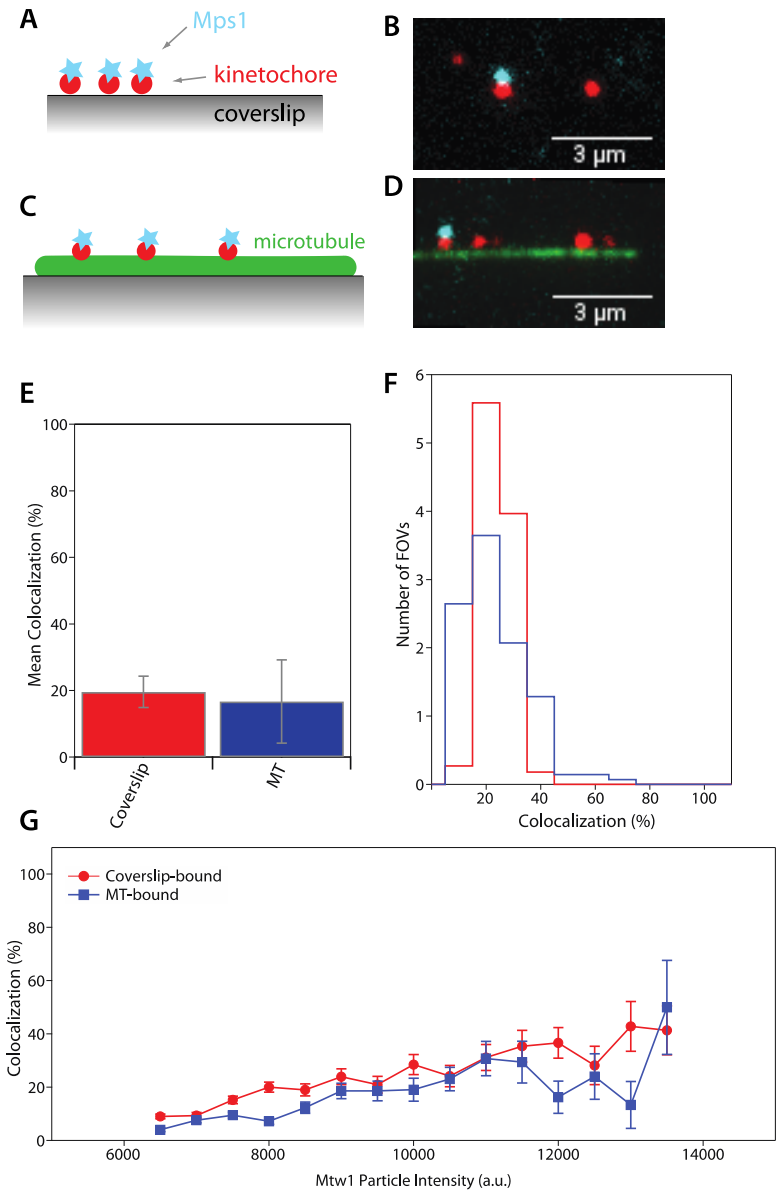

Figure 4.6: Individual wildtype Dsn1 kinetochores bound to the side of microtubules retain Mps1, similar to Dsn1-2D kinetochores. (A) Image showing individual kinetochores specifically linked to a coverslip. The Mps1 component labeled with SNAP-549 is indicated in cyan and the Mtw1 fiducial component labeled with CLIP-647 is indicated in red. (B) Schematic of the assay set up for lipid-tethered kinetochores. The kinetochores are immobilized through linkers to a coverslip surface with biotinylated lipid in a flow chamber. (C) Image showing kinetochores linked directly to the side of a microtubule. (D) Schematic of the assay setup in (C). (E) Mean Mps1 colocalization of coverslip-bound kinetochores compared to laterally-bound kinetochores. (F) Probability density comparison between laterally-bound and coverslip-bound kinetochores. (G) Mean Mps1 colocalization compared over increasing Mtw1 particle sizes.

Table 4.1: All yeast strains used in this study. SBY 15285 is the is the yeast strain from which the Mtw1-CLIP-647, Mps1-SNAP-549 kinetochores were isolated for most of the experimentation in this study.

Strain	Genotype
SBY4880	*MATa ura3-1 leu2-3,112 his3-11 trp1-1 LYS2 bar1-1 can1-100 ade2-1 Pds1-myc18:LEU2*
SBY8066	*MATa ura3-1 leu2-3,112 his3-11:Dsn1-2D-HIS3 trp1-1 lys2Δ bar1 PDS1-myc18:LEU2 ade2-1 dsn1ΔKanMX*
SBY10485	*MATa ura3-1 leu2-3,112 his3-11 trp1-1 can1-100 ade2-1 bar1-1 Dsn1-HIS-FLAG:URA3 Mtw1-CLIP:KanMX6 Nuf2-SNAP:HPH*
SBY12571	*MATa ura3-1 leu2-3,112 his3-11 trp1-1 can1-100 ade2-1 bar1-1 Dsn1-HIS-FLAG:URA3 Mps1-SNAP:Hph Mtw1-CLIP:KanMX6*
SBY 15282	*MATa ura3-1 leu2-3,112 his3-11 trp1-1 can1-100 ade2-1 bar1-1 Dsn1-2D-6HIS-3Flag::URA3 Nuf2-SNAP:Hph Mtw1-CLIP:KanMX6*
SBY 15285	*MATa ura3-1 leu2-3,112 his3-11 trp1-1 can1-100 ade2-1 bar1-1 Dsn1-2D-6HIS-3Flag::URA3 Mtw1-CLIP:KanMX6 Mps1-SNAP:HPH*
SBY16381	*MATa ura3-1 leu2-3,112 his3-11 trp1-1 can1-100 ade2-1 bar1-1 Dsn1-6HIS-3FLAG:URA3 Mps1-SNAP:Hph Mtw1-CLIP:KanMX6 Pds1-myc18:LEU2*
SBY16417	*MATa ura3-1 leu2-3,112 his3-11 trp1-1 can1-100 ade2-1 bar1-1 Dsn1-2D-6HIS-3Flag::URA3 Pds1-myc18::LEU2 Mps1-SNAP:Hph Mtw1-CLIP:KanMX*

Chapter 5. CONCLUSIONS & FUTURE DIRECTIONS

Briefly, I have shown that I can purify native functional budding yeast kinetochores with detectable checkpoint proteins. I have also developed a system to analyze the particles after TIRF image acquisition. Finally, I showed that the Mps1 kinase does not directly compete with microtubules for binding to kinetochores at the single particle level using the purified kinetochores. The assays that I have developed can be further altered to answer other scientific questions relating to mitosis in the future.

5.1 The Path To The Successful Mps1 Kinase Assay

The first checkpoint protein genes, Bub1, Bub3, Mad1 and Mad2, were discovered via genetic screens in budding yeast cells (18, 19). The MAD and BUB proteins are recruited to unattached kinetochores early in mitosis and disappear from the kinetochores when they form attachments to microtubules (26). My first efforts to study the spindle assembly checkpoint were focused on successfully purifying dual-labeled kinetochores that could be detected at the single particle level using a TIRF assay. Once that was successful, I turned my attention towards Bub1. My goal was to purify kinetochores with fluorescent labels on Mtw1 and Bub1. I chose to focus, first, on Bub1 because it had been extensively studied. Also, at the time the checkpoint signaling cascade was not as well understood. The dependence of Bub1 and Mad1 recruitment on Mps1 phosphorylation had not been fully realized.

I purified kinetochores with the SNAP- and CLIP-tags on Bub1 and Mtw1, respectively. I then measured the Bub1 colocalization when kinetochores were bound to a coverslip surface, and when they were attached to taxol-stabilized microtubules. I determined a colocalization that ranged from anywhere between 3% to 10% when the kinetochores were coverslip-tethered, and

10% to 40% when attached to taxol-stabilized microtubules (Figs 5.1 & 5.2). However, at the time we thought the particles I was purifying had too much heterogeneity. The heterogeneity in the particles is evident in acquired images, as well as in the analysis of the brightness of the particles (Figs. 3.4 and 3.6). Also, the colocalization measured for the particles was very low. Our initial hypothesis was that Bub1 and Mad1 colocalization would be lower for microtubule-bound particles based on evidence that the checkpoint proteins are released from kinetochores when they go from being unattached to attached to microtubules. However, we saw an increase in colocalization of microtubule-bound particles, which was the exact opposite of what we expected based on our initial hypothesis. Due to the very low colocalization levels I measured, we worried that the increase in microtubule-bound colocalization could simply be an artefact of microtubules selecting for more complete kinetochore particles. The very low baseline colocalization, combined with the heterogeneity in purified particles, made interpretation of the data quite challenging. The implication of the observed increase in colocalization with respect to our hypothesis was unclear. Given the heterogeneity in the purified kinetochores, we devoted a considerable amount of effort to purifying more stable kinetochores. I also devoted some effort to ensuring that the kinetochores were not falling apart in buffer during the experiment. Kinetochores are kept in buffer with 15% glycerol during the purification process to help keep the kinetochores stable in solution, and especially during the multiple freeze-thaws they undergo. However, during the assays I developed for TIRF imaging, there was no glycerol in the buffer. To ensure that lack of glycerol was not the cause for the low colocalization, I tested the kinetochores in a 15% glycerol buffer. I did not observe any increase in colocalization (Fig. 5.3). We also tried to increase the number of larger and more stable kinetochore particles by passing them through a size-exclusion column after purification. I tested this in Mtw1 and Nuf2-labeled

kinetochores, and saw very minimal increase in the level of colocalization (Fig. 5.4). One other disadvantage with using the column was that it resulted in reduced concentration of the kinetochore particle samples. Attempts to increase the population of brighter, stable particles by running the kinetochores through a sucrose gradient also yielded minimal effect on colocalization, and resulted in dilution.

Mad1 was the second checkpoint protein I focused on. I purified kinetochores with a SNAP-tag-dependent fluorescent label on Mad1 and a second label on Mtw1. Mad1 exhibited even lower and more variable colocalization when bound to the coverslip surface. I measured colocalization levels between <1% and 10% for these kinetochores, over a wide range of experiments. Another idea we developed to generate brighter particles was a dual purification procedure using two different tags. Briefly, the kinetochores were purified through a FLAG tag on Dsn1. We also endogenously engineer a V5 tag on Spc24, which is a component of the Ndc80 protein. We could, thus, first pull down kinetochores using the FLAG epitope and then re-purify them via the V5 epitope tag on the Spc24 protein. This would, in principle, select kinetochores with more microtubule-binding elements from the already FLAG-tag purified kinetochores. Again, I saw some increase in the colocalization level, but not high enough to continue to pursue this purification method for my assays (Fig. 5.6). The other disadvantage with this dual purification method was that it took longer, which usually results in more kinetochores falling apart. The above-mentioned strategies were used to try to improve the measured kinetochore colocalization levels early in the project, with little to no success. The success that I eventually saw on this project can be attributed to several specific alterations in the kinetochore purification process and the single particle assays.

First, work done by several labs that identified Mps1 upstream of the checkpoint signaling cascade was very critical to the success of this project. Mps1 kinase phosphorylation is what recruits and localizes Bub1 and Mad1 to the kinetochore (30–33). These findings allowed me to switch focus from trying to purify stable Mad1 and Bub1-labeled kinetochores to Mps1, and proved to be a major turning point in this project. Second, we decided to test Dsn1-2D kinetochores. As mentioned earlier in this document, the mutation in the two sites in Dsn1 results in more stable particles. Third, I switched from using a blender to using the Freezer Mill to lyse frozen harvested cells during kinetochore purification. Using the blender involved stopping the blender and adding dry ice to the frozen yeast cells in time intervals to reduce the heat generated from the machine. This helped to prevent the cells from completely melting. The Freezer Mill, however, does not require any interference when grinding cells. The frozen cells are ground while simultaneously submerged in liquid nitrogen. This prevents any temperature fluctuations that may be detrimental to the proteins being purified. Fourth, the development of the phospholipid bilayer for surface passivation helped to remove the tediousness and time consumption associated with blocking surfaces with PEG. Poorly passivated coverslips could be easily remade using the phospholipid bilayer. Finally, the introduction of the focus detection lock allowed large amounts of data to be collected on the TIRF system. This gave us a lot of confidence in our data.

I believe these improvements in the purification and TIRF assay were the most important in driving this project forward. It would be very interesting to test Bub1 and Mad1-labeled kinetochores with the purification process and assays as currently established. I mentioned earlier that our hypothesis was that colocalization would be reduced in microtubule-bound kinetochores. In retrospect, it is quite possible that the increased colocalization in Bub1-labeled

kinetochores when attached to taxol-stabilized microtubules is true, given how our Mps1 results turned out.

5.2 Future Directions

5.2.1 *In vitro Measurement of Mps1 Separation*

I have shown, through my *in vitro* assays, using isolated kinetochores that Mps1 and microtubules do not directly compete for binding to kinetochores. This is contrary to evidence provided in bulk assays using recombinant fragments of Mps1 and Ndc80 (51, 118). Other evidence suggests that microtubule binding doesn't directly compete off Mps1 from kinetochores. Per an alternative model, end-on microtubule attachment to the kinetochore results in the CH domain of Ndc80 being pulled outward. Since Mps1 binds to the CH domain of Ndc80, the model argues that Mps1 is separated from Spc105 rendering it unable to phosphorylate Spc105. This results in the silencing of the spindle assembly checkpoint (114). I propose that this model could be tested *in vitro* using our assay system.

The assays I have developed can be used to measure intermolecular distances between Mps1 and other core kinetochore components. The architecture of the kinetochore has already been mapped out in several experiments with nanometer accuracy (140–142). Kinetochores carrying SNAP- and CLIP-tags on Mps1 and a core kinetochore component, respectively, can be isolated. The kinetochores can, then, be tethered specifically to a phospholipid bilayer as described previously using linkers. The distance between Mps1 and the core kinetochore component can be measured with nanometer precision using the TIRF system. The distance measurements can also be repeated in the presence of microtubules.

In the first experiment, taxol-stabilized fluorescent microtubules could be tethered to the phospholipid bilayer. The kinetochores could be attached laterally to the microtubules. The intermolecular distance could then be measured for kinetochores that are attached to the microtubules with detectable Mps1 and core components. During cell division, kinetochores first attach laterally to microtubules. Lateral attachments are converted to end-on attachments as dynamic microtubules go through cycles of assembly and disassembly (131, 132, 134). Thus, the intermolecular distance between Mps1 and a core inner kinetochore protein in two physiologically relevant attachment conformations in the absence of tension, could also be determined. Changes in distance when kinetochores are bound to the ends of taxol-stabilized and when they are bound to and tracking progressively with the end of shrinking microtubules could also be determined. Movies of end-associated kinetochores, as well as kinetochores tracking processively with dynamic microtubules can be collected.

Changes in the intermolecular distance between Mps1 and the corresponding core kinetochore protein when the kinetochores is bound to the side of the microtubule, and when it is bound to and tracking processively with the dynamic microtubule tip could be measured and compared. Such experiments could provide a clear and direct observation of singe molecule events, and help determine if kinetochore-microtubule attachment causes spatial separation of Mps1. Mps1 kinase phosphorylates MELT motifs in Spc105. Therefore, it would be ideal to endogenously engineer the CLIP-tag into the Spc105 core kinetochore protein.

5.2.2 *Release of Mps1 from Kinetochore via Autophosphorylation*

We discovered in our *in vitro* assays that Mps1 is not released from kinetochores when they are bound to microtubules. We, therefore, proposed a model that relies on phosphorylation-mediated Mps1 release. Mps1 autophosphorylation has been shown to increase the kinase

activity of Mps1 and is also required for mitotic progression (123, 137, 138). The kinase activity of Mps1 has also been shown to be enhanced by the presence of microtubules (139). In the model I am proposing, stable bioriented end-on microtubule binding to kinetochores enhances the kinase activity of Mps1, resulting in the release of Mps1 from the kinetochore via autophosphorylation. This model can be tested via a series of experiments.

First, the response of Mps1 to phosphorylation can be tested by adding kinase in a bulk biochemical assay. Kinetochores carrying SNAP- and CLIP-tags on Mps1 and Mtw1, respectively, can be purified as previously described (52). After the 30-minute dye-labeling step during the kinetochore purification, Mps1 kinase buffer (500 μL of 1 M HEPES-KOH pH 8.0, 100 μL of 1 M $MgCl_2$, 100 μL of 50% glycerol, 20 μL of 100 mM ATP, 30 μL of distilled H_2O) can be added to the Dynabeads with the kinetochores. The kinase can be allowed to react with the kinetochores for 30 minutes at a temperature of 30 ^oC. After the 30-minute incubation period, the supernatant can be aspirated, and the kinetochores eluted from the Dynabeads. Based on our model, if Mps1 is released from the kinetochore via autophosphorylation then the supernatant should contain more Mps1 than in the eluate. In preliminary experiments, I have shown that Mps1 kinase does indeed release from the kinetochore when phosphorylated in a bulk reaction. I ran the proteins in comparison to a control experiment without ATP on an SDS/PAGE gel, and then performed a typhoon scan to determine the level of Mps1 and Mtw1 in the proteins (Fig. 5.1). I then took the kinetochores from the bulk assay and specifically tethered them to a biotinylated phospholipid surface in a coverslip flow chamber. I imaged the kinetochores, determined the level of Mps1 colocalization and compared that to the kinetochores that did not undergo a kinase reaction. I found that the colocalization was reduced in the kinetochores as

expected from the typhoon scan (Fig. 5.1). The Mps1 release in the bulk assay via kinase addition was detectable at the single particle level using TIRF.

An analogous assay can also be performed at the single particle level, by first tethering kinetochores to the phospholipid surface, and then flowing in Mps1 kinase buffer. Image acquisition and analysis can then be performed to measure the colocalization of the kinetochore particles. In a preliminary experiment, I have seen a small reduction in the level of colocalization of specifically tethered kinetochores that have undergone a 30-minute kinase buffer incubation (Fig. 5.1). As mentioned earlier, microtubule binding enhances the kinase activity of Mps1. I have proposed in our model that this enhanced kinase activity could result in Mps1 release from the kinetochore. Thus, in a separate experiment, Mps1 kinase buffer can be added to kinetochores that are already bound to microtubules. This assay can be performed for kinetochores bound to the sides of microtubules as well as kinetochores that are attached to the ends of microtubules. The differences can be assessed to determine if the level of Mps1 release correlates with how kinetochores are attached to microtubules.

5.2.3 *Determining the Role of Tension in Mps1 Release*

For proper chromosome segregation to occur there must be proper and stable kinetochore attachment and, possibly, tension. As the body of knowledge on checkpoint activation and silencing continues to grow there continues to be an attachment versus tension debate (14). There is evidence to show that attachment of kinetochores to microtubules is sufficient to turn off checkpoint activity during cell division (24). There is also other evidence that indicates that lack of tension at the kinetochore leads to checkpoint activation and, thus, tension is a requirement for ‘wait’ signal silencing (23). One of the major reasons for this debate is the inability of *in vivo* assays to unambiguously distinguish between the attachment status of kinetochores and levels of

tension, due to both phenomena happening almost simultaneously. I believe that an *in vitro* single particle biophysical assay that allows attachment status and levels of tension to be independently measured provides the best solution to this problem. To this end, a dual instrumentation system that combines optical tweezers with multi-color TIRF imaging has been developed to address this problem (107). The system allows fluorescent single kinetochores to be monitored with nanometer precision, whilst simultaneously applying mechanical tension to kinetochore-microtubule attachments. It also incorporates video-enhanced differential interference contrast (VE-DIC) microscopy to allow the use of unlabeled microtubule in assays. This helps to reduce the risk of photobleaching and photodamage during image acquisition.

Dual-tagged kinetochores with fluorescent labels on Mps1 and Mtw1 can be specifically tethered to a biotinylated phospholipid surface in a coverslip flow chamber. Polymerized taxol-stabilized microtubules can then be fed into the chamber and allowed to make end-on attachments with the tethered kinetochores. Kinesin-functionalized polystyrene beads can be introduced into the flow chamber gently. After a brief period of incubation, the slide can then be mounted onto the microscope stage and a 'search' can be done to identify end-on attached kinetochores carrying both fluorescent tags. Next, the bead can be trapped and the VE-DIC can then be used to help guide the bead to the microtubule. After attachments on both ends of the microtubule are established, a customized LabVIEW program can be used, through the piezo stage, to apply pico-Newton level forces to the kinetochore-microtubule attachment. While tension is being applied through the optical tweezers, TIRF images and movies can be acquired to determine if the level of Mps1 is reduced during the application of tension. This will provide a direct measurement of the effect of tension on Mps1 release. Intermolecular spatial distance changes between Mps1 and Mtw1 can also be monitored using the images collected.

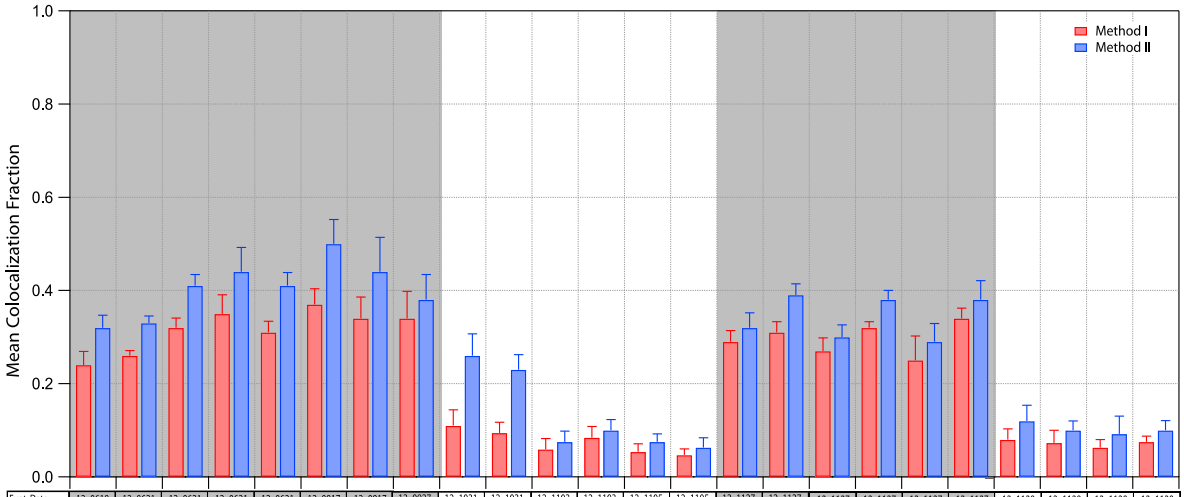

	Expt. Date	12_0618	12_0621	12_0621	12_0621	12_0621	12_0917	12_0917	12_0927	12_1031	12_1031	12_1103	12_1103	12_1105	12_1105	12_1127	12_1127	12_1127	12_1127	12_1127	12_1127	12_1129	12_1129	12_1129	12_1129
	Expt. #	I	I	II	III	IV	I	II	I	I	II	I	II	I	II	I	II	III	IV	I	II	I	II	III	IV
	Strain	SBY10485	SBY10485	SBY10485	SBY10485	SBY10485	SBY10485	SBY10485	SBY10485	SBY10696	SBY10696	SBY10696	SBY10696	SBY10696	SBY10696	SBY10485	SBY10485	SBY10485	SBY10485	SBY10485	SBY10485	SBY10696	SBY10696	SBY10696	SBY10696
	Made by:	N.D.	N.D.	N.D.	N.D.	N.D.	N.D.	N.D.	S.C.	S.C.	S.C.	S.C.	S.C.	S.C.	S.C.	S.C.	S.C.	S.C.	S.C.	S.C.	S.C.	S.C.	S.C.	S.C.	S.C.
	Made on:	12_0507	12_0507	12_0507	12_0507	12_0507	12_0507	12_0507	12_0925	12_1010	12_1010	12_1010	12_1010	12_1010	12_1010	12_0925	12_0925	12_0925	12_0925	12_0925	12_0925	12_1010	12_1010	12_1010	12_1010
	Fiducial	Mtw1	Mtw1	Mtw1	Mtw1	Mtw1	Mtw1	Mtw1	5x-Mtw1	Mtw1	Mtw1	Mtw1	Mtw1	Mtw1	Mtw1	5x-Mtw1	5x-Mtw1	5x-Mtw1	5x-Mtw1	Mtw1	Mtw1	Mtw1	Mtw1	Mtw1	Mtw1
	Secondary	Nuf2	Nuf2	Nuf2	Nuf2	Nuf2	Nuf2	Nuf2	Nuf2	Bub1	Bub1	Bub1	Bub1	Bub1	Bub1	Nuf2	Nuf2	Nuf2	Nuf2	Nuf2	Nuf2	Bub1	Bub1	Bub1	Bub1
	Coverslip	Plasma	Plasma	Plasma	Plasma	Plasma	Plasma	Plasma	Plasma	Plasma	Plasma	Plasma	Plasma	Plasma	Plasma	Plasma	Plasma	Plasma	Plasma	Plasma	Plasma	Plasma	Plasma	Plasma	Plasma
	Fiducial Tag	CLIP-547	CLIP-547	CLIP-547	CLIP-547	CLIP-547	CLIP-647	CLIP-647	CLIP-647	CLIP-647	CLIP-647	CLIP-647	CLIP-647	CLIP-647	CLIP-647	CLIP-647	CLIP-647	CLIP-647	CLIP-647	CLIP-647	CLIP-647	CLIP-647	CLIP-647	CLIP-647	CLIP-647
	Secondary Tag	SNAP-488	SNAP-488	SNAP-488	SNAP-488	SNAP-488	SNAP-549	SNAP-549	SNAP-549	SNAP-549	SNAP-549	SNAP-549	SNAP-549	SNAP-549	SNAP-549	SNAP-549	SNAP-549	SNAP-549	SNAP-549	SNAP-549	SNAP-549	SNAP-549	SNAP-549	SNAP-549	SNAP-549
	Wash	YES	YES	YES	YES	YES	NO	NO	NO	NO	NO	YES	YES	YES	YES	YES	YES	YES	YES	YES	YES	YES	YES	YES	YES
	Coloc (m1)	0.24±0.029	0.26±0.011	0.32±0.021	0.35±0.041	0.31±0.024	0.37±0.034	0.34±0.046	0.34±0.058	0.11±0.034	0.094±0.023	0.059±0.023	0.084±0.024	0.054±0.017	0.047±0.013	0.29±0.024	0.31±0.023	0.27±0.028	0.32±0.013	0.25±0.052	0.34±0.022	0.080±0.023	0.073±0.027	0.063±0.017	0.075±0.012
	Coloc (m2)	0.32±0.027	0.33±0.015	0.41±0.024	0.44±0.052	0.41±0.028	0.50±0.052	0.44±0.074	0.38±0.054	0.26±0.047	0.23±0.032	0.075±0.023	0.010±0.023	0.075±0.017	0.063±0.021	0.32±0.032	0.39±0.024	0.30±0.026	0.38±0.020	0.29±0.039	0.38±0.041	0.12±0.034	0.10±0.020	0.092±0.038	0.10±0.021
Spots per Field	Fiducial	474±30	398±30	472±16	212±15	209±14	210±18	161±19	252±35	116±17	150±32	87±16	129±22	191±12	96±13	164±17	258±24	196±19	209±11	96±12	91±4	131±11	127±16	133±12	120±6
	Secondary	501±14	455±28	541±18	420±16	403±6	630±61	563±92	310±24	542±19	508±23	64±9	85±8	111±11	62±9	196±13	369±56	186±15	237±14	146±12	171±12	136±15	142±10	122±14	111±9

Figure 5.1: Summary of early data from coverslip-tethered Nuf2 and Bub1-labeled kinetochores. Several experiments were performed using Nuf2 kinetochores and Bub1 kinetochores attached to coverslip surfaces. The kinetochores used in these experiments were prepared using a blender to grind harvested cells. Also, the kinetochores were immobilized on the coverslip surface without a phospholipid bilayer. The Nuf2 data is shaded grey. The kinetochore colocalization levels were very low in the Bub1 experiments.

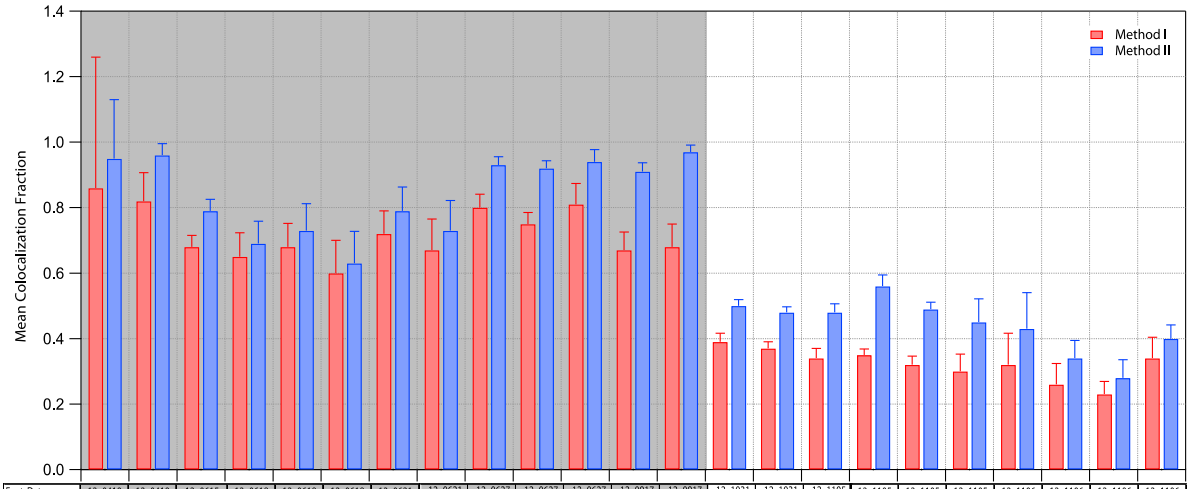

	Expt. Date	12_0419	12_0419	12_0615	12_0618	12_0618	12_0618	12_0621	12_0621	12_0627	12_0627	12_0627	12_0917	12_0917	12_1031	12_1031	12_1105	12_1105	12_1105	12_1105	12_1106	12_1106	12_1106	12_1106
	Expt. #	I	II	I	I	II	III	I	II	I	II	III	I	II	I	II	I	II	III	IV	I	II	III	IV
	Strain	SBY10458	SBY10458	SBY10485	SBY10485	SBY10485	SBY10485	SBY10485	SBY10485	SBY10485	SBY10485	SBY10485	SBY10485	SBY10485	SBY10696	SBY10696	SBY10696	SBY10696	SBY10696	SBY10696	SBY10696	SBY10696	SBY10696	SBY10696	SBY10696
	Made by:	N.D.	N.D.	N.D.	N.D.	N.D.	N.D.	N.D.	N.D.	N.D.	N.D.	N.D.	N.D.	N.D.	S.C.	S.C.	S.C.	S.C.	S.C.	S.C.	S.C.	S.C.	S.C.	S.C.	S.C.
	Made on:	12_0413	12_0413	12_0507	12_0507	12_0507	12_0507	12_0507	12_0507	12_0507	12_0507	12_0507	12_0507	12_0507	12_1010	12_1010	12_1010	12_1010	12_1010	12_1010	12_1010	12_1010	12_1010	12_1010	12_1010
	Fiducial	Mtw1	Mtw1	Mtw1	Mtw1	Mtw1	Mtw1	Mtw1	Mtw1	Mtw1	Mtw1	Mtw1	Mtw1	Mtw1	Mtw1	Mtw1	Mtw1	Mtw1	Mtw1	Mtw1	Mtw1	Mtw1	Mtw1	Mtw1	Mtw1
	Secondary	Nuf2	Nuf2	Nuf2	Nuf2	Nuf2	Nuf2	Nuf2	Nuf2	Nuf2	Nuf2	Nuf2	Nuf2	Nuf2	Bub1	Bub1	Bub1	Bub1	Bub1	Bub1	Bub1	Bub1	Bub1	Bub1	Bub1
	Fiducial Tag	CLIP-488	CLIP-488	CLIP-488	CLIP-547	CLIP-547	CLIP-547	CLIP-547	CLIP-547	CLIP-547	CLIP-647	CLIP-647	CLIP-647	CLIP-647	CLIP-647	CLIP-647	CLIP-647	CLIP-647	CLIP-647	CLIP-647	CLIP-647	CLIP-647	CLIP-647	CLIP-647	CLIP-647
	Secondary Tag	SNAP-549	SNAP-549	SNAP-549	SNAP-488	SNAP-488	SNAP-488	SNAP-488	SNAP-488	SNAP-488	SNAP-549	SNAP-549	SNAP-549	SNAP-549	SNAP-549	SNAP-549	SNAP-549	SNAP-549	SNAP-549	SNAP-549	SNAP-549	SNAP-549	SNAP-549	SNAP-549	SNAP-549	SNAP-549
	Coverslip	PEGylated	PEGylated	PEGylated	PEGylated	PEGylated	PEGylated	PEGylated	PEGylated	PEGylated	PEGylated	PEGylated	PEGylated	Plasma	Plasma	Plasma	Plasma	Plasma	Plasma	Plasma	PEGylated	PEGylated	PEGylated	PEGylated	PEGylated
	Wash	YES	YES	YES	YES	YES	YES	YES	YES	YES	YES	YES	YES	YES	YES	YES	YES	YES	YES	YES	YES	YES	YES	YES	YES
	Coloc (m1)	0.86±.040	0.82±0.087	0.68±0.035	0.65±0.073	0.68±0.072	0.60±0.10	0.72±0.070	0.67±0.095	0.80±0.041	0.75±0.035	0.81±0.064	0.67±0.055	0.68±0.070	0.39±0.026	0.37±0.020	0.34±0.030	0.35±0.018	0.32±0.026	0.30±0.052	0.32±0.096	0.26±0.064	0.23±0.039	0.34±0.064
	Coloc (m2)	0.95±.018	0.96±0.035	0.79±0.035	0.69±0.068	0.73±0.082	0.63±0.097	0.79±0.073	0.73±0.092	0.93±0.025	0.92±0.023	0.94±0.037	0.91±0.027	0.97±0.021	0.50±0.019	0.48±0.017	0.48±0.026	0.56±0.034	0.49±0.021	0.45±0.071	0.43±0.11	0.34±0.054	0.28±0.055	0.40±0.042
Spots per Field	Fiducial	80±13	32±12	89±14	133±28	131±14	91±22	69±17	87±36	87±12	83±16	56±14	60±17	99±31	134±25	157±19	112±31	116±18	107±38	88±18	64±20	56±17	72±46	45±16
	Secondary	188±34	61±24	237±36	140±27	148±18	82±28	70±18	96±44	171±19	173±27	161±31	132±29	156±37	83±14	93±10	89±28	91±13	74±24	75±12	38±16	30±10	32±16	26±12
Spots per Mask Area	Fiducial (x100)	0.11±0.014	0.22±0.045	0.076±0.0077	0.15±0.014	0.18±0.025	0.17±0.016	0.22±0.020	0.18±0.030	0.11±0.011	1.00±0.012	0.072±0.016	0.15±0.017	0.23±0.031	0.26±0.038	0.26±0.029	0.21±0.031	0.27±0.052	0.21±0.041	0.16±0.026	0.22±0.034	0.16±0.011	0.16±0.084	0.19±0.017
	Secondary (x100)	0.25±0.013	0.42±0.043	0.20±0.0086	0.16±0.024	0.20±0.028	0.16±0.036	0.22±0.016	0.19±0.040	0.21±0.0010	0.21±0.012	0.21±0.021	0.35±0.038	0.37±0.040	0.16±0.008	0.16±0.014	0.17±0.025	0.21±0.031	0.14±0.015	0.14±0.0066	0.12±0.024	0.085±0.014	0.074±0.013	0.10±0.017

Figure 5.2: Summary of early data from taxol-stabilized microtubule-attached Nuf2- and Bub1-labeled kinetochores. Several experiments were performed using Nuf2 kinetochores and Bub1 kinetochores attached to microtubules. The kinetochores used in these experiments were prepared using a blender machine to grind harvested cells. The microtubules were attached to the coverslip surface using rigor kinesin on. The Nuf2 data is shaded grey.

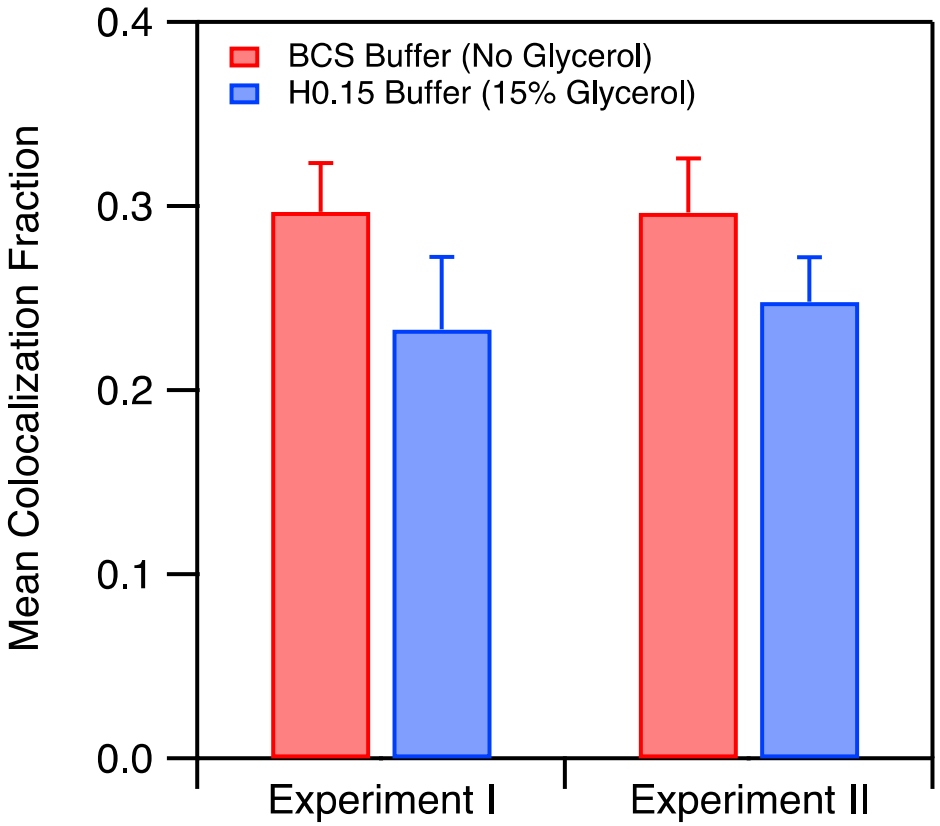

Figure 5.3: Addition of glycerol to TIRF assay buffer does not improve colocalization. Kinetochores are purified in a 15% glycerol buffer. However, using the same glycerol concentration in the TIRF assay buffer did not show any improvement in Nuf2-Mtw1 colocalization when the kinetochores were immobilized on a coverslip surface.

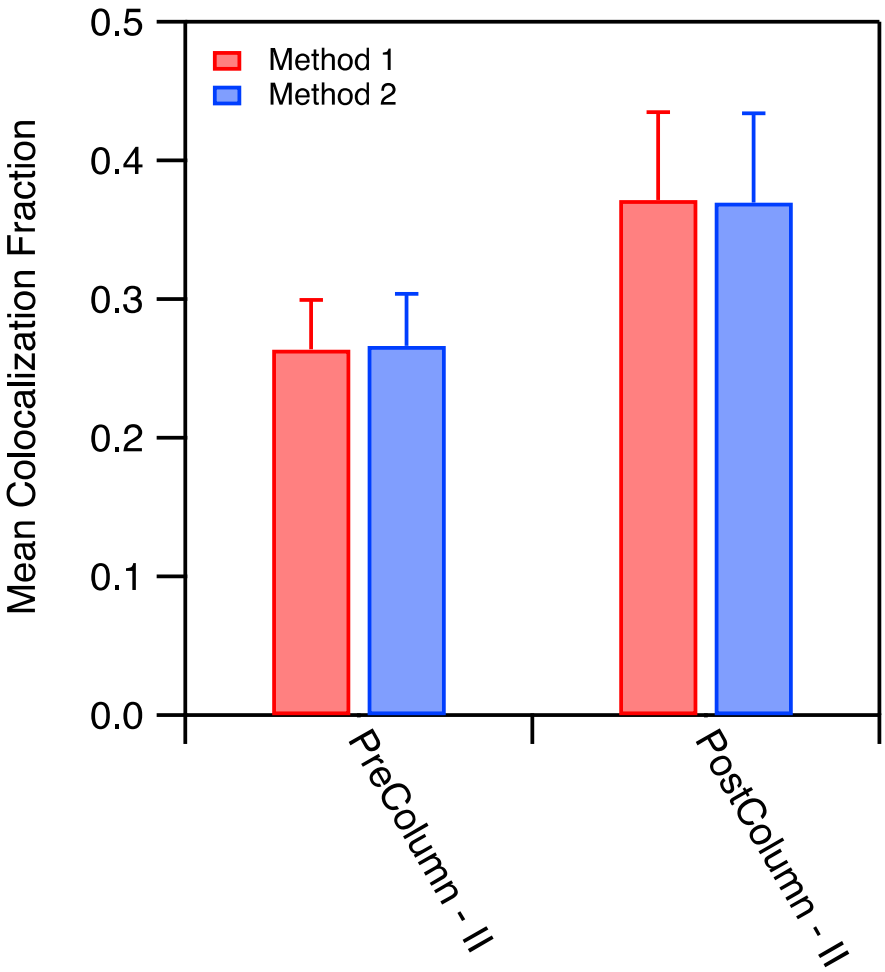

Figure 5.4: Column separation does not significantly increase kinetochore colocalization. To help generate more stable kinetochores, Nuf2-labeled kinetochores were ran through a size exclusion column after purification. This process did not increase the level of colocalization of the kinetochore particles.

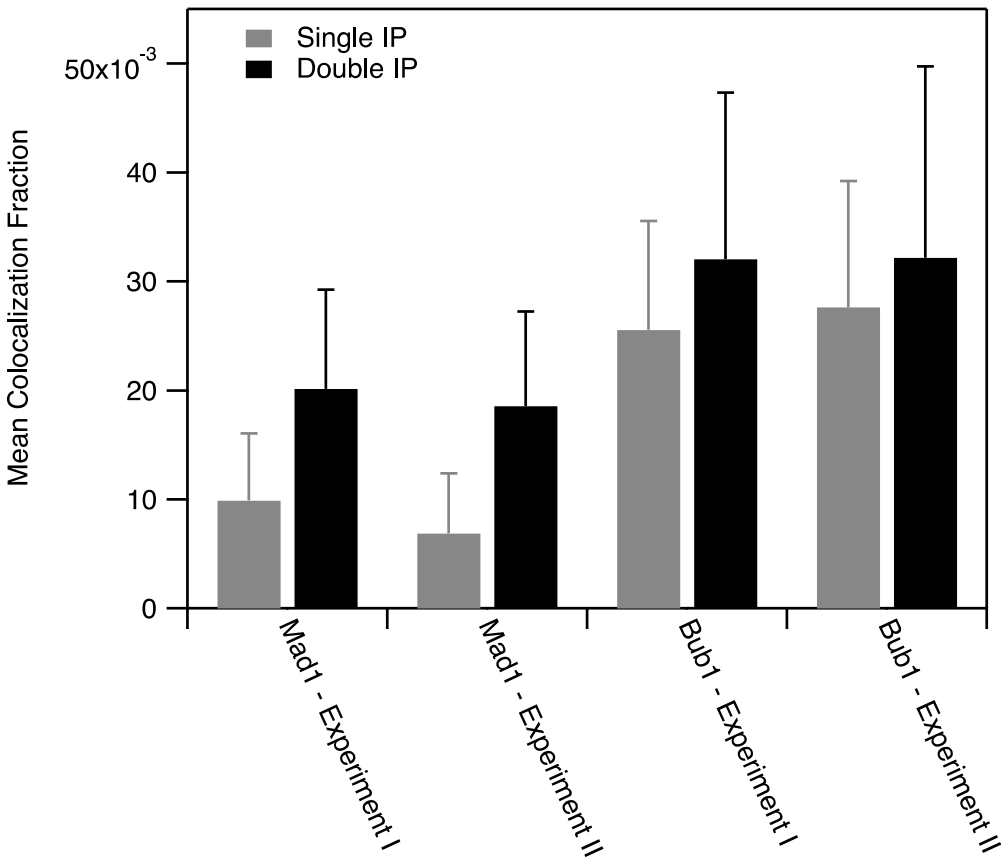

Figure 5.5: Dual purification of the kinetochores does not significantly increase colocalization levels. A 3V5 tag was endogenously engineered into the Spc24 core component of the kinetochore to help improve purification. These kinetochores were purified via FLAG first, and then a second purification was done on the immunoprecipitation kinetochore sample using the V5 epitope. The resulting Mad1- and Bub1-labeled kinetochores did not show significant increase in colocalization.

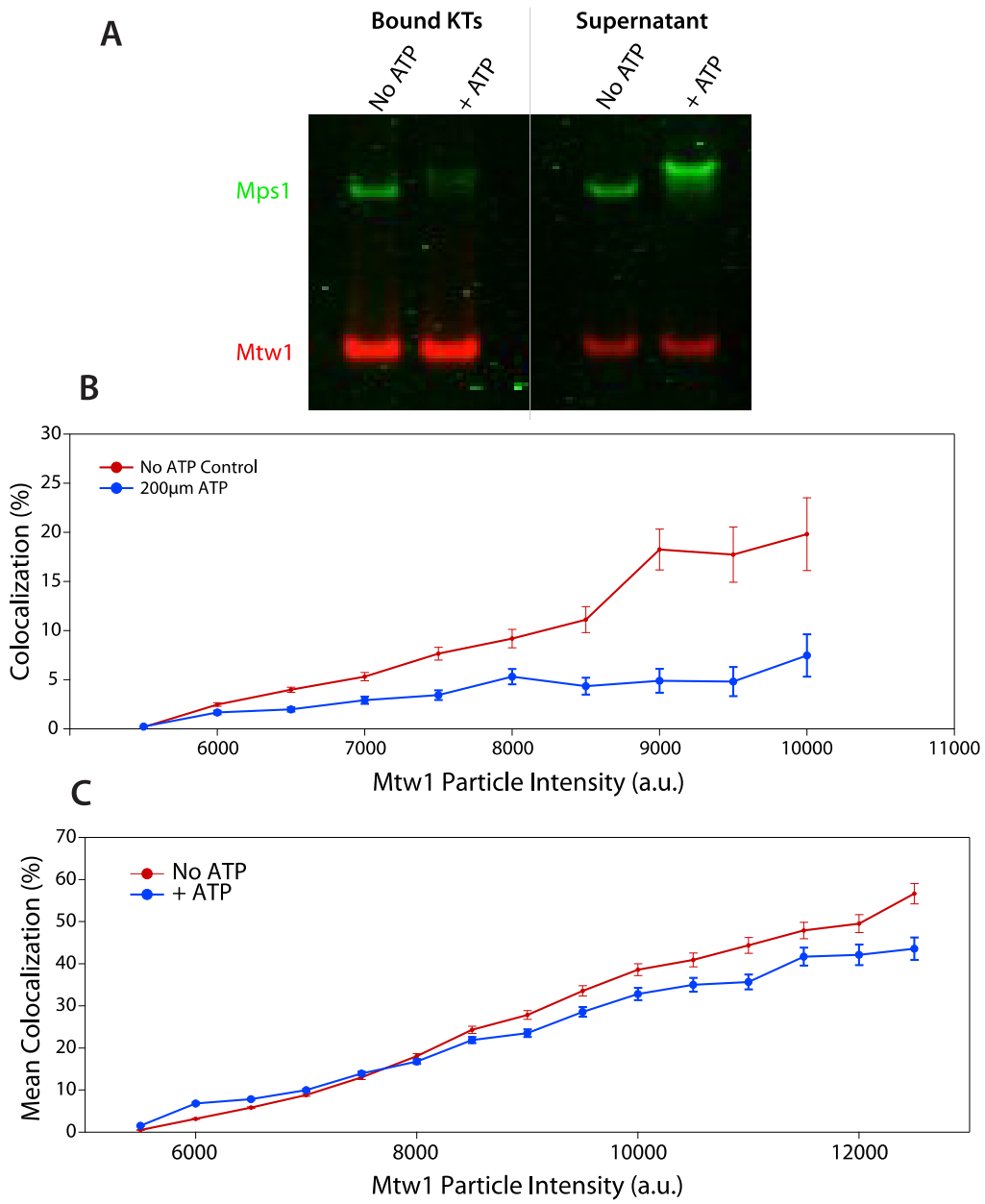

Figure 5.6: Preliminary experiments indicate that Mps1 is released from kinetochores upon addition of ATP. (A) The resultant supernatant and bound kinetochores from a kinase buffer treated kinetochore preparation indicated that the Mps1 upon ATP treatment were released from the kinetochore as seen in the typhoon scan. A shift in the Mps1 band is also seen in the scan. (B) the kinetochores from this experiment were then observed in TIRF and showed a significant decrease in colocalization. (C) Preliminary experiments showed very moderate decrease in level of colocalization when kinetochores already specifically adsorbed to a phospholipid bilayer were treated with ATP. This experiment needs to be further explored in the future.

BIBLIOGRAPHY

1. Hartwell LH (1991) Twenty-five years of cell cycle genetics. *Genetics* 129(4):975–980.
2. Cleveland DW, Mao Y, Sullivan KF (2003) Centromeres and kinetochores: from epigenetics to mitotic checkpoint signaling. *Cell* 112(4):407–21.
3. Clarke L, Carbon J (1985) The structure and function of yeast centromeres. *Ann Rev Genet* 19:29–56.
4. Cheeseman IM, Desai A (2008) Molecular architecture of the kinetochore-microtubule interface. *Nat Rev Mol Cell Biol* 9(1):33–46.
5. McAinsh AD, Tytell JD, Sorger PK (2003) Structure, function, and regulation of budding yeast kinetochores. *Annu Rev Cell Dev Biol* 19:519–539.
6. Cho U, Harrison SC (2011) Ndc10 is a platform for inner kinetochore assembly in budding yeast. *Nat Struct Mol Biol* 19(1):48–55.
7. Biggins S (2013) The composition, functions, and regulation of the budding yeast kinetochore. *Genetics* 194(4):817–46.
8. Joglekar AP, et al. (2008) Molecular architecture of the kinetochore-microtubule attachment site is conserved between point and regional centromeres. *J Cell Biol* 181(4):587–594.
9. Gonen S, et al. (2012) The structure of purified kinetochores reveals multiple microtubule-attachment sites. *Nat Struct Mol Biol* 19(9):925–929.
10. Lara-Gonzalez P, Westhorpe FG, Taylor SS (2012) The spindle assembly checkpoint. *Curr Biol* 22(22):R966-80.
11. Mitchison TJ, Kirschner MW (1984) Dynamic instability of microtubule growth. *Nature*

312(5991):237–242.

12. Burbank KS, Mitchison TJ (2006) Microtubule dynamic instability. *Curr Biol* 16(14):516–517.

13. Tanaka K, Kitamura E, Kitamura Y, Tanaka TU (2007) Molecular mechanisms of microtubule-dependent kinetochore transport toward spindle poles. *J Cell Biol* 178(2):269–281.

14. Pinsky BA, Biggins S (2005) The spindle checkpoint: tension versus attachment. *Trends Cell Biol* 15(9):486–93.

15. Lampson M a, Renduchitala K, Khodjakov A, Kapoor TM (2004) Correcting improper chromosome-spindle attachments during cell division. *Nat Cell Biol* 6(3):232–7.

16. Tanaka TU, et al. (2002) Evidence that the Ipl1-Sli15 (Aurora Kinase-INCENP) Complex Promotes Chromosome Bi-orientation by Altering Kinetochore-Spindle Pole Connections. *Cell* 108(3):317–329.

17. Winey M, et al. (2004) Three-dimensional ultrasctructural analysis of the Saccharomyces cerevisiae mitotic spindle. *J Cell Biol* 129(6):1601–1615.

18. Hoyt MA, Totis L, Roberts BT (1991) S. cerevisiae genes required for cell cycle arrest in response to loss of microtubule function. *Cell* 66(3):507–17.

19. Li R, Murray AW (1991) Feedback control of mitosis in budding yeast. *Cell* 66(3):519–31.

20. Winey M, Goetsch L, Baum P, Byers B (1991) MPS1 and MPS2: Novel yeast genes defining distinct steps of spindle pole body duplication. *J Cell Biol* 114(4):745–754.

21. Lauze E, et al. (1995) Yeast spindle pole body duplication gene MPS1 encodes an essential dual specificity protein kinase. *EMBO J* 14(8):1655–1663.

22. Weiss E, Winey M (1996) The Saccharomyces cerevisiae spindle pole body duplication gene MPS1 is part of a mitotic checkpoint. *J Cell Biol* 132(1–2):111–23.

23. Li X, Nicklas B (1995) Mitotic forces control a cell-cycle checkpoint. *Nature* 373(6515):630–632.

24. Rieder CL, Cole RW, Khodjakov A, Sluder G (1995) The checkpoint delaying anaphase in response to chromosome monoorientation is mediated by an inhibitory signal produced by unattached kinetochores. *J Cell Biol* 130(4):941–948.

25. Mcewen BF, Heagle AB, Cassels GO, Buttle KF, Rieder CL (1997) Kinetochore fiber maturation in PtK1 cells and its implications for the mechanisms of chromosome congression and anaphase onset. *J Cell Biol* 137(7):1567–1580.

26. Howell BJ, et al. (2004) Spindle Checkpoint Protein Dynamics at Kinetochores in Living Cells. *Curr Biol* 14(11):953–964.

27. Lan W, Cleveland DW (2010) A chemical tool box defines mitotic and interphase roles for Mps1 kinase. *J Biol Chem* 190(1):21–24.

28. Saurin AT, van der Waal MS, Medema RH, Lens SM a, Kops GJPL (2011) Aurora B potentiates Mps1 activation to ensure rapid checkpoint establishment at the onset of mitosis. *Nat Commun* 2(May):316.

29. Nijenhuis W, et al. (2013) A TPR domain-containing N-terminal module of MPS1 is required for its kinetochore localization by Aurora B. *J Cell Biol* 201(2):217–231.

30. London N, Ceto S, Ranish JA, Biggins S (2012) Phosphoregulation of Spc105 by Mps1 and PP1 regulates Bub1 localization to kinetochores. *Curr Biol* 22(10):900–906.

31. Shepperd L a, et al. (2012) Phosphodependent recruitment of Bub1 and Bub3 to Spc7/KNL1 by Mph1 kinase maintains the spindle checkpoint. *Curr Biol* 22(10):891–9.

32. Yamagishi Y, Yang C-H, Tanno Y, Watanabe Y (2012) MPS1/Mph1 phosphorylates the kinetochore protein KNL1/Spc7 to recruit SAC components. *Nat Cell Biol* 14(7):746–52.

33. London N, Biggins S (2014) Mad1 kinetochore recruitment by Mps1-mediated phosphorylation of Bub1 signals the spindle checkpoint. *Genes Dev* 28(2):140–152.

34. Howell BJ, Hoffman DB, Fang G, Murray AW, Salmon ED (2000) Visualization of Mad2 dynamics at kinetochores, along spindle fibers, and at spindle poles in living cells. *J Cell Biol* 150(6):1233–50.

35. Luo X, Tang Z, Rizo J, Yu H (2002) The Mad2 spindle checkpoint protein undergoes similar major conformational changes upon binding to either Mad1 or Cdc20. *Mol Cell* 9(1):59–71.

36. Sironi L, et al. (2002) Crystal structure of the tetrameric Mad1-Mad2 core complex: implications of a "safety belt" binding mechanism for the spindle checkpoint. *EMBO J* 21(10):2496–506.

37. Antoni A De, et al. (2005) The Mad1 / Mad2 Complex as a Template for Mad2 Activation in the Spindle Assembly Checkpoint. *Curr Biol* 15(3):214–225.

38. Mapelli M, Massimiliano L, Santaguida S, Musacchio A (2007) The Mad2 conformational dimer: structure and implications for the spindle assembly checkpoint. *Cell* 131(4):730–43.

39. Musacchio A (2015) The molecular biology of spindle assembly checkpoint signaling dynamics. *Curr Biol* 25(20):R1002–R1018.

40. Stucke VM, Sillje HHW, Arnaud L, Nigg EA (2002) Human Mps1 kinase is required for the spindle assembly checkpoint but not for centrosome duplication. *EMBO J* 21(7):1723–1732.

41. Jelluma N, Dansen TB, Sliedrecht T, Kwiatkowski NP, Kops GJPL (2010) Release of Mps1 from kinetochores is crucial for timely anaphase onset. *J Cell Biol* 191(2):281–90.

42. Ito D, Saito Y, Matsumoto T (2012) Centromere-tethered Mps1 pombe homolog (Mph1) kinase is a sufficient marker for recruitment of the spindle checkpoint protein Bub1, but not Mad1. *Proc Natl Acad Sci* 109(1):209–14.

43. Kemmler S, et al. (2009) Mimicking Ndc80 phosphorylation triggers spindle assembly checkpoint signalling. *EMBO J* 28(8):1099–1110.

44. Heinrich S, Windecker H, Hustedt N, Hauf S (2012) Mph1 kinetochore localization is crucial and upstream in the hierarchy of spindle assembly checkpoint protein recruitment to kinetochores. *J Cell Sci* 125(20):4720–4727.

45. Wei RR, Al-Bassam J, Harrison SC (2007) The Ndc80/HEC1 complex is a contact point for kinetochore-microtubule attachment. *Nat Struct Mol Biol* 14(1):54–59.

46. Ciferri C, et al. (2008) Implications for Kinetochore-Microtubule Attachment from the Structure of an Engineered Ndc80 Complex. *Cell* 133(3):427–439.

47. Primorac I, et al. (2013) Bub3 reads phosphorylated MELT repeats to promote spindle assembly checkpoint signaling. *Elife* 2:e01030.

48. Kim S, Sun H, Tomchick DR, Yu H, Luo X (2012) Structure of human Mad1 C-terminal domain reveals its involvement in kinetochore targeting. *Proc Natl Acad Sci* 109(17):6549–6554.

49. Moyle MW, et al. (2014) A Bub1-Mad1 interaction targets the Mad1-Mad2 complex to unattached kinetochores to initiate the spindle checkpoint. *J Cell Biol* 204(5):647–657.

50. Hiruma Y, et al. (2015) Competition between MPS1 and microtubules at kinetochores regulates spindle checkpoint signaling. *Science (80-)* 348(6240):1264–1267.

51. Ji Z, Gao H, Yu H (2015) Kinetochore attachment sensed by competitive Mps1 and microtubule binding to Ndc80C. *Science (80-)* 348(6240):1260–1264.

52. Akiyoshi B, et al. (2010) Tension directly stabilizes reconstituted kinetochore-microtubule attachments. *Nature* 468(7323):576–9.

53. Deniz AA, Mukhopadhyay S, Lemke EA (2008) Single-molecule biophysics: at the interface of biology, physics and chemistry. *J R Soc Interface* 5(18):15–45.

54. Hirschfeld T (1976) Optical microscopic observation of single small molecules. *Appl Opt* 15(12):2965–2966.

55. Neher E, Sakmann B (1976) Single-channel currents recorded from membrane of denervated frog muscle fibres. *Nature* 260(5554):799–802.

56. De Vlaminck I, Dekker C (2012) Recent advances in magnetic tweezers. *Annu Rev Biophys* 41:453–72.

57. Lionnet T, et al. (2012) Single-molecule studies using magnetic traps. *Cold Spring Harb Protoc* 7(1):34–49.

58. Lipfert J, Lee M, Ordu O, Kerssemakers JWJ, Dekker NH (2014) Magnetic tweezers for the measurement of twist and torque. *J Vis Exp* 19(87):1–18.

59. Strick TR, Croquette V, Bensimon D (2000) Single-molecule analysis of DNA uncoiling by a type II topoisomerase. *Nature* 404(6780):901–904.

60. Garzon-Coral C, Fantana HA, Howard J (2016) A force-generating machinery maintains the spindle at the cell center during mitosis. *Science (80-)* 352(6289):1124–7.

61. Ashkin A, Dziedzic JM, Bjorkholm JE, Chu S (1986) Observation of a single-beam gradient force optical trap for dielectric particles. *Opt Lett* 11(5):288–290.

62. Svoboda K, Schmidt CF, Schnapp BJ, Block SM (1993) Direct observation of kinesin

stepping by optical trapping interferometry. *Nature* 365(6448):721–727.

63. Neuman KC, Block SM (2004) Optical trapping. *Rev Sci Instrum* 75(9):2787–2809.

64. Moffitt JR, Chemla YR, Smith SB, Bustamante C (2008) Recent advances in optical tweezers. *Annu Rev Biochem* 77:205–28.

65. Koch MD, Shaevitz JW (2017) Optical Tweezers. *Methods Mol Biol* 1486(1):3–24.

66. Binnig G, Quate CF (1986) Atomic Force Microscope. *Phys Rev Lett* 56(9):930–933.

67. Seo Y, Jhe W (2008) Atomic force microscopy and spectroscopy. *Reports Prog Phys* 71(1):1–23.

68. Fischer-Friedrich E, Hyman AA, Jülicher F, Müller DJ, Helenius J (2014) Quantification of surface tension and internal pressure generated by single mitotic cells. *Sci Rep* 4:6213.

69. Cattin CJ, et al. (2015) Mechanical control of mitotic progression in single animal cells. *Proc Natl Acad Sci* 112(36):11258–11263.

70. Jonkman J, Brown CM (2015) Any Way You Slice It-A Comparison of Confocal Microscopy Techniques. *J Biomol Tech* 26(2):54–65.

71. Ha T, et al. (1996) Probing the interaction between two single molecules: fluorescence resonance energy transfer between a single donor and a single acceptor. *Proc Natl Acad Sci* 93(13):6264–6268.

72. Axelrod D (2001) Total internal reflection fluorescence microscopy in cell biology. *Traffic* 2(11):764–774.

73. Leake MC, et al. (2006) Stoichiometry and turnover in single, functioning membrane protein complexes. *Nature* 443(7109):355–358.

74. Ulbrich MH, Isacoff EY (2007) Subunit counting in membrane-bound proteins. *Nat Methods* 4(4):319–21.

75. Sarangapani KK, et al. (2014) Sister kinetochores are mechanically fused during meiosis I in yeast. *Science (80-)* 346(6206):248–252.

76. Vale RD, et al. (1996) Direct observation of single kinesin molecules moving along microtubules. *Nature* 380(6753):451–453.

77. Yildiz A, et al. (2003) Myosin V walks hand-over-hand: Single fluorophore imaging with 1.5-nm localization. *Science (80-)* 300(5628):2061–2065.

78. Hoskins AA, et al. (2011) Ordered and dynamic assembly of single spliceosomes. *Science (80-)* 331(March):1289–1295.

79. Dickson RM, Cubitt AB, Tsien RY, Moerner WE (1997) On / off blinking and switching behaviour of single molecules of green fluorescent protein. *Nature* 388(July):355–358.

80. Grohmann D, Werner F, Tinnefeld P (2013) Making connections — strategies for single molecule fluorescence biophysics. *Curr Opin Chem Biol* 17(4):691–698.

81. Keppler A, et al. (2004) Labeling of fusion proteins of O6 -alkylguanine-DNA alkyltransferase with small molecules in vivo and in vitro. *Methods* 32(4):437–444.

82. Gautier A, et al. (2008) An engineered protein tag for multiprotein labeling in living cells. *Chem Biol* 15(2):128–136.

83. Lamichhane R, Solem A, Black W, Rueda D (2010) Single-molecule FRET of protein-nucleic acid and protein-protein complexes: Surface passivation and immobilization. *Methods* 52(2):192–200.

84. Sofia SJ, Premnath V, Merrill EW (1998) Poly(ethylene oxide) grafted to silicon surfaces: Grafting density and protein adsorption. *Macromolecules* 9297(97):5059–5070.

85. Elbert DL, Hubbell JA (1996) Surface treatments of polymers for biocompatibility. *Annu Rev Mater Sci* 26(1):365–394.

86. Radi L, et al. (2016) Methods of protein surface PEGylation under structure preservation for the emulsion-based formation of stable nanoparticles. *R Soc Chem* 7:21–39.

87. Sackmann E (1996) Supported membranes: Scientific and practical applications. *Science (80-)* 271(5245):43–48.

88. Livnah O, Bayer EA, Wilchek M, Sussman JL (1993) Three-dimensional structures of avidin and the avidin- biotin complex. *Proc Natl Acad Sci* 90(11):5076–5080.

89. Chivers CE, Koner AL, Lowe ED, Howarth M (2011) How the biotin–streptavidin interaction was made even stronger: investigation via crystallography and a chimaeric tetramer. *Biochem J* 435(1):55–63.

90. Paweletz N (2001) Walther Flemming: pioneer of mitosis research. *Nat Rev Mol Cell Biol* 2(1):72–75.

91. Heald R, Khodjakov A (2015) Thirty years of search and capture : The complex simplicity of mitotic spindle assembly. *J Cell Biol* 211(6):1103–1111.

92. London N, Biggins S (2014) Signalling dynamics in the spindle checkpoint response. *Nat Rev Mol Cell Biol* 15(11):735–747.

93. Jain A, et al. (2011) Probing cellular protein complexes using single-molecule pull-down. *Nature* 473(7348):484–8.

94. Miller MP, Asbury CL, Biggins S (2016) A TOG Protein Confers Tension Sensitivity to Kinetochore-Microtubule Attachments. *Cell* 165(6):1–12.

95. Sarangapani KK, et al. (2014) Sister kinetochores are mechanically fused during meiosis I in yeast. *Science (80-)* 346(6206):248–251.

96. Schwarzacher T (2003) Meiosis, recombination and chromosomes: A review of gene isolation and fluorescent in situ hybridization data in plants. *J Exp Bot* 54(380):11–23.

97. Marston AL, Amon A (2004) Meiosis: cell-cycle controls shuffle and deal. *Nat Rev Mol Cell Biol* 5(12):983–997.

98. Goldstein LSB (1981) Kinetochore structure and its role in chromosome orientation during the first meiotic division in male D . melanogaster. *Cell* 25(3):591–602.

99. Paliulis L V, Nicklas RB (2000) The reduction of chromosome number in meiosis is determined by properties built into the chromosomes. *J Cell Biol* 150(6):1223–1231.

100. Li X, Dawe RK (2009) Fused sister kinetochores initiate the reductional division in meiosis I. *Nat Cell Biol* 11(9):1103–1108.

101. Corbett KD, et al. (2010) The monopolin complex crosslinks kinetochore components to regulate chromosome-microtubule attachments. *Cell* 142(4):556–567.

102. Castoldi M, Popov A V (2003) Purification of brain tubulin through two cycles of polymerization – depolymerization in a high-molarity buffer. *Protein Expr Purif* 32(1):83–88.

103. Churchman LS, Okten Z, Rock RS, Dawson JF, Spudich JA (2005) Single molecule high-resolution colocalization of Cy3 and Cy5 attached to macromolecules measures intramolecular distances through time. *Proc Natl Acad Sci U S A* 102(5):1419–1423.

104. Churchman LS, Spudich JA (2012) Colocalization of Fluorescent Probes : Accurate and Precise Registration with Nanometer Resolution. *Cold Spring Harb Protoc* 2012(2):141–149.

105. Churchman LS, Spudich JA (2012) Single-molecule high-resolution colocalization of single probes. *Cold Spring Harb Protoc* 2012(2):242–245.

106. Goshtasby A (1988) Image registration by local approximation methods. *Image Vis Comput* 6(4):255–261.

107. Deng Y, Asbury CL (2017) Simultaneous manipulation and super-resolution fluorescence imaging of individual kinetochores coupled to microtubule tips. *Methods Mol Biol* 1486(1):437–467.

108. Compton DA (2011) Mechanisms of aneuploidy. *Curr Opin Cell Biol* 23(1):109–13.

109. Thompson SL, Compton DA (2008) Examining the link between chromosomal instability and aneuploidy in human cells. *J Cell Biol* 180(4):665–72.

110. Murray AW (2011) A brief history of error. *Nat Cell Biol* 13(10):1178–1182.

111. Liu X, Winey M (2012) The MPS1 family of protein kinases. *Annu Rev Bioochemistry*:561–585.

112. Primorac I, et al. (2013) Bub3 reads phosphorylated MELT repeats to promote spindle assembly checkpoint signaling. *Elife* 2013(2):1–20.

113. Chmielewska AE, Tang NH, Toda T (2016) The hairpin region of Ndc80 is important for the kinetochore recruitment of Mph1/MPS1 in fission yeast. *Cell Cycle* 15(5):740–747.

114. Aravamudhan P, Goldfarb AA, Joglekar AP (2015) The kinetochore encodes a mechanical switch to disrupt spindle assembly checkpoint signalling. *Nat Cell Biol* 17(7):868–879.

115. Hervas-Aguilar A, Millar JBA (2016) Mph1/MPS1 checks in at the kinetochore. *Cell Cycle* 15(10):1313–1314.

116. Etemad B, Kops GJ (2016) Attachment issues: kinetochore transformations and spindle checkpoint silencing. *Curr Opin Cell Biol* 39(a015826):101–108.

117. Sacristan C, Kops GJPL (2015) Joined at the hip: kinetochores, microtubules, and spindle assembly checkpoint signaling. *Trends Cell Biol* 25(1):21–28.

118. Hiruma Y, et al. (2015) Competition between MPS1 and microtubules at kinetochores

regulates spindle checkpoint signaling. *Science (80-)* 348(6240):1264–1267.

119. Joglekar AP, Bouck DC, Molk JN, Bloom KS, Salmon ED (2006) Molecular architecture of a kinetochore-microtubule attachment site. *Nat Cell Biol* 8(6):581–5.

120. Johnston K, et al. (2010) Vertebrate kinetochore protein architecture: protein copy number. *J Cell Biol* 189(6):937–43.

121. Aravamudhan P, Felzer-Kim I, Joglekar AP (2013) The budding yeast point centromere associates with two Cse4 molecules during mitosis. *Curr Biol* 23(9):1–16.

122. Suzuki A, Badger BL, Salmon ED (2015) A quantitative description of Ndc80 complex linkage to human kinetochores. *Nat Commun* 6:8161.

123. Wang X, et al. (2014) Dynamic Autophosphorylation of Mps1 Kinase Is Required for Faithful Mitotic Progression. *PLoS One* 9(9):1–10.

124. Akiyoshi B, Nelson CR, Biggins S (2013) The aurora B kinase promotes inner and outer kinetochore interactions in budding yeast. *Genetics* 194(3):785–789.

125. Dimitrova YN, Jenni S, Valverde R, Khin Y, Harrison SC (2016) Structure of the MIND complex defines a regulatory focus for yeast kinetochore assembly. *Cell* 167(4):1014–1021.

126. Powers AF, et al. (2009) The Ndc80 kinetochore complex forms load-bearing attachments to dynamic microtubule tips via biased diffusion. *Cell* 136(5):865–875.

127. Kirschner M, Mitchison TJ (1986) Beyond self-assembly : From microtubules to morphogenesis. *Cell* 45(3):329–342.

128. Huang B, Huffaker TC (2006) Dynamic microtubules are essential for efficient chromosome capture and biorientation. *J Cell Biol* 175(1):17–23.

129. Rieder CL, Alexander SP (1990) Kinetochores Are Transported Poleward along a Single

Astral Microtubule during Chromosome Attachment to the Spindle in Newt Lung Cells. *J Cell Biol* 110(1):81–95.

130. Tanaka K, et al. (2005) Molecular mechanisms of kinetochore capture by spindle microtubules. *Nature* 434(7036):987–94.

131. Magidson V, et al. (2011) The spatial arrangement of chromosomes during prometaphase facilitates spindle assembly. *Cell* 146(4):555–567.

132. Kalinina I, et al. (2012) Pivoting of microtubules around the spindle pole accelerates kinetochore capture. *Nat Cell Biol* 15(1):82–87.

133. Kalantzaki M, et al. (2015) Kinetochore–microtubule error correction is driven by differentially regulated interaction modes. *Nat Cell Biol* 17(4):421–433.

134. Tanaka TU (2010) Kinetochore–microtubule interactions: steps towards bi-orientation. *EMBO J* 29(24):4070–4082.

135. Tauchman EC, Boehm FJ, DeLuca JG (2015) Stable kinetochore-microtubule attachment is sufficient to silence the spindle assembly checkpoint in human cells. *Nat Commun* 6:8987.

136. Smith CA, Mcainsh AD, Burroughs NJ (2016) Human kinetochores are swivel joints that mediate microtubule attachments. *Elife* 5(e16159):1–15.

137. Mattison CP, et al. (2007) Mps1 Activation Loop Autophosphorylation Enhances Kinase Activity. *J Biol Chem* 282(42):30553–30561.

138. Kang J, Chen Y, Zhao Y, Yu H (2007) Autophosphorylation-dependent activation of human Mps1 is required for the spindle checkpoint. *Proc Natl Acad Sci* 104(51):20232–20237.

139. Stucke VM, Baumann C, Nigg EA (2004) Kinetochore localization and microtubule

interaction of the human spindle checkpoint kinase Mps1. *Chromosoma* 113(1):1–15.

140. Wan X, et al. (2009) Protein architecture of the human kinetochore microtubule attachment site. *Cell* 137(4):672–84.

141. Joglekar AP, Bloom K, Salmon ED (2009) In vivo protein architecture of the eukaryotic kinetochore with nanometer scale accuracy. *Curr Biol* 19(8):694–9.

142. Aravamudhan P, Felzer-Kim I, Gurunathan K, Joglekar AP (2014) Assembling the Protein Architecture of the Budding Yeast Kinetochore-Microtubule Attachment using FRET. *Curr Biol* 24(13):1437–46.

VITA

Kwaku Nyame Opoku was born on July 10th, 1985 in Koforidua, a town in the Eastern Region of Ghana to John Theophilus Opoku and Salome Opoku, who hail from Akuase. Kwaku attended Naylor SDA Primary School in Tema until Class 5 when his family moved to Takoradi, Ghana. In Takoradi, he attended Ridge International School. He attended Mfantsipim School, also known as 'The School'. After senior secondary school in Ghana, Kwaku made a solo journey through the help of his parents and other individuals to Moorhead, Minnesota to attend Concordia College.

At Concordia College, he pursued a dual-degree with the University of Minnesota in Minneapolis. He obtained an Applied Science degree and Mathematics minor from Concordia College and a Biomedical Engineering degree from the University of Minnesota. At the University of Minnesota, he had his first real experience doing scientific research in the lab of Dr. David Odde. He spent approximately two years in the lab of Dr. David Odde studying glioblastoma cell division, shape and migration *in vitro*. He was spurred by this experience to pursue a graduate degree. He moved to Seattle Washington in the fall of 2011 to pursue a PhD in Molecular and Cellular Biology in the lab of Dr. Chip Asbury.